

Copyright is owned by the Author of the thesis. Permission is given for a copy to be downloaded by an individual for the purpose of research and private study only. The thesis may not be reproduced elsewhere without the permission of the Author.

COMPARATIVE ANALYSIS OF A PRESSURE VESSEL

**Finite Element Analysis versus
Speckle Photography**

ZUPING WANG

1994

**A thesis presented in fulfilment
of the requirements for the degree of
Master of Technology
Massey University**

CONTENTS

Abstract	1
Acknowledgements	2
1 Introduction	3
2 Literature Survey	8
2.1 History of Finite Element Method	8
2.2 A brief survey of Speckle Photography	10
3 Finite Element Computations	12
3.1 Finite Element Computational Model	12
3.2 MYSTRO and LUSAS Programs	14
4 Pressure Vessel Model	18
4.1 Configuration	18
4.2 Features and Attributes	19
4.3 Meshes	24
4.4 Geometry, Materials, Support and Loading	31
5 Running LUSAS	44
5.1 Running LUSAS	44
5.2 Running expose	47
6 Results Analysis	51
6.1 Displacement	52
6.2 Deformation	56
6.3 Stress	58
6.4 A summary of the results from FEM	62
6.5 Results from the pressure vessel design formulas	77

6.6 Results from Laser Speckle Photography Experiment	78
6.7 Comparison of displacements and stresses determined by FEA, LSP and the pressure vessel design formulas	80
7 Conclusions	85
8 Thoughts on further work	87
9 References	89
10 Index	92
Appendices	A1
Appendix I Equilibrium, Compatibility and the Stress/Strain law	A1
Appendix II Input data list	A3
Appendix III Output data list	A20

ABSTRACT

A detailed explanation and analysis are presented of the Finite Element Method used to solve the stress/strain situation in a small pressure vessel. A pressure vessel was modelled whose displacement characteristics were previously analysed using speckle photography. The Mystro/Lusas finite element software was used on a PC 486 computer system. A linear and static analysis was made. Contour plots of direct stress and shear stress distribution are presented which also show the highest stress areas. A comparison of the results from Finite Element Method and Speckle Photography Method as well as the pressure vessel design formulas are presented. Advantages of the Finite Element Method are discussed.

ACKNOWLEDGEMENTS

I would particularly like to express my gratitude to my supervisor Dr.E.W.Smith for his guidance, advice, valuable suggestions, constructive criticism and encouragement during all my work.

I wish to express my special thanks to Mr.Len Chisholm, System programmer, Department of Production Technology, for his specialised expertise and skill in computer systems.

I would like to thank Mr.Farshad Nourozi, Electronics/Software Technical Officer and Mrs. Vicki Spagnolo, Computer Programmer, for providing me with skilled assistance for the Macintosh computer and laser printer. I also would like to thank Miss Heather North, Graduate Assistant, Department of Production Technology, for sharing her knowledge in Laser Speckle Photography and providing encouragement.

I am indebted to the New Zealand government and Massey University for the award of a MERT scholarship whilst carrying out this study.

I also wish to take the opportunity to express my deepest gratitude to my parents and my family, as well as those who have loved, cared and helped me.

Words are inadequate to express my profound gratitude.

ZUPING WANG

1 Introduction

The Finite Element Method is a numerical procedure for analysing structures and continua. Usually the problem addressed is too complicated to be solved satisfactorily by classical analytical methods. The problem may concern stress analysis, heat conduction, or any of several other areas. The finite element procedure produces many simultaneous algebraic equations, which are generated and solved on a digital computer. Results are rarely exact.

The Finite Element Method originated as a method of stress analysis. Today finite elements are also used to analyse problems of heat transfer, fluid flow, lubrication, electric and magnetic fields and many other areas. Problems that previously were utterly intractable are now solved routinely. Finite element procedures are used in the design of buildings, electric motors, heat engines, ships, airframes and spacecraft. Manufacturing companies and large design offices typically have one or more large finite element programs in-house. Smaller companies usually have access to a large program through a commercial computing centre or use a smaller program on a personal computer.

The fundamental concept of the finite element method is that any continuous quantity can be approximated by a discrete model composed of a set of piecewise continuous functions defined over a finite number of sub-domains. The piecewise continuous functions are defined using the values of the continuous quantity at a finite number of points in its domain.

The more common situation is where the continuous quantity is unknown and we wish to determine the values of this quantity at certain points within the region. The construction of the discrete model is most easily explained, however, if we assume that we already know the numerical value of the quantity at every point within the domain. We

shall return to the common situation shortly. The discrete model is constructed as follows.

1. A finite number of points in the domain are identified. These points are called nodal points or nodes.
2. The value of the continuous quantity at each nodal point is denoted as a variable which is to be determined.
3. The domain is divided into a finite number of subdomains called elements. These elements are connected at common nodal points that collectively approximate the shape of the domain.
4. The quantity is approximated over each element by a polynomial that is defined using the nodal values of the continuous quantity. A different polynomial is defined for each element, but the element polynomials are selected in such a way that continuity is maintained along the element boundaries.

Laser Speckle Photography is an optical technique for measuring strains and displacements in structures. It has the advantage of being a nondestructive and qualitative analysis system, enabling complete structural areas to be assessed for points of high displacement gradients, as well as providing quantitative displacement results.

Speckle Photography involves recording two laser speckle patterns obtained from an optically rough object surface, before and after displacement, with the use of a photographic camera and high resolution film. If the processed negative is then illuminated with a narrow beam of coherent light, fringes representing displacement vectors are obtained.

A diagram of the optical arrangement for double exposure Laser Speckle Photography is shown in figure 1.1

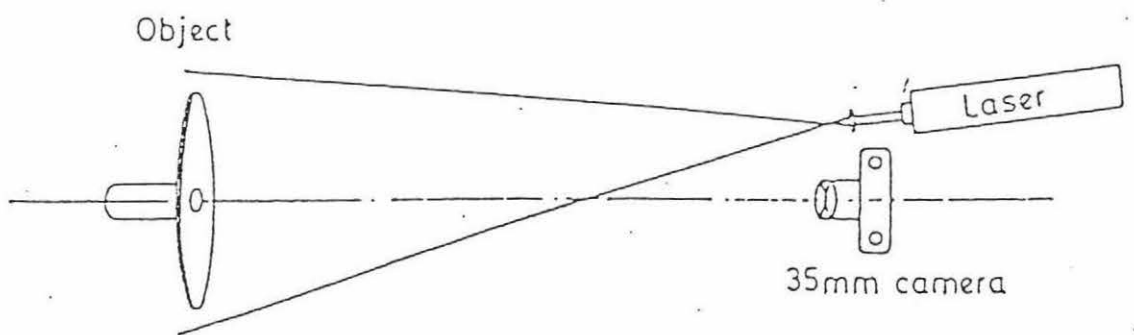


Fig.1.1 Optical arrangement for double exposure Laser Speckle Photography

When an optically rough surface is illuminated with laser light the scattered radiation forms speckle patterns in all directions and at all distances from the surface. The speckle pattern is related to the object and its surface texture, and is displaced if the object or part of it is moved.

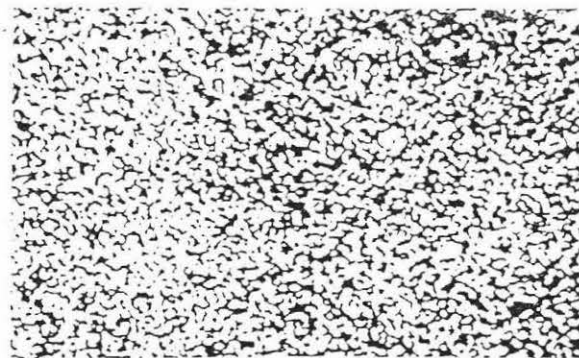


Fig.1.2 Example of an enlarged speckle pattern

A camera is then used to record two superimposed images of the surface, one before and one after the surface has moved. From the processed negative the main form of displacement that can be measured from the object surface is lateral in-plane movement.

Once the double exposed speckle pattern, from the displaced object surface, has been recorded, analysis can be made and the separation between the two speckle patterns determined. Analysis can be performed either by a point by point or a full-field method. A diagram of point by point analysis is shown in figure 1.3

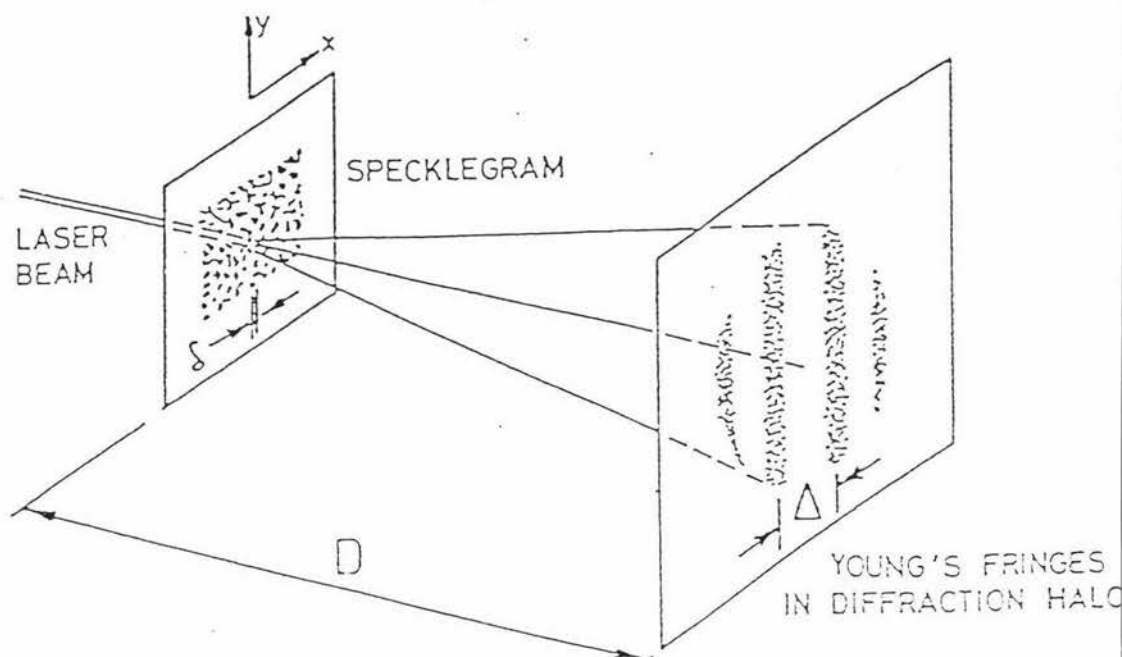


Fig.1.3 Point-by-Point filtering setup

The fringe pattern consists of a set of parallel straight fringes (Young's fringes) whose spacing is inversely proportional to the speckle (and therefore object surface) displacement, and whose direction lies at right angles to the displacement direction.

Here the displacement δ can be established as follows:

$$\delta = \frac{D\lambda}{\Delta}$$

where D is distance from negative to screen.

λ is wavelength of the laser light.

Δ is fringe separation distance.

The alternative method of analysis is to perform a type of full field spatial filtering on the specklegram as shown in Figure 1.4

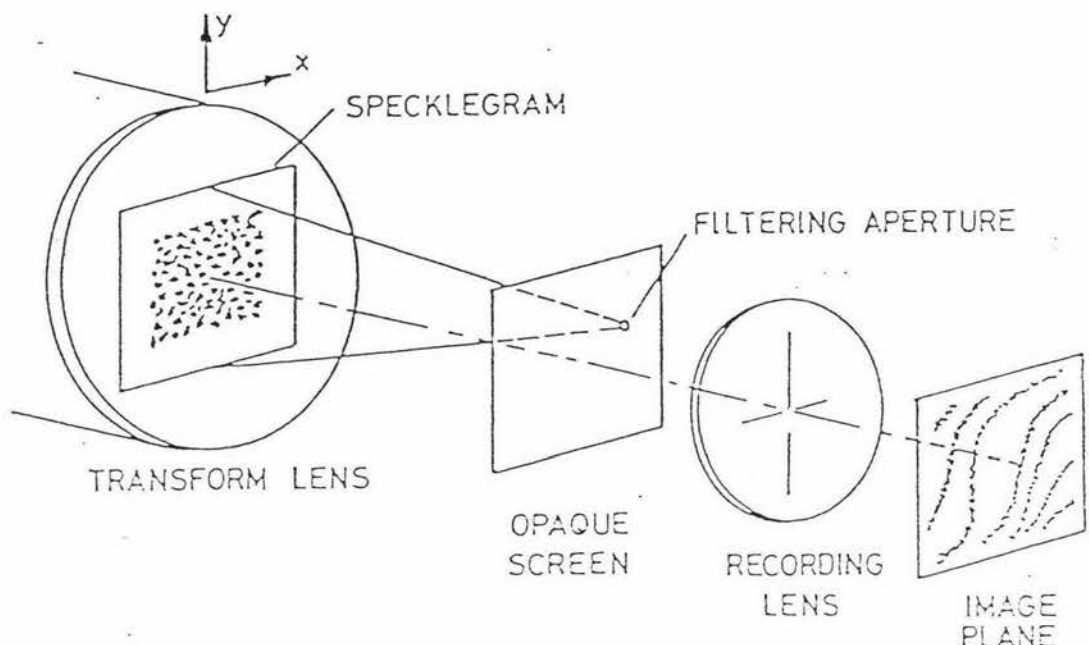


Fig.1.4 Full field filtering setup

The method involves illuminating the whole film with light and after performing spatial filtering, followed by re-imaging with a lens, a fringe pattern is obtained which corresponds to a large area on the surface being analysed.

2 Literature survey

2.1 History of Finite Element Method

The label " Finite Element Method " appeared in 1960 in a paper by Clough (1) concerning plane elasticity problems. However the method had its birth in the aerospace industry in the early 1950s. Early work on numerical solution of boundary value problems can be traced to the use of finite difference schemes. The beginnings of the finite element method actually stem from early numerical methods and the frustration associated with attempting to use finite difference methods on more difficult, geometrically irregular problems.

Beginning in the mid 1950s, efforts to solve continuum problems in elasticity using small, discrete "elements" to describe the overall behaviour of simple elastic bars began to appear. Argyris (2) and Turner et al. (3) were the first to publish on the use of such techniques for the aircraft industry.

An important theoretical contribution was made in 1963 when Melosh (4) showed that the finite element method was really a variation of the well known Raleigh-Ritz procedure.

The early use of finite elements was restricted to the application of such techniques to structural problems and much of the early work is on non-linear problems. However, the versatility of the method and its underlying rich mathematical basis were soon recognised by others for application in non structural areas. Zienkiewicz and Cheung (5) were among the first to apply the finite element method to field problems (e.g., heat conduction, irrational fluid flow, etc.) involving the solution of Laplace and Possion equations. Efforts to model heat transfer problems with complex boundaries are discussed in Huebner (6); a comprehensive three-dimensional finite element model for heat conduction is described by Heuser (7). An early application of the finite element technique to viscous fluid flow is given by Martin (8).

A virtual explosion in usage of the method has occurred since the mid 1970s. Excellent reviews and descriptions of the method can be found in the texts by Finlayson (9), Desai (10), Becker et al (11), Fletcher (12), Reddy (13), Segerlind (14), Hughes (15), Bickford (16), and Zienkiewicz and Taylor (17). A rigorous mathematical discussion is given in the text by Johnson (18), and programming the finite element method is described by Smith (19). A short monograph on development of the finite element method is given by Owen and Hinton (20).

The underlying mathematical basis of the finite element method first lies with the classical Rayleigh-Ritz method and variational calculus procedures introduced by Rayleigh (21) and Ritz (22). The theories provided the reasons why the finite element method worked well for the class of problems in which variational statements could be obtained (e.g., linear diffusion-type problems). However, as interest expanded in applying the finite element method to more areas, especially in mechanics, classical theory could no longer be used to describe such problems. This is particularly evident in fluid-related problems involving convection.

Extension of the mathematical basis to nonlinear and nonstructural problems was achieved through the method of weighted residuals, originally conceived by Galerkin (23) in the early 20th century. The method of weighted residuals was found to provide the ideal theoretical basis for a wide set of problems, including those to which the Rayleigh-Ritz method can be applied. Basically, the method requires the governing differential equation to be multiplied by a set of predetermined weights and the resulting product to be integrated over space; this integral is then required to vanish. Technically, Galerkin method is a particular case of the general weighted residuals procedure where various types of weights can be utilised; in the case of Galerkin's method, the weights are chosen to be same as the functions used to define the unknown variables. Galerkin's method yields results identical to the Rayleigh-Ritz approximations for linear, elliptic equations. By using constant weights instead of functions, the weighted residual method yields the finite volume technique. A rigorous

description of the method of weighted residuals can be found in Finlayson (9).

2.2 A brief survey of Speckle Photography

Speckle photography, which is usually based on laser illumination, enables measurements of displacement (static or dynamic) and shape to be made on optically rough surfaces at sensitivities significantly greater than the wavelength of light.

Operation of the first cw HeNe laser in 1960 revealed an unexpected phenomenon: that objects viewed in highly coherent light acquire a peculiar granular appearance.

Speckle photography takes its name from the phenomenon of this laser speckle pattern. Burch and Tokarski (24) explained that successively displaced laser speckle patterns can generate interference fringes similar to an array of fine pinholes. Archbold and Ennos (25) described methods for measuring surface displacement, based on the recording of laser speckle patterns with a photographic camera and high-resolution film. It was shown that two complementary techniques were possible, one for the measurement of very small displacements (a few wavelengths of light in magnitude), the other for applications where the surface movement was relatively large (tens of micrometers). The transition between the ranges occurs when the displacement to be measured equals the apparent diameter of an individual laser speckle referred back to the object.

The techniques for measurement of the very small displacements utilise the interference effects between two speckle fields, as first described by Leendertz (26). Archbold and Ennos demonstrated the practicality of the method for displacement analysis using laser illumination and a 35mm camera capable of double exposures, with magnifications of the order of unity down to one tenth. Their demonstrations showed a limited object size due to the need for laser illumination.

To overcome the problems of using laser illumination, Burch and Forno (27) proposed the use of white light speckle , this pattern simply taking the form of random black and white marks on the object surface. Boone and De Backer (28), using a suitable speckle pattern on the surface of the object in white light, showed the method was feasible without resorting to special aperture masks. Asundi and Chiang (29) illustrated that many natural surface textures will create a suitable speckle pattern if photographed in the correct light configuration. Measurement of speckle movement will allow object displacements and strains to be calculated in 2-D and 3-D. Establishing speckle movement may be performed by suitable spatial filtering or direct observation of the speckles. The simplest and quickest method is to use point by point spatial filtering using an unexpanded laser beam.

The earliest mathematical investigations of speckle-like phenomena were those of Verdet and Strutt (30), who were concerned with the properties of "coronas", now more commonly known as Fraunhofer rings. Later, in a series of papers dealing with the scattering of light from a large number of particles, Laue (31) derived many basic results that have direct relevance to speckle.

Speckle photography works well when applied to relatively small objects, but little use has been made of the technique to look at large objects. Those for measurement of larger movements did so by observing the optical transform of the double-exposed recording of the speckle pattern, it was employed by Archbold and Ennos (25).

The work of Cloud & Conley (32) and Smith & North (33), looking at the movement of glacier ice, used the sun as the light source.

3 Finite Element Computations

3.1 Finite Element Computational Model

We are often confronted with practical physical and engineering problems whose solution is too difficult or even impossible by conventional analytical methods. Of particular concern are three-dimensional elastic bodies acted upon by sets of externally applied forces. The pressure vessel used in the Optical Engineering Research Lab at Massey University is such a problem. The Finite Element Method, in conjunction with automatic computation, constitutes a very effective and elegant device for solving complex physical problems, whose solution by any other means can be too difficult.

The following is a typical finite element computational model (34).

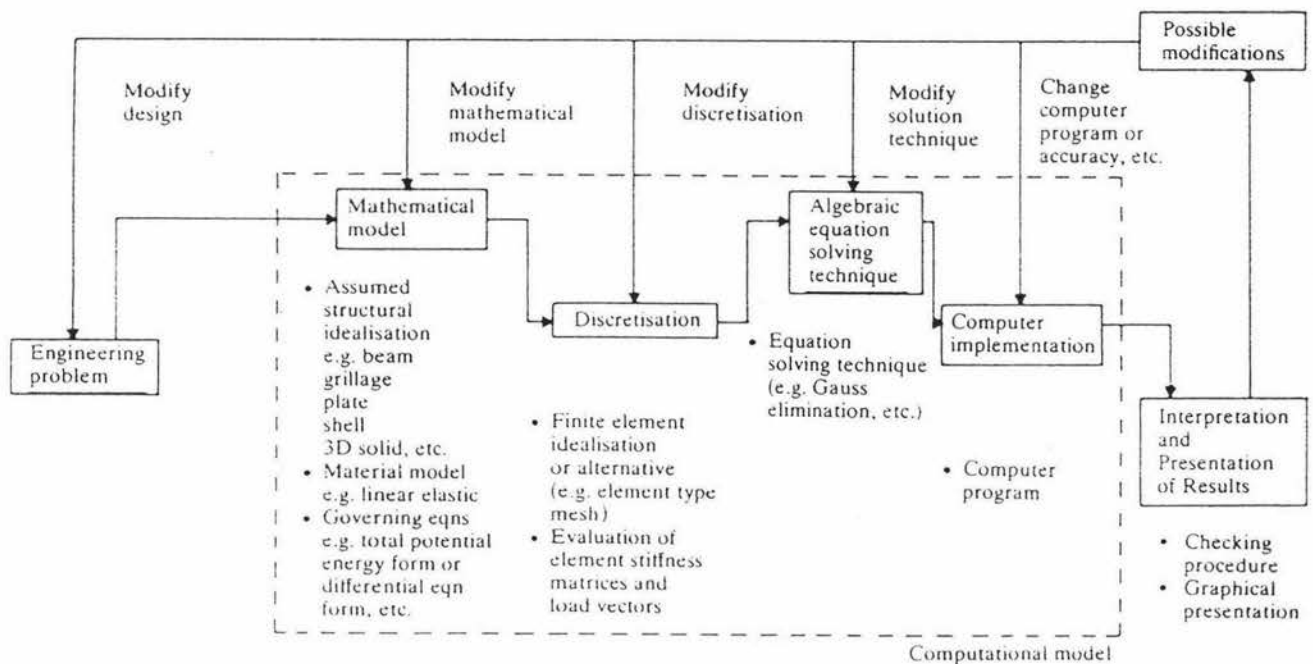


Fig. 3.1 A finite element computational model

The basic steps in the development of a typical finite element computational model are as follows:

- (1) Starting with the physical reality or an engineering problem, it is first necessary to select an appropriate mathematical model .
- (2) Having decided upon the mathematical model, a finite element is chosen.
- (3) For each element (e), the stiffness matrices $[K]^e$ and the load vectors $\{F\}^e$ are evaluated .
- (4) The element stiffness and load terms are then assembled into the overall stiffness matrix [K] and load vector {F}.
- (5) The resulting linear simultaneous equations $[K]\{\delta\} = \{F\}$ are solved for the unknown displacement variables $\{\delta\}$ using an algorithm for equation solving.
- (6) Having evaluated the displacements $\{\delta\}$ the strains and hence the stresses or stress resultants $\{\sigma\}$ may be evaluated. Reactions at nodes restrained against movement are also calculated .
- (7) To achieve the solution steps (3-6) it is necessary to obtain a computer implementation of the finite element method by use of a specially developed program. Here the LUSAS program is used.
- (8) After a successful computer run, the next step involves the interpretation and presentation of the results. This is known as post-processing. Results are frequently presented graphically to aid interpretation and checking.

(9) Having studied the finite element results, the analyst may consider several possible modifications which may be made at various stages in the finite element analysis.

3.2 MYSTRO and LUSAS programs

MYSTRO is a full interactive finite element graphics system, it includes two parts: Pre-processor and Post-processor. Pre-processor may be used interactively to generate full working finite element models. The Pre-processing facilities available include:

- * Interactive model definition in terms of points, lines, surfaces and volumes.
- * Automatic or manual model scaling.
- * Automatic regular or irregular line, surface and volume mesh generation.
- * Meshing point visualisation and mesh drawing in full or dashed line, and exploded or outline plots.
- * Transformation and viewing of the finite element model in isometric or perspective projection with hidden line removal.
- * Interactive definition and assignment of element properties, support and loading conditions.
- * Generalised load generation and visualisation.
- * Printing, labelling and interactive modifying of the components of the model.
- * Load and support condition visualisation.
- * Automatic generation of the LUSAS datafile.

Post-processor MYSTRO possesses a range of manipulative and graphical facilities which allow effective interpretation and display of the analysis results. These facilities include:

- * Manipulation of displacements, velocities, accelerations, strains and stresses, field potentials and fluxes.
- * Graphical display of results as vectors, smoothed or element by element contours, or X-Y graphs.
- * Layer by layer representation of composite or nonlinear shells .
- * Printing of selected numerical results.
- * Generation of time/load history X-Y graphs for dynamic and nonlinear analyses.
- * Post-processing of Fourier and Harmonic response analyses.
- * Line and slice sections through 2 and 3-dimensional structures .
- * Bending moment and shear force diagrams for frame structures .
- * Yield flag and crack pattern plots for materially nonlinear elasto/plastic and concrete analyses.
- * Calculation and plotting of steel reinforcement requirements according to Wood-Armer specification.
- * Combination, transformation, factoring and enveloping of applied load cases and inbuilt results calculator.
- * Colour fill for elements and contours with full or selective colour definition.
- * Read and write access to existing model and picture files.
- * Use of multiple windows with line and text annotations to create compound pictures.
- * Selective zoom in/out facility to investigate areas of particular interest.

- * External process control for running a LUSAS analysis or obtaining a hard copy plot.
- * Interactive or command file operation, with a full session log.
- * Free format command interpreter with context sensitive prompting .

The relationship between MYSTRO and LUSAS, and the various types of interface files used are shown diagrammatically in Fig (3.2).

The LUSAS program suite consists of the following components:

- * LUSAS Finite Element System.
- * MYSTRO Pre-processor and Post-processor.
- * The EXPOSE Plotting Utility.

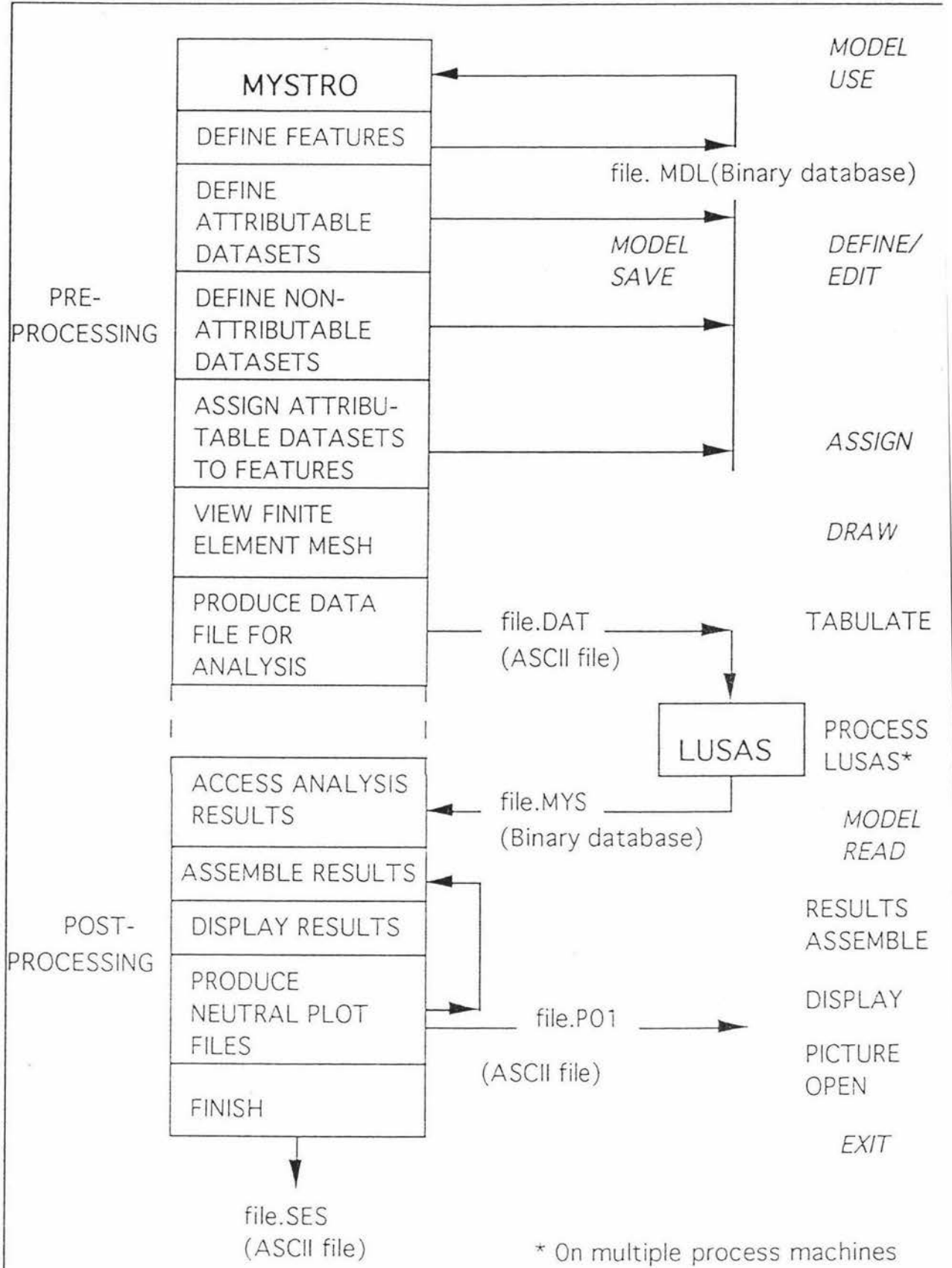


Fig.3.2 The Relationship Between MYSTRO and LUSAS

4 Pressure Vessel Model

- * The descriptions in chapter 4 provide detailed instructions for modelling the pressure vessel.

4.1 Configuration

Using the finite element computational model, the pressure vessel will be considered as a practical example of modelling a three-dimensional object. The shape and data of the pressure vessel are as follows. (35)

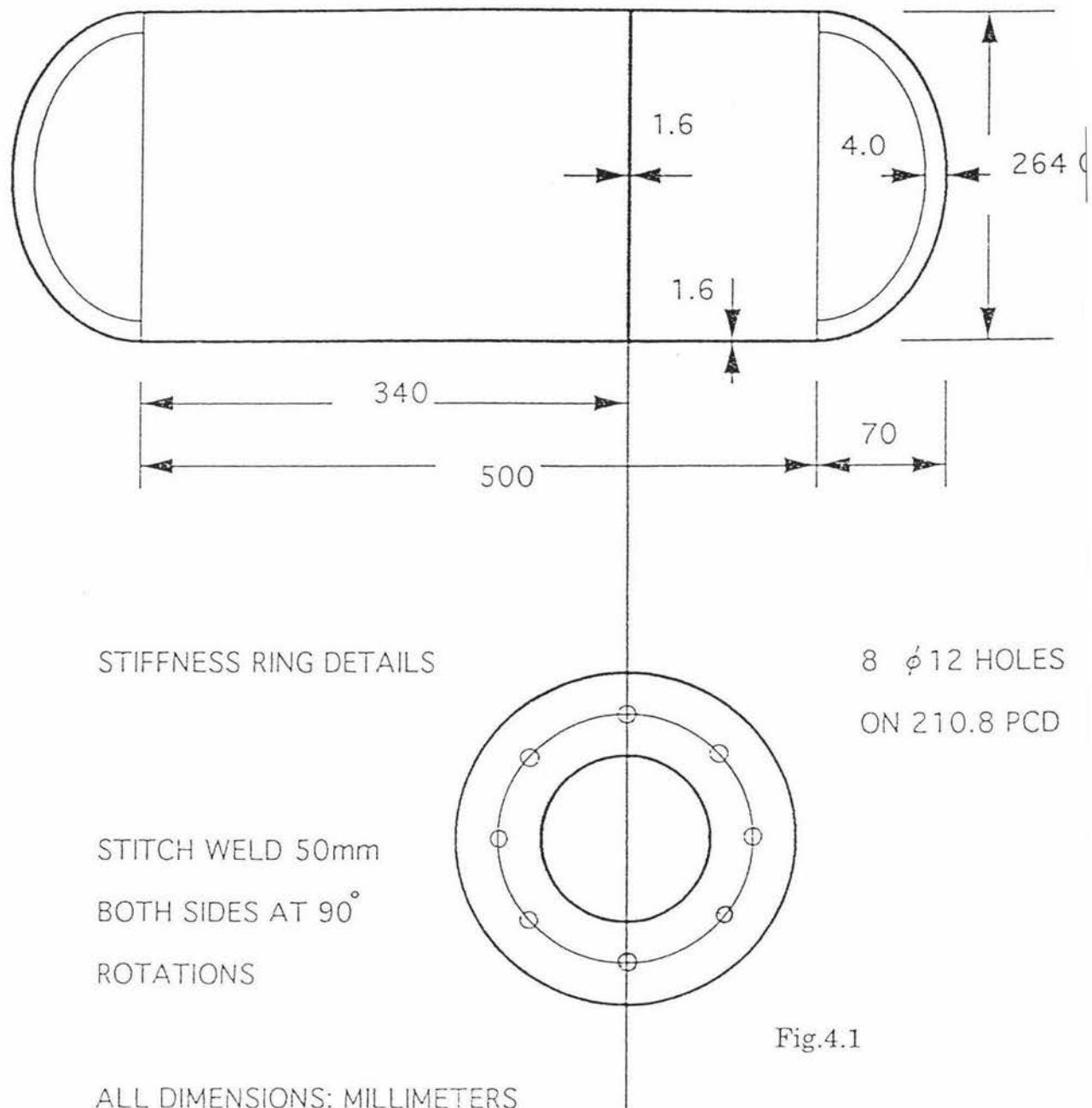


Fig.4.1

ALL DIMENSIONS: MILLIMETERS

MATERIALS: MILD STEEL

Length of Cylinder Section: 0.5m

Material Type: Mild Steel

$$E = 200 \times 10^9 N / m^2$$

$$\sigma_y = 207 \times 10^6 N / m^2$$

Thickness of cylinder 1.6mm

Thickness of end caps 4.0 mm

Max. allowable pressure $1.3MN / m^2$

The pressure vessel is subjected to a uniform internal pressure. Its properties (material, supports, geometry and loading etc.) are symmetric about its centre so only 1/4 need be taken as a model.

4.2 Features and Attributes

The first parameter to be defined is the angle of viewing the pressure vessel.(i.e.. choice of view eye position)

1 (x)

1 (y)

-1 (z)

Figure 4.2.1 , 4.2.2 and 4.2.3 shows the view of the pressure vessel from the chosen position (x=1, y=1, z=-1)

RAYSTRO : 10.1-2

DATE : 5 - 2 - 93

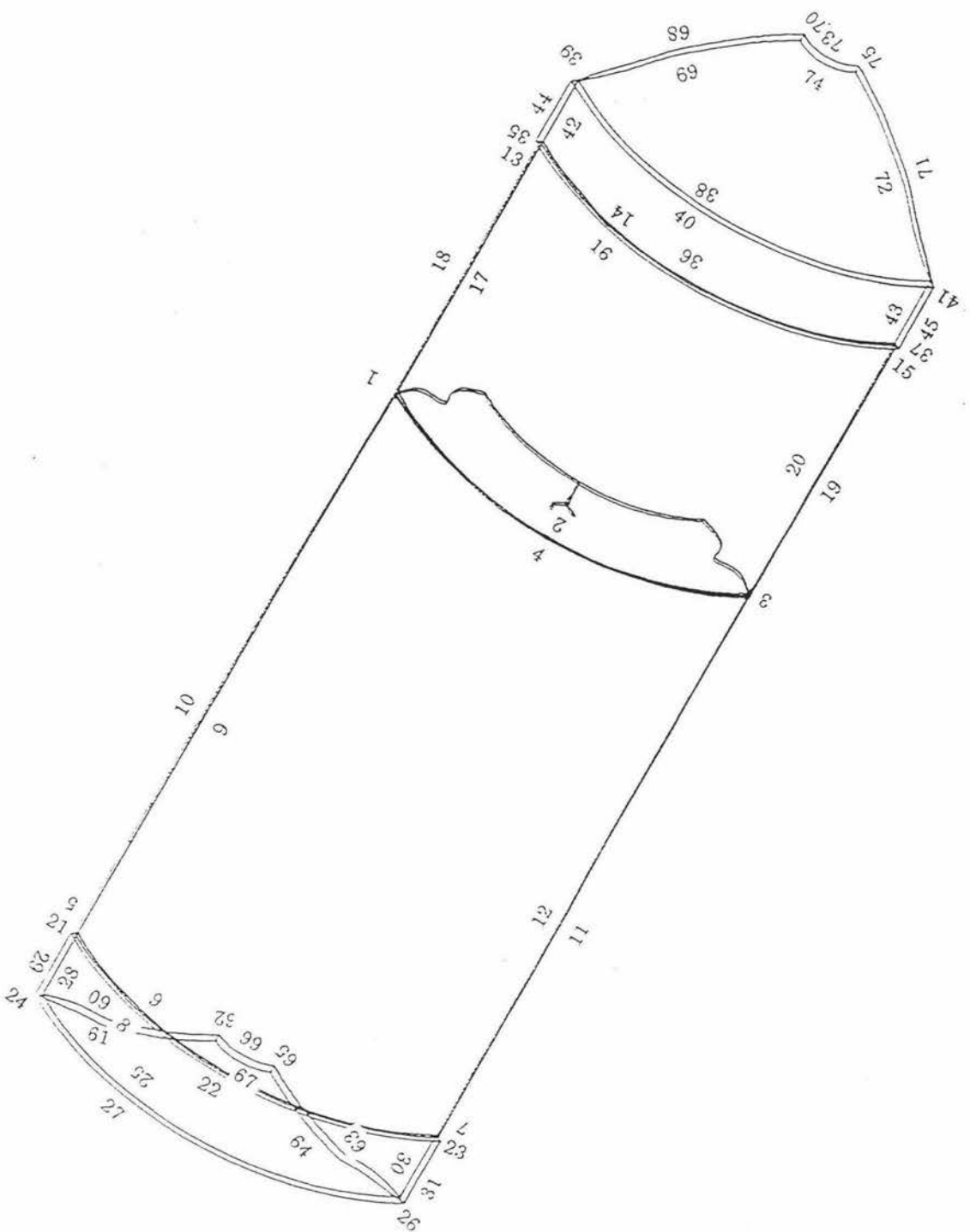


Fig.4.2.1 Lines

- * 1. $S(t)$ means top surface
- $S(b)$ means bottom surface
- 2. Surfaces and volumes of ring are shown in Fig.4.3

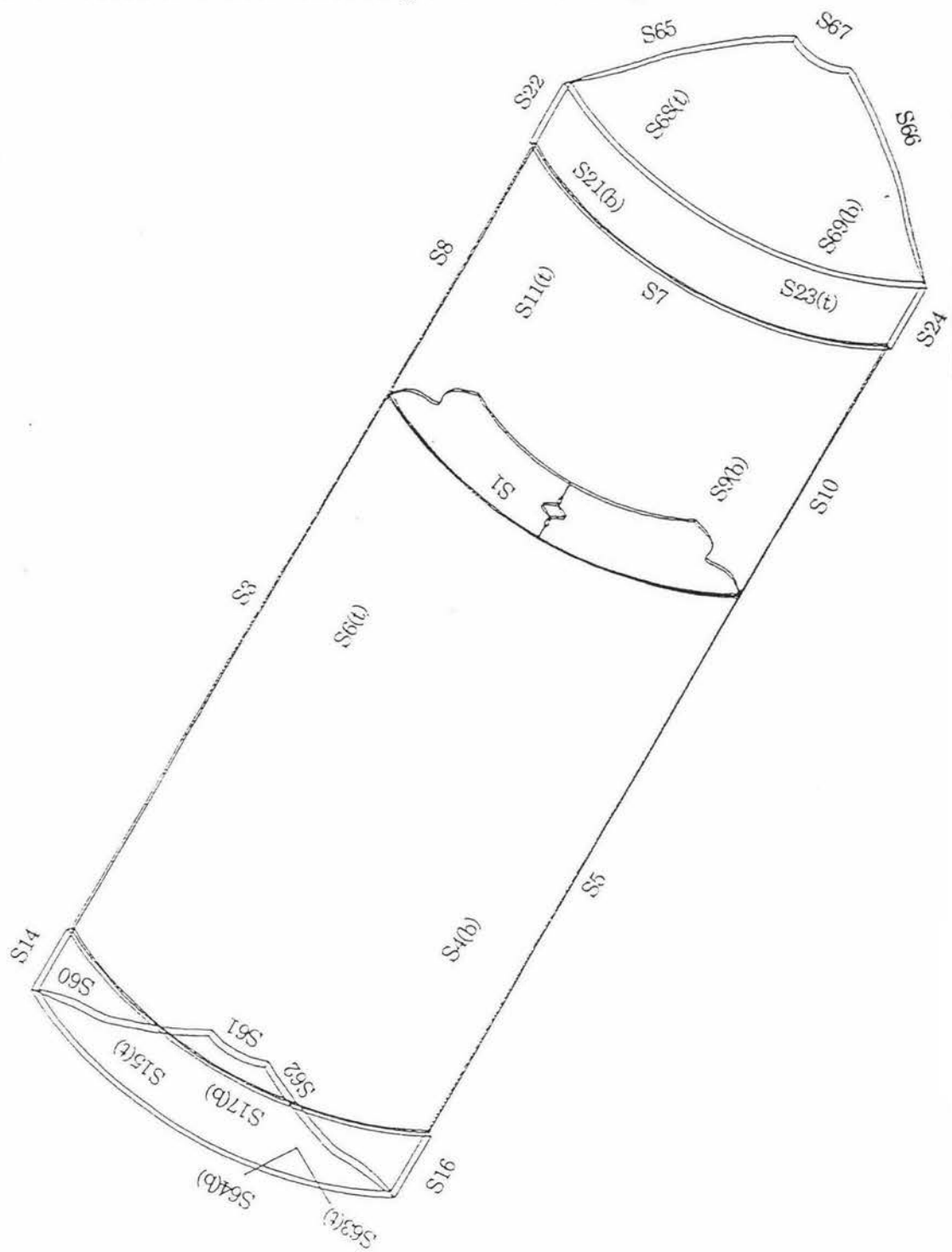


Fig.4.2.2 Surfaces

MYSTRO: 10.1-2

DATE: 5-2-93

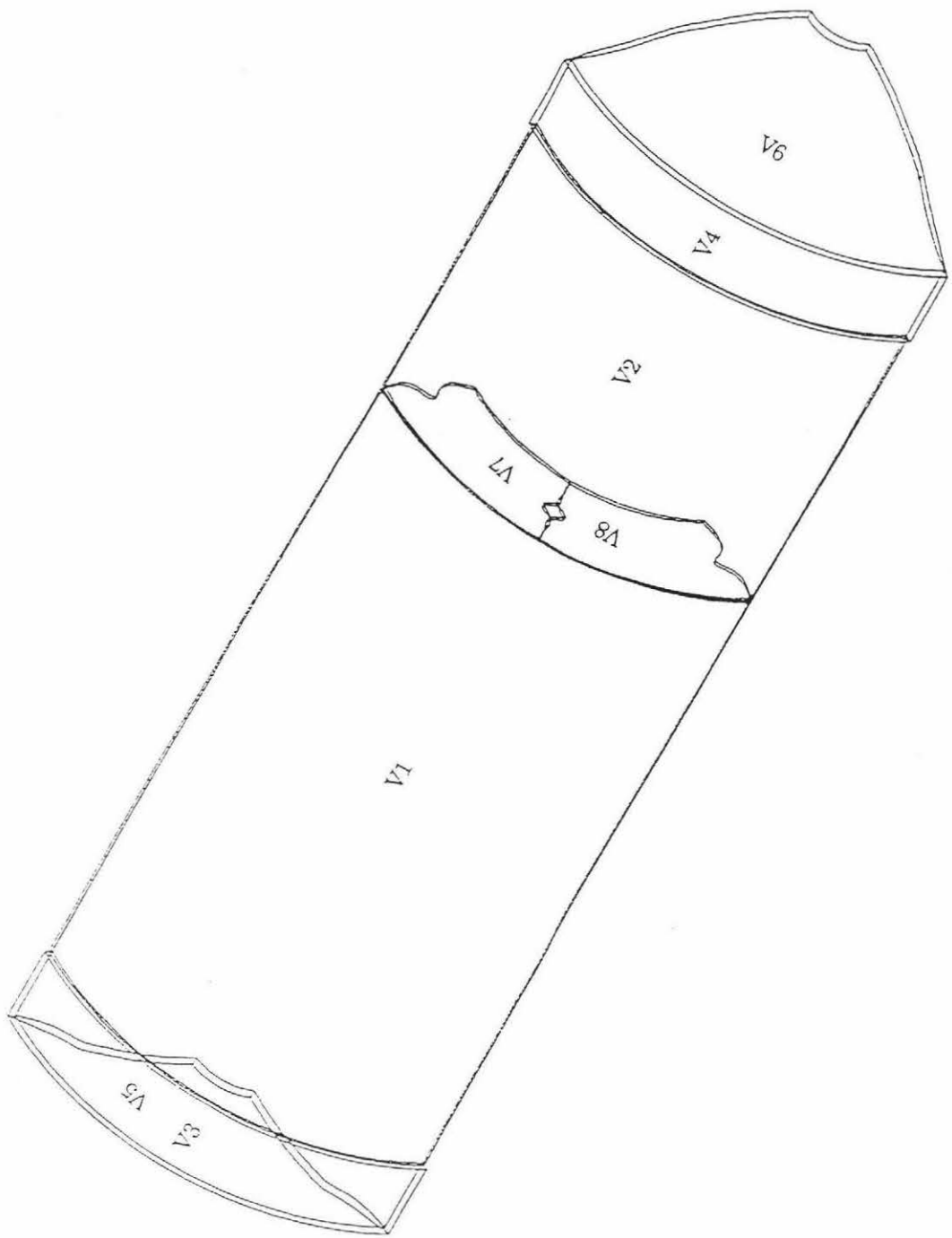
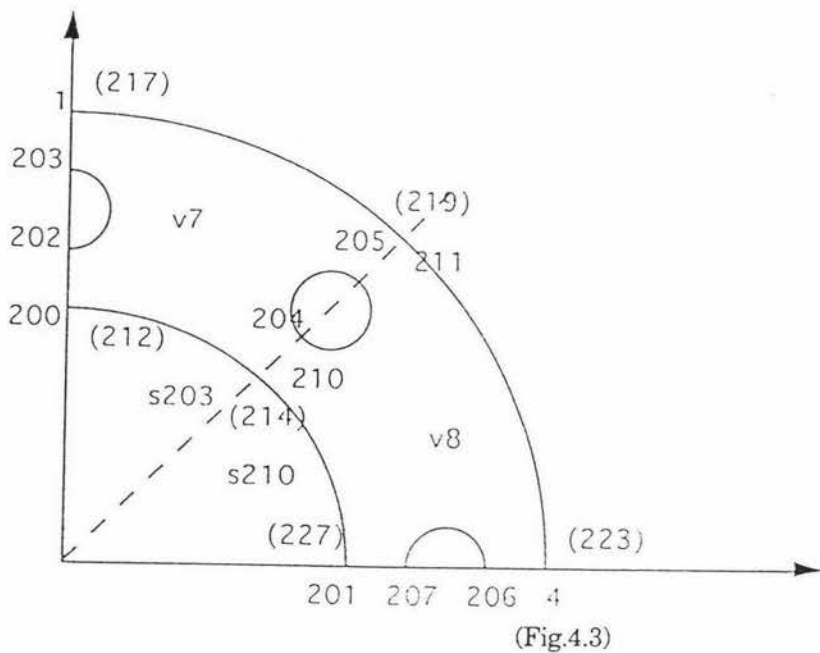


Fig.4.2.3 Volumes

Figure 4.3 shows a quarter of the stiffness ring which will be used for the model (see Fig.4.1)



where; number means front point

 (number) means back point

S means surface

V means volume

The steps used in drawing figure 4.2 and 4.3 were:

Define points:

By coordinates

Define lines:

Straight lines by point

Arc by rotation (2 points, radius)

Define surfaces:

By lines

By points

Minor/Major arc surfaces by sweep line

By coordinates

Define volumes:

By surfaces

By lines

By sweeping surface

4.3 mesh

The following is an example of a 3-dimensional mesh. Its thickness is of a similar magnitude to its length and width. It is considered as a 3-dimensional continuum so that the element is a curved, isoparametric hexahedral in direct approximation to a curved shell, as shown in Fig(4.4) (36)

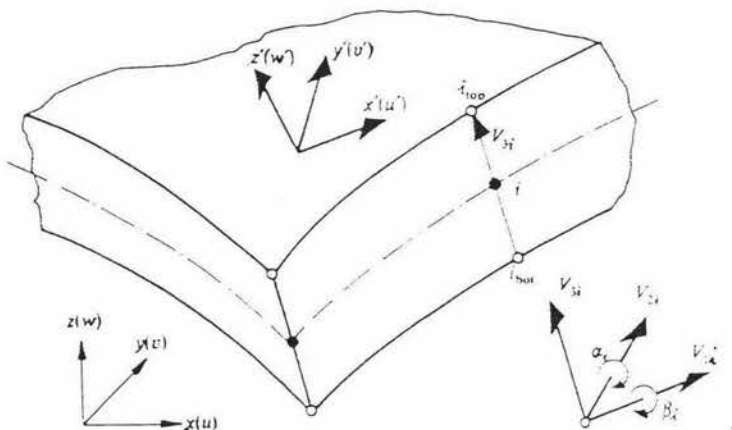


Fig. 4.4 Local and global co-ordinates

The external faces of the element are curved, while the sections across the thickness are generated by straight lines. Pairs of points, i_{top} and i_{bottom} , each with given Cartesian co-ordinates, prescribe the shape of the element.

Let ξ, η be the two curvilinear co-ordinates in the middle plane of the shell and ζ a linear co-ordinate in the thickness direction, where ξ, η, ζ vary between -1 and +1 on the respective faces of the element. A relationship between the Cartesian co-ordinates and the curvilinear co-ordinates of any point of the shell can be written in the form:

$$\begin{Bmatrix} x \\ y \\ z \end{Bmatrix} = \sum N_i(\xi, \eta) \frac{(1+\zeta)}{2} \begin{Bmatrix} x_i \\ y_i \\ z_i \end{Bmatrix}_{top} + \sum N_i(\xi, \eta) \frac{(1-\zeta)}{2} \begin{Bmatrix} x_i \\ y_i \\ z_i \end{Bmatrix}_{bottom}$$

Here $N_i(\xi, \eta)$ is a shape function taking a value of unity at the node i and zero at all other nodes.

The following steps were used in drawing the mesh :

Mesh Techniques: Regular meshing

Element meshes: HX8 (hexahedral mesh)

Mesh Define:

(a) Line Mesh

(line diagram in Fig.4.2.1)

Dataset Define Mesh 1

Mesh line type Element=11

Spacing Ratios are: 1.000 1.000 1.000 1.000
1.000 1.000 1.000 1.000
1.000 1.000 1.000

Assign Mesh Dataset Number 1 to Line 9, Line 10, Line 11
Line 12.

Dataset Define Mesh 2

Mesh line type Element=6

Spacing Ratios are: 1.000 1.000 1.000 1.000
1.000 1.000

Assign Mesh Dataset number 2 to Line 2, Line 4, Line 6, Line 8,
Line14, Line16, Line25, Line27, Line38, Line40, Line 66, Line 67,
Line 73, Line 74.

Dataset Define Mesh 3

Mesh line type Element=1

Spacing Ratios are: 1.000

Assign Mesh Dataset Number 3 to Line1, Line3, Line5, Line7,
Line13, Line15, Line21, Line23, Line 24, Line 26, Line28, Line29,
Line 30, Line31, Line35, Line37, Line39, Line41, Line42, Line43,
Line44, Line45, Line62, Line65, Line70, Line75.

Dataset Define Mesh 6

Mesh line type Element=5

Spacing Ratios are: 1.000 1.000 1.000 1.000 1.000

Assign Mesh Dataset Number 6 to Line17, Line18, Line19,
Line20.

Dataset Define Mesh 7

Mesh line Type Element=4

Spacing Ratios are: 1.000 1.000 1.000 1.000

Assign Mesh Dataset Number 7 to Line60, Line61, Line63,
Line64, Line68, Line69, Line71, Line72.

Dataset Define Mesh 8

Mesh Line type Element=3

Spacing Ratios are: 1.000 1.000 1.000

Assign Mesh Dataset Number 8 to Line203, Line209, Line210,

Line211 (RING)

(b) Surface Mesh (surface diagram in Fig.4.2.2)

Dataset Define Type Meshtype=1

Assign Mesh Dataset Number4 to all of the surfaces

(c) Volume Mesh (volume diagram in Fig.4.2.3)

Dataset Define Mesh 5

Mesh Volume Type=HX8

Meshtype=1

Assign Mesh Dataset Number 5 to all of the volumes

Mesh Figures shown in Fig 4.5.1 and 4.5.2

ie, Mesh(black) and volumes.

MYSTRO: 10.1-2

DATE: 5- 2-93

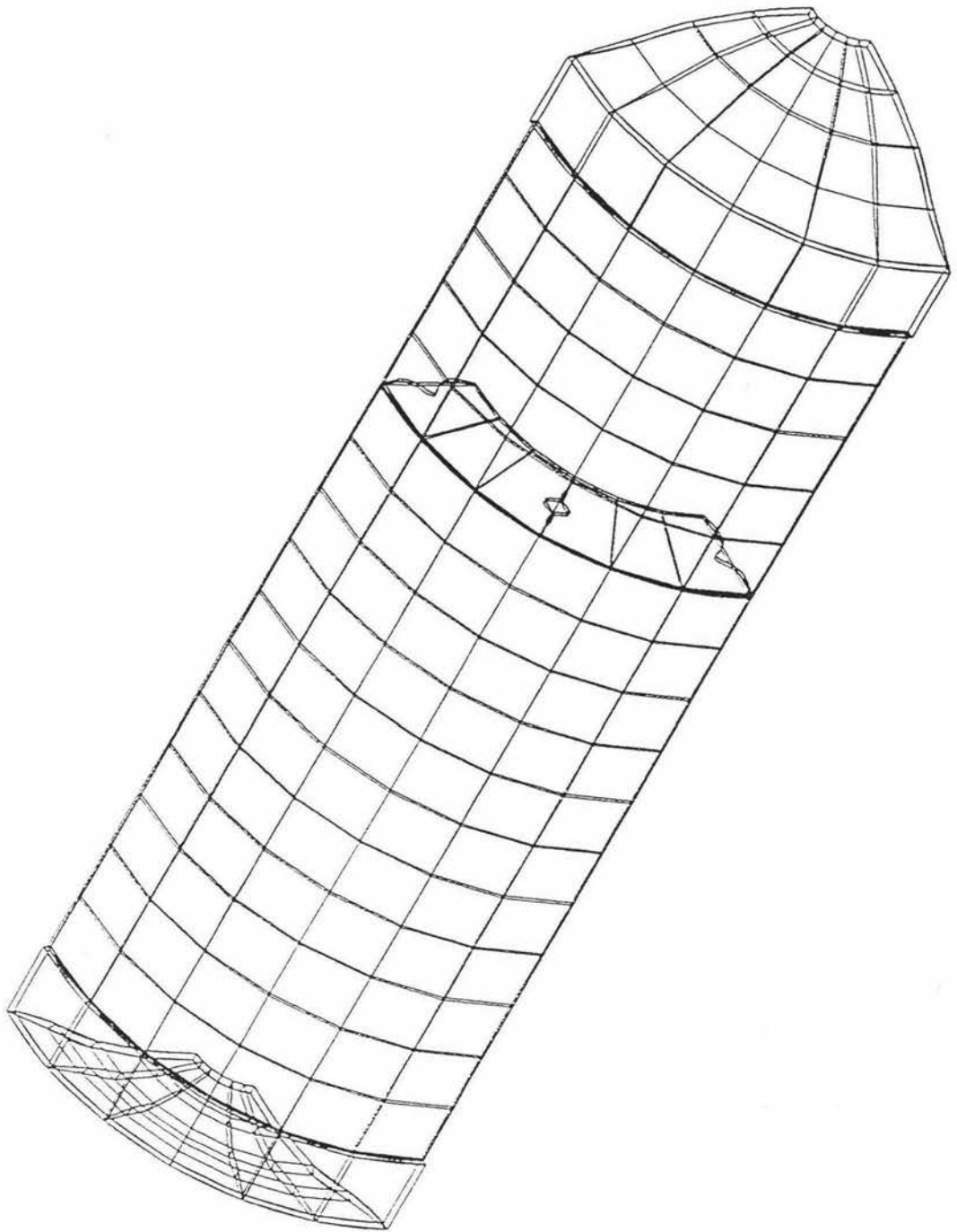


Fig.4.5.1 Side view mesh of a quarter of the pressure vessel

HYSTRO : 10. 1-2

DATE: 3-11-92

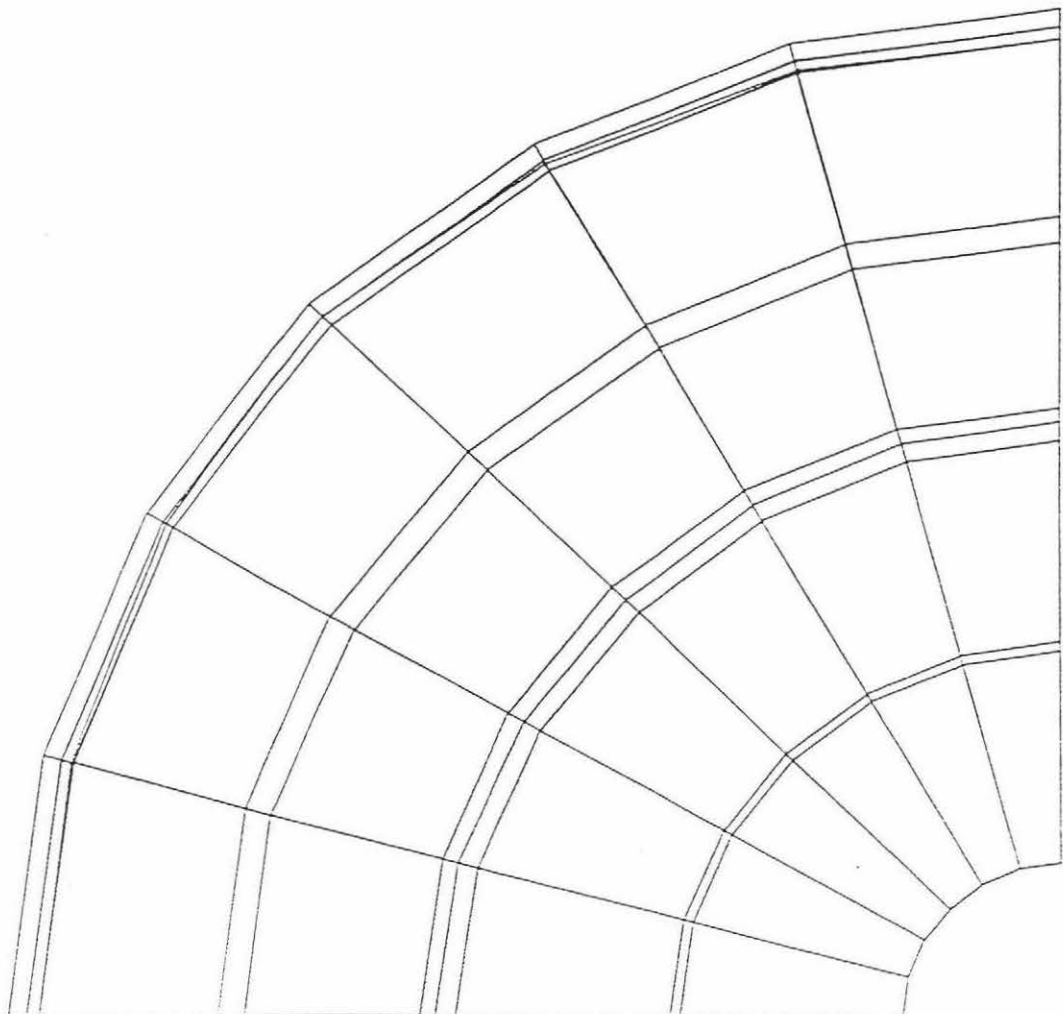


Fig.4.5.2 End view mesh of a quarter of the pressure vessel

The results shown on the screen were:

Volume 1 with 66 HX8 elements

Volume 2 with 30 HX8 elements

Volume 3 with 6 HX8 elements

Volume 4 with 6 HX8 elements

Volume 5 with 24 HX8 elements

Volume 6 with 24 HX8 elements

Volume 7 with 3 HX8 elements

Volume 8 with 3 HX8 elements

Total number of elements=162

Largest element number=1321

Total number of nodes=418

Largest node number=2089

Element Topology shown in Appendix II

4.4 Geometry, Materials, Support and Loading

In general, geometry and loading data may be independently specified in Cartesian, cylindrical or spherical coordinate systems. A variety of

different loadings may be applied to any part of the structure, with up to 13 independent loading cases. These include the following: (Table 4.1)

Loading Type	Reference	Load Components
Concentrated loads	CL	$P_x, P_y, P_z, M_x, M_y, M_z, M_{L1}, M_{L2}$
Prescribed displacement	PDSP	$U, V, W, T_{Hx}, T_{Hy}, T_{Hz}, T_{HL1}, T_{HL2}$
Body forces	CBF	$A_x, A_y, A_z, O_{Mx}, O_{My}, O_{Mz}, A_{Lx}, A_{Ly}, A_{Lz}$
Body forces (field)	FCBF	Q
Uniformly distributed loads	UDL	w_x, w_y, w_z
Structure face loads	FLD	p_x, p_y, p_z
Field face loads	FFLD	$q \dots$
Temperature loads	TMPE	$T_1, dT_1/dx, dT_1/dy, dT_1/dz, T_0, dT_0/dx, dT_0/dy, dT_0/dz$
Temperature face loads	TMPF	T_1, T_0
Environmental temp. loads	ENVT	T, bc, hr
Nodal temperature loads	TEMP	$T_1, dT_1/dx, dT_1/dy, dT_1/dz, T_0, dT_0/dx, dT_0/dy, dT_0/dz$
General point loads	POINT	X, Y, P
General patch loads	PATCH	X, Y, P

KEY.	
P_x, P_y, P_z	Concentrated loads in global directions
M_x, M_y, M_z	Moments
M_{L1}, M_{L2}	Loof moments
U, V, W	Displacements
T_{Hx}, T_{Hy}, T_{Hz}	Rotations
T_{HL1}, T_{HL2}	Loof rotations
w_x, w_y, w_z	Uniformly distributed loads
p_x, p_y, p_z	Face loads in local directions
$A_x, A_y, A_z,$	Linear accelerations
O_{Mx}, O_{My}, O_{Mz}	Angular velocities
A_{Lx}, A_{Ly}, A_{Lz}	Angular accelerations
Q	Potentials
T_1	Final temperature
T_0	Initial temperature
$dT_1/dx, dT_1/dy, dT_1/dz$	Final temperature gradient
$dT_0/dx, dT_0/dy, dT_0/dz$	Initial temperature gradient
T	External temperature
bc, hr	Convective and radiative heat transfer coefficients
X, Y, P	Location and load magnitude

Table 4.1 Summary Of Loading Types And Components

Both linear and nonlinear material property models are available. A summary of the material type parameter for each of the available LUSAS material models is shown in Table 4.2

Material Description	Material Type
LINEAR	
Isotropic	1
Orthotropic plane strain	3
Orthotropic axisymmetric	3
Orthotropic plane stress	4
Orthotropic thick	16
Orthotropic solid	14
Anisotropic	12
Anisotropic solid	15
Rigidities	6
Rigidities shell	7
Field isotropic	5
Field orthotropic	8
Field orthotropic Solid	17
Field link	18
Field link	19
NONLINEAR	
Uniaxial concrete	23
Biaxial concrete	24
Elasto-plastic plane interface	27
Elasto-plastic solid interface	26
Elasto-plastic Tresca	29
Elasto-plastic resultant	61
Elasto-plastic von-Mises	62
Elasto-plastic Mohr-Coulomb	63
Elasto-plastic Drucker-Prager	64
Backward Euler Von-Mises (elasto-plastic)	72/75
User-Defineable Material Model	99

Table 4.2 Material Property Type Numbers

Support conditions may be specified in two ways:

First, by specifying the support codes for each degree of freedom type contained in the MYSTRO freedom library. The required support codes are:

'F' for a 'free' or unrestrained freedom(default)

'R' for a 'restrained' freedom

'S' for a 'sprung' freedom

and the freedom library is arranged in the following order:

U Translation in the global X-direction

V Translation in the global Y-direction

W Translation in the global Z-direction

THX Rotation about the global X-axis

THY Rotation about the global Y-axis

THZ Rotation about the global Z-axis

THL1 Local rotation about the first loof point

THL2 Local rotation about the second loof point

DU Hierarchical displacement

DTHX Hierarchical local rotation

In this manner, the order in which the support codes is significant, and intermediate unrestrained freedoms must be defined explicitly.

Secondly, by specifying which freedoms from the library are restrained, and in what manner the restraints are to be applied. Since the support codes refer directly to the freedom name, the order in which they are specified is unimportant, and unrestrained freedoms may be implied using the default condition.

The data for geometry, materials, support and loading are entered as follows:

Geometry:

Define Geometry

Dataset number 1

Property type number 6

Thickness default

Assign geometry to all of the surfaces.

Materials:

Define Material

Dataset number 1

Property type number 1 (isotropic)

Young's Modules $E = 200,000 N / mm^2$

Posson's Ratio $\vartheta = 0.3$

Mass Density RHO= $7.7028E-05 N / mm^3$

Coefficient of Thermal Expansion ALPHA= $1.1000E-05 / C$

A Stiffness Rayleigh Damping Constant ar= $0.0000E+00$

B Stiffness Rayleigh Damping Constant br= $0.0000E+00$

TEMP T=17

Assign material to all of the volumes.

Data storage locations used=13

Support:

Define Support, (Dataset Define Support 1 found)

Dataset number 1

Translation in the global x-direction U=R

Translation in the global y-direction V=F

Translation in the global z-direction W=F

Rotation about the global X-axis THX=F

Rotation about the global Y-axis THY=F

Rotation about the global Z-axis THZ=F

Local rotation about the first loof point THL1=F

Local rotation about the second loof point THL2=F

Hierachical displacement DU=F

Hierarchical local rotation DTHX=F

Assign support 1 to Surface 3, Surface 8, Surface 14,

Surface 22, Surface 60, Surface 65.

Define Support,

Dataset number 2

V=R THL1=F

W=F THL2=F

THX=F DU=F

$\text{THY} \equiv \text{F}$ $\text{DTHX} \equiv \text{F}$

Assign support 2 to Surface 5, Surface 10, Surface 16,

Surface 24, Surface 62, Surface 66.

Define Support

Dataset number 3

U=R	THZ=F
V=R	THL1=F
W=F	THL2=F
THX=F	DU=F
THY=F	DTHX=F

Assign support 3 to Surface61.

Define Support

Dataset number 4

U=R	THZ=F
V=R	THL1=F
W=R	THL2=F
THX=F	DU=F
THY=F	DTHX=F

Assign support 4 to Surface67.

Loading: (surface diagram in Fig.4.2.2)

Surface 4: the area of the $S_4 = \frac{1}{4} 2\pi \times 128 \times 340 = 68361 \text{ mm}^2$

the value of structure face loads=68361×1.3=88870 (N)

Surface 9: the area of the $S_9 = \frac{1}{4} 2\pi \times 128 \times 160 = 32169.9 \text{ mm}^2$

the value of structure face loads=32169.9×1.3=41820(N)

Surface 17, Surface 21:

the areas of the $S_{17}, S_{21} = \frac{1}{4} 2\pi \times 128 \times 39 = 7841.4 \text{ mm}^2$

the value of structure face loads=7841.4×1.3=10190(N)

Surface 64, Surface 69:

Due to the fact that S64 and S69 are irregular curved surfaces, so divide them into 5 small surfaces, then calculate the areas of each.

$$S_{100} = \frac{130 + 132}{2} \times 26.4 = 3458.4 \text{ mm}^2 \approx 3458.4 + 20 = 3478.4 \text{ mm}^2$$

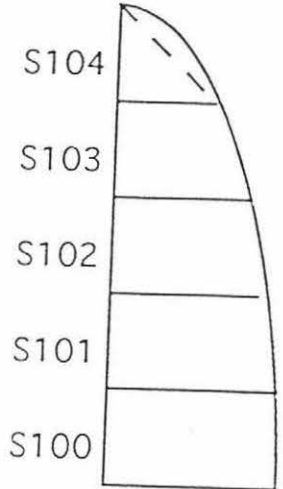
$$S_{101} = \frac{130 + 122}{2} \times 26.4 = 3326.4 \text{ mm}^2 \approx 3326.4 + 20 = 3346.4 \text{ mm}^2$$

$$S_{102} = \frac{107 + 122}{2} \times 26.4 = 3022.8 \text{ mm}^2 \approx 3022.8 + 20 = 3042.8 \text{ mm}^2$$

$$S_{103} = \frac{81 + 107}{2} \times 26.4 = 2481.6 \text{ mm}^2 \approx 2481.6 + 20 = 2501.6 \text{ mm}^2$$

$$S_{104} = \frac{9 + 26.4}{2} \times 66 + \frac{9 + 12}{2} = 1222.2 \text{ mm}^2 \approx 1222.2 + 120 = 1342.2 \text{ mm}^2$$

the loads on each areas as:



$$F_{100} = 3478.4 \times 1.3 = 4521.92(N)$$

$$F_{101} = 3346.4 \times 1.3 = 4350.32(N)$$

$$F_{102} = 3042.8 \times 1.3 = 3955.64(N)$$

$$F_{103} = 2501.6 \times 1.3 = 3252.08(N)$$

$$F_{104} = 1342.2 \times 1.3 = 1744.86(N)$$

Total loads on the S64 and S69 are:

Fig.4.6

$$\begin{aligned} F_{100} + F_{101} + F_{102} + F_{103} + F_{104} &= 4521.92 + 4350.32 + 3955.64 + 3252.08 + 1744.86 \\ &= 17824.82(N) \end{aligned}$$

S203 and S210 (RING):

$$\frac{1}{4} 2\pi \times 79.6 \times 1.6 = 200 \text{ mm}^2$$

the areas of the S203 and S210 =

the value of the structure loads = $200 \times 1.3 = 260.1(N)$

(b) Loading values which are input into the computer

Dataset Define Loading 1

Loading Type=FLD

Loading values are:

$$F_x = 0.0000E + 00$$

$$F_y = 0.0000E + 00$$

$$F_z = -0.8887E + 05$$

Assign loading dataset number 1 to surface 4

Dataset Define Loading 2

Loading Type=FLD

Loading values are:

$$F_x = 0.0000E + 00$$

$$F_y = 0.0000E + 00$$

$$F_z = -0.4182E + 05$$

Assign loading dataset number 2 to surface 9

Dataset Define Loading 3

Loading Type =FLD

Loading values are:

$$F_x = 0.0000E + 00$$

$$F_y = 0.0000E + 00$$

$$F_z = -0.1019E + 05$$

Assign loading dataset number 3 to surface 17 and surface 21

Dataset Define Loading 4

Loading Type = FLD

Loading values are:

$$F_x = 0.0000E + 00$$

$$F_y = 0.0000E + 00$$

$$F_z = -0.1782E + 05$$

Assign loading dataset number4 to surface 64 and surface 69

Dataset Define Loading 5

Loading Type = FLD

Loading values are:

$$F_x = 0.0000E + 00$$

$$F_y = 0.0000E + 00$$

$$F_z = -260.1$$

Assign loading dataset number5 to surface 203 and surface 210

Support and loading are shown in Fig (4.7)

The green arrows show the position of support and the blue arrows show the position of loading.

MYSTRO: 10.1-2

DATE: 5- 2-93

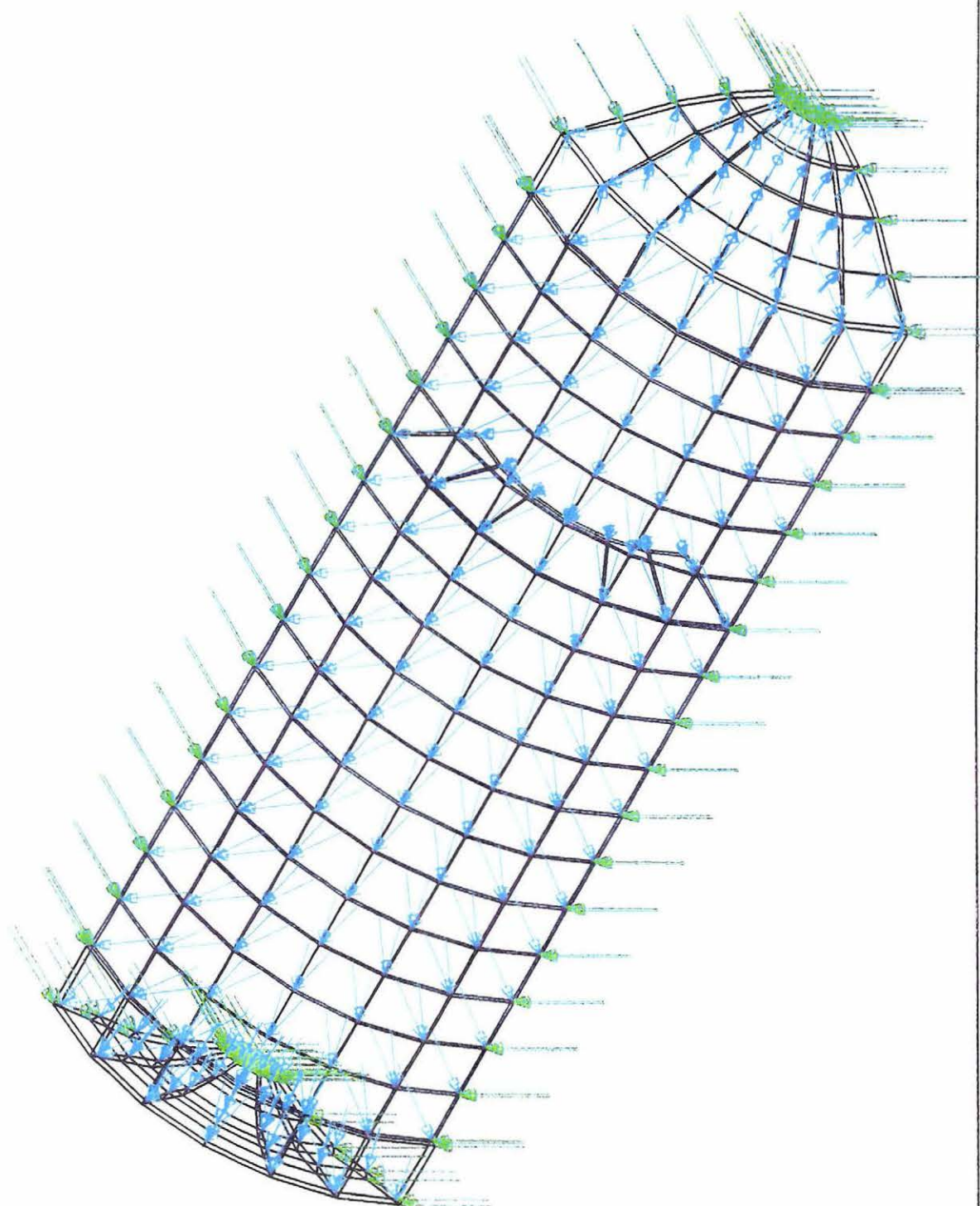


Fig.4.7

TITLE: Mesh Support and Loading

5 Running LUSAS

Using the model previously defined and data previously input, LUSAS is run to calculate displacements and stresses.

5.1 Running LUSAS

Create a LUSAS datafile from MYSTRO using command:

TABULATE (file name)

The command to spawn a LUSAS analysis process is:

PROCESS LUSAS

This will run and automatically create the files:

(file name). file. OUT Results file (readable ASCII)

(file name). file. LOG Analysis Log (readable ASCII)

7488 k bytes of extended memory is required for this model.

The following information is shown in the screen:

- (time) Processing elements
- Processing co-ordinates and supports
- Processing properties and supports
- Processing loads
- Cross checking data
- Assembling elements
- Solving equations
- Recovering stresses
- Writing output
- Writing plot file

The output information from the LUSAS run is:

Total number of nodes = 418

Largest node number = 2089

Total number of elements = 162

Largest element number = 1321

Largest material assignment set number = 1

Total number of material assignment set = 8

Total number of support nodes = 132

Largest node number = 1756

Number of loaded nodes or elements = 648

Total number of loading cases = 1

Maximum frontwidth of stiffness matrix = 90

Root mean square of frontwidth = 60

Total number of equations = 1254

Total number of active nodes = 418

The results of the LUSAS analy-

post-analysis model file may be accessed using the command:
- MODEL READ file_name.MVC

SUMMARY OF POST PROCESSING OPERATIONS

SET LOADCASE Set the loadcase

SET RESULTS (DISPLACEMENT STRAIN STRESS)
Set the results record

RESULTS ASSEMBLE Assemble the results

RESULTS DEFORMATION Assemble deformations

* * * * *

PRINT RESULTS							Print selected results
*	*	*	*	*	*	*	
DRAW MESH							Draw mesh
*	*	*	*	*	*	*	
DISPLAY DIAGRAM							Frame diagram
DISPLAY PEAK							Peak value locations
DISPLAY VALUE							Peak values
DISPLAY YILED							Nonlinear material states
DISPLAY VECTOR							Vectors (only for 2D)
*	*	*	*	*	*	*	
RESULTS USER							User supplied datasets
RESULTS HISTORY							Time history datasets
SECTION LINE							Line section datasets
SET GRAPH NUMBER							Graph number
SET GRAPH XAXIS							X-axis dataset
SET GRAPH YAXIS							Y-axis dataset/control
DISPLAY GRAPH AXES							Graph axes
DISPLAY GRAPH DATA							Graph data
*	*	*	*	*	*	*	
DISPLAY CONTOUR							Contours
ANNOTATE							Annotate contours
*	*	*	*	*	*	*	
SECTION LINE							Line section (for 2D)
SECTION SLICE							Slice section (for 3D)

5.2 Running EXPOSE:

EXPOSE is the module which generates hardcopies from LUSAS runs.

a) picture file:

To enable hard copy plots to be produced, MYSTRO creates a neutral file known as the picture file.

Processing the picture file may be implemented in following way:

PICTURE OPEN	Open a picture file
SET PICTURE TITLE	Give the title
ERASE	Ensure title appears
DRAW MESH (or other graphs)	Draw picture
PICTURE SAVE	Close and save picture file

All the screen changes caused by commands issued between the PICTURE OPEN and PICTURE SAVE commands will be saved in the picture file. Smartening up the picture can be done using the ANNOTATE commands in MYSTRO.

The neutral plotting files are converted to the appropriate drivers using the plotting utility EXPOSE.

Run EXPOSE by typing:

C:/FEA / STUDENT> **Expose**

Input picture filename: **L&F2. pic**

DEVICE > 3 (no colour fill)

Output file name: **L&F2. hp**

Input number of pens to be used: 6

b) Colour print:

To print the coloured pictures, the computer must be rebooted typing:

> Choose: **P**
 > [PTPrt] C: / > **FEA**
 > [PTPrt] C / FEA / student > **A4Plot L&F2.hp**

The above instructions will cause all the necessary graphs to be printed.

c) Configuration file:

Expose can be configured to suit the plotter that was installed by editing the enclosed configuration file:CONFIG.FIL.

The following is an example of CONFIG.FIL. and its contents:

(IDEV/Device number -1)

Idev	Dvscl	IP1	IP2	IP3	IP4	IS1	IS2	IS3	IS4	XS1	XS2	XS3	XS4
1	0.10	0	0	0	0	0	0	0	0	0.0	0.0	0.0	0.0
2	10.0	0	0	0	0	0	0	0	0	0.0	0.0	0.0	0.0
3	40.0	0	0	13520	9600	0	13520	0	9600	0.0	0.0	0.0	0.0
4	3.00	0	0	0	0	0	0	0	0	0.0	0.0	0.0	0.0
5	40.0	0	0	13520	9600	0	13520	0	9600	0.0	0.0	0.0	0.0
6	27.0	0	0	338	240	0	0	0	0	0.0	0.0	0.0	0.0
7	40.0	11160	1600	13600	9600	20	1	1	0	0.05	0.05	0.0	0.0
8	40.0	11160	1600	13600	9600	20	1	1	0	0.05	0.05	0.0	0.0
9	40.0	0	0	13520	9600	0	13520	0	9600	0.0	0.0	0.0	0.0
10	40.0	0	0	13520	9600	0	13520	0	9600	0.0	0.0	0.0	0.0
11	40.0	0	0	13520	9600	0	13520	0	9600	0.0	0.0	0.0	0.0
12	40.0	0	0	13520	9600	0	13520	0	9600	0.0	0.0	0.0	0.0

Table 5.1

The first number in line 1 is IDEV and if IDEV is set to -1, then EXPOSE will prompt the user for the desired device number from the supported list. The remaining lines define the set-up and the numbers refer to the following parameters:

EXPOSE CONFIGURATION DETAILS

IDEV/DEVICE number	-1
--------------------	----

DVSCL/ESCALE (plot units/mm)	40.0
------------------------------	------

HPGL PARAMETER DESCRIPTION	VALUE
-----------------------------------	--------------

IP1/Minimum X value IP	0
------------------------	---

IP2/Minimum Y value IP	0
------------------------	---

IP3/Maximum X value IP	13520
------------------------	-------

IP4/Maximum Y value IP	9600
------------------------	------

IS1/Minimum X value SC	0
------------------------	---

IS2/Maximum X value SC	13520
------------------------	-------

IS3/Minimum Y value SC	0
------------------------	---

IS4/Maximum Y value SC	9600
------------------------	------

XS1/Unused	0.0
------------	-----

XS2/Unused	0.0
------------	-----

XS3/Unused	0.0
------------	-----

XS4/Unused	0.0
------------	-----

POSTSCRIPT PARAMETER DESCRIPTION	VALUE
---	--------------

IP1/Translate X of Origin	11160
---------------------------	-------

IP2/Translate y of Origin	1600
---------------------------	------

IP3/Bounding Box Size X (EPS only)	13600
------------------------------------	-------

IP4/Bounding Box Size Y (EPS only)	9600
------------------------------------	------

IS1/Linewidth	20
---------------	----

IS2/Linejoin	1
IS3/Linecap	1
IS4/Unused	0
XS1/Scale X	0.05
XS2/Scale Y	0.05
XS3/Unused	0.0
XS4/Unused	0.0

MYSTRO produces plot files in different paper sizes depending on the commands issued when creating the PICTURE file. The maximum plot area is set within MYSTRO as follows:

PLOTSIZE (MM)	MYSTRO
PLOTTER UNITS (DVSCLE=40.0)	COMMAND
1168 by 800 (46720 by 32000)	SET PLOTSIZE A0
800 by 574 (32000 by 22960)	SET PLOTSIZE A1
574 by 400 (22960 by 13520)	SET PLOTSIZE A2
338 by 240 (13520 by 9600)	SET PLOTSIZE A3
240 by 169 (9600 by 6760)	SET PLOTSIZE A4
xs by ys (40. xs by 40. ys)	SET PLOTSIZE xs ys

Table 5.2 MYSTRO plotsize

6 Results Analysis

Analysis Types:

Static analysis is used to determine displacements, strains, stresses, and forces in structures under applied loads. Elastic, plastic, creep and swelling material behaviours are available. Stress stiffening and large deflection effects may be included.

Graphic Displays

The graphics capabilities of the MYSTRO pre- and post-processor provide many options for verification of model geometry and loads. Windowing on a model can be done by limiting included nodes, elements, or geometric distances. The geometry may be limited in any defined co-ordinate system. Surfaces may be plotted as well as defined co-ordinate systems. All boundary conditions (displacements, forces, moments, pressures, and degrees of freedom) may be displayed on element or node plots. Element, node, material, support, loading, or member property numbering can be shown on plots of the model. Section views through three dimensional structures, plots of model edges, and hidden line plots are all available for further checking of model geometry and for presentation .

The LUSAS analysis program may be activated as an external process at any time during the MYSTRO session. Any previously created LUSAS datafile may be analysed using the command:

PROCESS LUSAS

All results are from the post-processors file.

6.1 Displacements

The following data are the actual displacements determined by the LUSAS run (Finite Element Method) at certain nodes which are of particular importance .Some of these points have also been analysed using Laser Speckle Photography by Hendel (35). They are three-dimensions with respect to the structure's axes. Other displacements determined by the LUSAS run are presented in the Appendix.

Nodal point No.	Displacement in x-direction $\times 10^{-5}$ m	Displacement in y-direction $\times 10^{-5}$ m	Displacement in z-direction $\times 10^{-5}$ m
1	0	2.38238	6.42835
2	0	2.34768	6.43892
5	2.38238	0	6.42835
6	1.71429	4.34860	6.42931
17	2.34768	0	6.43892
70	0	5.45467	6.31879
71	0	6.16685	6.27216
73	0	6.44746	6.21430
75	0	6.53613	6.13688
76	0	6.61395	6.07377
91	5.45467	0	6.31879
92	6.16685	0	6.27216
96	6.53613	0	6.13688

97	6.61395	0	6.07377
137	4.62226	4.62226	6.15044
138##	4.70197	4.70197	6.07834
283	0	6.58007	6.07374
345	4.67810	4.67810	6.07706
587	0	0.73642	6.18326
588	0	0.72787	6.29184
597	0.72787	0	6.29184
605	0.73642	0	6.18326
671	0	0.75724	6.47868
673	0.75724	0	6.47868
681 *	0	0.74852	6.36268
689	0.74852	0	6.36268
1039	0.15952	0.15952	7.4757
1228	0	4.32069	6.48469
1229#	0	6.03063	6.59390
1230	0	6.50287	6.68666
1237	4.32069	0	6.48469
1238@	6.03063	0	6.59390
1239	6.50287	0	6.68666
1240*	5.53683	0	6.72497
1247	6.06548	1.82455	6.54414
1248	6.35939	1.76317	6.64513
1249*	5.34644	1.43087	6.69258
1253*	4.80760	2.77416	6.64185
1256	4.90233	4.90233	6.52501
1263	1.82455	6.06548	6.54414

1264	1.76317	6.35939	6.64513
1316	0	5.99370	6.64782
1317	0	6.46713	6.67740
1324	4.28331	0	6.60363
1325	5.99370	0	6.64782
1326	6.46713	0	6.67740
1327*	5.50567	0	6.63758
1335	6.32733	1.74689	6.62845
1336*	5.31656	1.42289	6.60276
1340*	4.78214	2.75781	6.54716
1345	3.84141	6.02092	6.41808
1351	1.74689	6.32733	6.62845
1429	0.18787	0.70324	6.29219
1430	0.36359	0.63080	6.29205
1433	0.70324	0.18787	6.29219
1441	0.19012	0.71142	6.18412
1442	0.36780	0.63798	6.18553
1443	0.52072	0.52072	6.18631
1444	0.63798	0.36780	6.18553
1445	0.71142	0.19012	6.18412
1489	0.18880	0.73357	6.47145
1490	0.37246	0.66005	6.45724
1493	0.73357	0.18880	6.47145
1501	0.18557	0.72547	6.35656
1504*	0.65319	0.36733	6.34507
1542^	0	0.37238	6.97320
1560	0.35202	0	6.95891

1579	0.08935	0.34420	6.94934
1580	0.17828	0.31441	6.92858
1582*	0.31441	0.17828	6.92858
1583	0.34420	0.08935	6.94934
1586*	0.20542	0.20542	6.83227
1646*	0.32907	0.19077	6.93958
2009	-0.03791	1.53211	11.5535
2046	-0.21212	1.41999	1.15538
2075	1.53211	-0.03791	11.5535
2089	1.41999	-0.21212	11.5538

Table 6.1 Displacements at nodes

- (1) The nodes whose displacements are compared with Laser Speckle Photography method are noted by *.
- (2) The node whose stress is the largest in the x-direction is node 1229, noted by #.
- (3) The nodes whose stress is the largest in the y-direction is node 1238, noted by @.
- (4) The node whose stresses are the largest in the z-direction are node 1542 , noted by ^.
- (5) The node whose stress is the largest in the xy-plane is node 138, noted by ##.

6.2 Deformation

An overall view of structural performance of the pressure vessel can be achieved from a deformed plot, which is generated by LUSAS as follows. The deformation of the pressure vessel is shown as are deformed shape, it is a static analysis.

Two kinds of deformed mesh can be drawn.

(1) A deformed mesh plot may be drawn using the commands:

```
SET LOADCASE
```

```
RESULTS DEFORMATION
```

```
DRAW MESH
```

(2) A deformed mesh may be superimposed over the original configuration using the commands:

```
SET LOADCASE
```

```
RESULTS DEFORMATION
```

```
DRAW MESH
```

```
RESULTS DEFORMATION OFF
```

```
DRAW MESH
```

The deformation mesh is superimposed over the original mesh in Fig.(6.1)

This shows:

- * Large displacements but small strains.

- * Large displacements occurred at the middle of the lines 9, 10, 11, 12, 17, and 18, 19, 20, as well as at the left side of the cap.

- * No displacements occurred at the end of the right side of the cap because it was fixed.

- * Small displacements occurred at the area around the ring and fixed end.

MYSTRO: 10, 1-2

DATE: 5-12-93

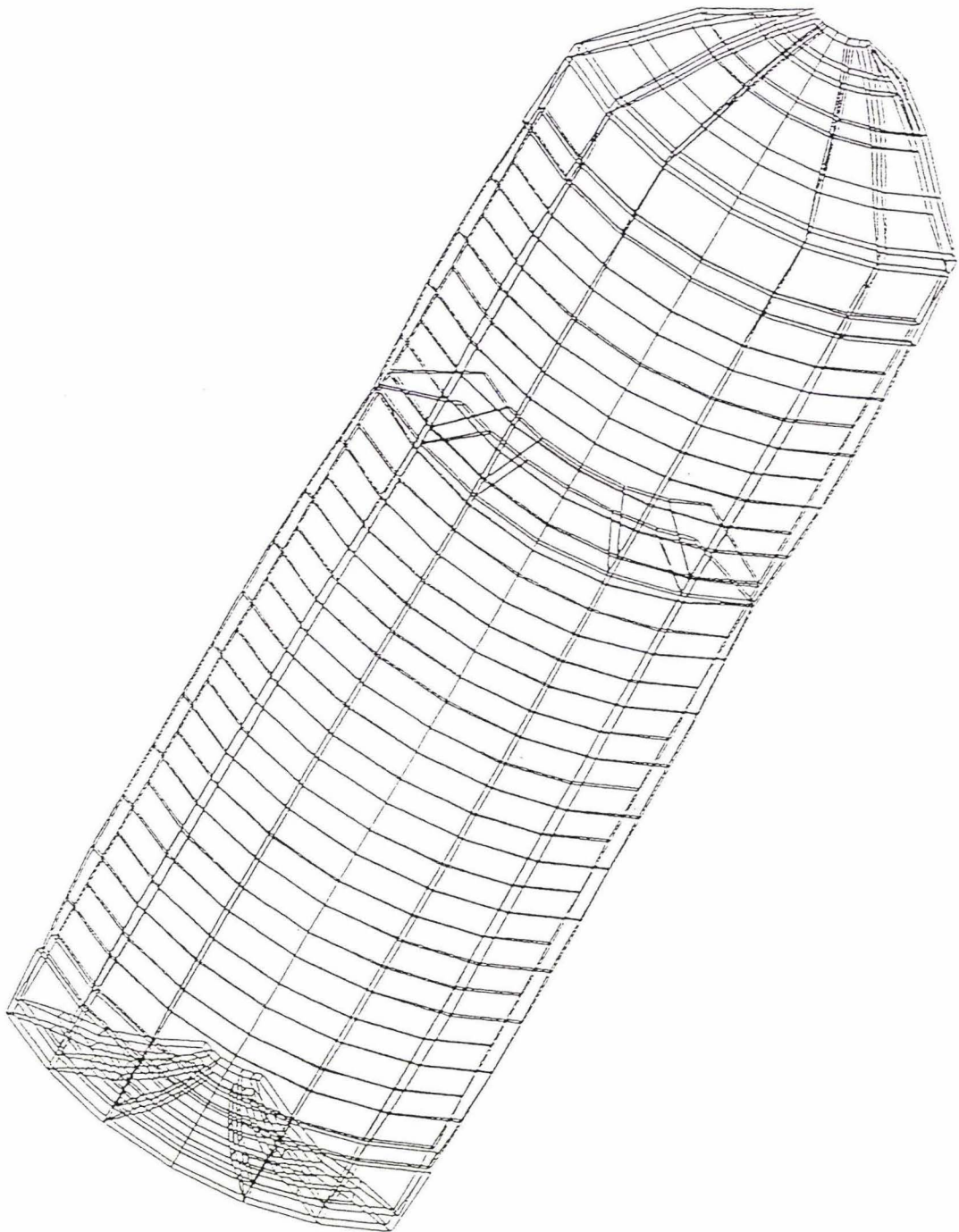


Fig.6.1

6.3 Stress

The direct and shear stress lists (table) show the output stresses for certain nodes which are of particular importance and some of them were also analysed using Laser Speckle Photography by Hendel (35).

The graphs of the stress contours are shown after the lists of stresses .

The areas of highest stress can be determined by comparing the list of stresses with the graphs of stress contours.

Other direct and shear stresses determined by the Finite Element Method are presented in Appendix.

ELT	Node	Compt	Compt	Compt	Compt	Compt	Compt
No.	No.	x-dirn	y-dirn	z-dirn	xy-dirn	yz-dirn	zx-dirn
		$\times 10^6$	$\times 10^6$	$\times 10^6$	$\times 10^6$	$\times 10^6$	$\times 10^6$
239	1	72.33	-17.83	20.67	71.88 [^]	17.32	3.62
244	5	-17.83	72.33	20.67	71.88 [^]	3.62	17.32
259	350	67.85	3.09	56.38	-65.21	0.49	0.54
	143	69.06	3.01	56.84	-65.73	1.35	-0.76
	133	32.70	32.02	56.65	-71.32	7.48	7.31
	340	33.53	33.06	55.66	-70.76	6.80	7.43
	351	60.68	11.36	56.78	-65.22	-0.41	-1.92
	144	62.49	11.71	57.44	-66.00	0.08	-2.70
	134	36.01	35.80	47.18	-70.19	-6.45	-4.58
	341	37.99	33.92	45.99	-70.37	-6.61	-4.52
262	320	-14.69	85.53	58.70	-44.19	-0.83	-11.97
	113	-13.58	84.97	58.85	-45.64	-2.12	-11.64
	92	-15.60	107.36	69.13	-6.53	-1.39	-15.82
	299	-15.25	105.05	69.24	-6.37	-0.80	-15.75
	321	-12.90	86.34	58.53	-46.96	0.49	7.91
	114	-12.49	85.21	58.50	-44.30	-0.42	8.12
	93	-15.25	105.76	68.90	-9.46	1.24	11.58
	300	-14.61	104.11	69.19	-9.34	1.47	11.64
277	137	33.20	31.43	57.91	-71.88	-2.73	-0.06
	344	31.43	33.20	57.14	-71.03	-2.71	-0.12
281	282	104.61	-14.90	57.50	-12.65	-2.13	-0.90
	75	106.66	-15.13	57.83	-12.76	-2.10	-0.86
	157	83.25	-12.39	57.79	-43.49	-2.74	1.34

	364	84.25	-12.58	57.48	-43.16	-2.74	1.33
	283	106.44	-14.65	57.89	-12.55	6.42	0.12
	76	108.57	-14.16	58.25	-12.67	6.44	0.16
	158	88.00	-12.74	58.20	-43.07	6.29	2.40
	365	87.92	-12.90	57.86	-42.73	6.28	2.38
283	137	31.00	36.33	57.62	-71.88	-3.34	-0.67
	138	31.99	36.76	57.89	-72.79^	4.96	5.42
768	1337	-12.96	33.75	27.31	-21.51	8.73	-3.37
771	1229	114.32*	-11.88	67.95	-10.89	48.88	7.21
776	1238	-16.88	114.32#	67.95	-1.89	7.01	48.96
777	1317	97.22	-13.35	63.22	-7.01	62.59	-5.79
	1351	97.64	-12.30	69.75	-45.24	55.57	19.04
	1264	98.01	-12.09	69.77	-43.69	55.60	20.23
	1230	92.47	-13.10	69.98	-7.18	62.95	-5.25
	1318	90.23	-12.98	68.39	-8.12	-64.75	-21.08
	1352	73.95	-12.13	67.81	-33.80	-61.98	5.06
	1265	73.38	-11.51	64.57	-34.11	-61.04	5.88
778	1231	89.52	-13.85	64.88	-8.23	-61.23	-5.01
779	1257	28.30	24.56	52.90	-61.92	-19.91	-46.45
781	1340**	25.60	26.21	55.94	-69.33	-8.75	-55.63
	1336**	-12.10	71.22	67.86	-37.55	-34.88	-53.25
	1249**	-12.59	70.65	64.64	-38.07	-33.96	-53.01
	1253**	0.26	62.95	43.34	-63.99	-7.70	-55.90
	1248	-12.52	80.22	69.32	-44.82	10.25	58.28
782	1326	-13.35	92.22	73.22	-17.02	-5.79	62.58
	1239	-13.11	92.47	69.98	-17.18	-4.99	63.96
	1336**	-12.14	86.95	67.81	-43.80	7.03	-63.97

	1240**	-13.85	79.52	64.88	-8.23	-20.93	-64.15
787	1253**	0.54	55.87	55.63	-59.99	33.95	25.68
788	1327**	-13.48	79.69	63.53	-8.13	-21.08	43.51
	1240**	-13.18	79.55	62.36	-8.24	-20.97	44.86
	1249**	12.39	78.26	69.85	-36.11	28.21	36.36
841	587	16.41	-14.68	38.26	-1.04	-70.39##	9.28
842	1441	-15.30	5.92	38.07	-4.84	-70.06	-13.81
845	1445	5.92	-15.30	38.07	-4.84	-13.81	-70.06
	1433	-0.12	2.98	83.86	-4.69	-13.33	-67.91
846	605	-14.68	16.41	38.26	-1.04	9.28	-70.20
	597	-14.32	10.05	37.42	-1.00	7.50	-70.39^^
899	673	-13.71	6.44	109.48	-1.00	-10.51	69.40
	689	-13.48	5.85	108.47	-0.96	31.55	69.39
	1505	-10.06	9.13	112.74@	-4.95	12.31	64.40
903	1501	5.67	-11.10	112.74@	-5.11	68.51	12.31
	1502	9.13	-0.60	101.22	-4.95	59.40	50.19
997	1542	2.91	-12.60	-112.75@	0.74	7.78	-5.42
	1501	5.23	-11.75	112.28	-5.38	25.17	18.84
	671	6.44	-13.81	112.70	-0.93	69.40	-9.29
1001	1489	5.75	-12.83	111.21	-4.39	52.60	4.27
1005	1491	6.02	5.94	102.13	-5.35	31.77	42.42
	1503	5.62	6.40	101.49	-5.96	14.92	26.26
1013	1492	-13.18	13.55	98.37	-4.27	32.36	41.77
	1505	-16.58	7.23	103.97	-3.73	-1.51	29.85
1017	673	31.89	39.29	39.37	-0.63	-9.29	69.40
	597	4.19	12.50	101.39	-0.74	8.34	-28.77
1285	2053	-6.70	-11.58	-2.12	2.17	20.38	-27.65

	1039	-12.80	-0.69	0.43	-0.31	-23.41	25.09
1319	1082	-11.58	-6.70	-2.11	2.17	-27.96	20.38
1321	2075	-14.16	-17.13	-6.22	-3.97	-22.55	6.98
	2089	-17.84	-13.40	-6.22	4.66	-22.81	7.31

Table 6.2 Direct and shear stresses in element

6.4 A summary of the results from FEM

Basic aspects of the Finite Element Methods, theory, input features and scope of MYSTRO and LUSAS programs have been presented. In addition, detailed input and numerical as well as graphical output illustrating linear response have been presented.

The output results show:

- (a) The highest direct stress in the X-direction occurred at node 1229 of the element 771, its value is $114.32 \times 10^6 N/m^2$, noted by *. Other values of the direct stresses in the X direction vary from $-17.84 \times 10^6 N/m^2$ to $114.32 \times 10^6 N/m^2$.
- (b) The highest direct stress in the Y-direction occurred at node 1238 of the element 776, its value is $114.32 \times 10^6 N/m^2$, noted by #. Other values vary from $-17.84 \times 10^6 N/m^2$ to $114.32 \times 10^6 N/m^2$.
- (c) The highest direct stress in the Z-direction occurred at node 1542 of the element 997, node 1501 of the element 903 and node 1505 of the element 899, their values are $-112.75 N/m^2$ and $112.74 \times 10^6 N/m^2$ respectively, noted by @. Other values vary from $-112.75 \times 10^6 N/m^2$ to $112.74 \times 10^6 N/m^2$.
- (d) The highest shear stress in the XY-plane occurred at node 138 of the element 283, its value is $-72.79 \times 10^6 N/m^2$, noted by ^. Other values of the

shear stresses in the XY plane vary from $-72.79 \times 10^6 N/m^2$ to $71.88 \times 10^6 N/m^2$.

(e) The highest shear stress in the YZ-plane occurred at node 587 of the element 841, its value is $-70.39 \times 10^6 N/m^2$, noted by ##. Other values vary from $-70.39 \times 10^6 N/m^2$ to $69.40 \times 10^6 N/m^2$.

(f) The highest shear stress in the ZX-plane occurred at node 597 of the element 846, its value is $-70.39 \times 10^6 N/m^2$, noted by ^^. Other values vary from $-70.39 \times 10^6 N/m^2$ to $69.40 \times 10^6 N/m^2$.

(g) The highest stress areas are indicated by asterisk sign on the stress contour graphs.

(h) The number of contours =12

(i) The elements whose stresses at all of the nodes in the x-direction are larger than others are element 251, 263, 269, 275, 281 and 287 (refer to Appendix III).

(j) The elements whose stresses at all of the nodes in the y-direction are larger than others are element 256, 262, 268, 274, 280, 286, 292 and 776 (refer to Appendix III).

(k) The nodes whose stresses in the z-direction are larger than others are nodes 673, 689, 1505, 1501, 1502, 671, 1542, 681, 1489, 1490, 1491, 1503, 1504, 1505, 1493, 1552, 1560, 605, 597. (refer to Appendix III).

(l) The elements whose stresses at all of the nodes in the xy-plane are larger than others are element 259, 260, 265 and 266 (refer to Appendix III).

(m) The nodes whose stresses in the yz-plane are larger than others are nodes 1317, 1230, 1318, 1352, 1265, 1231, 587, 1441, 1501, 671(refer to Appendix III).

- (n) The elements whose stresses at all of the nodes in the zx-plane are larger than others are element 776 and 782 (refer to Appendix III).
- (o) The nodes whose displacements are compared with Laser Speckle Photography Method are noted by **.

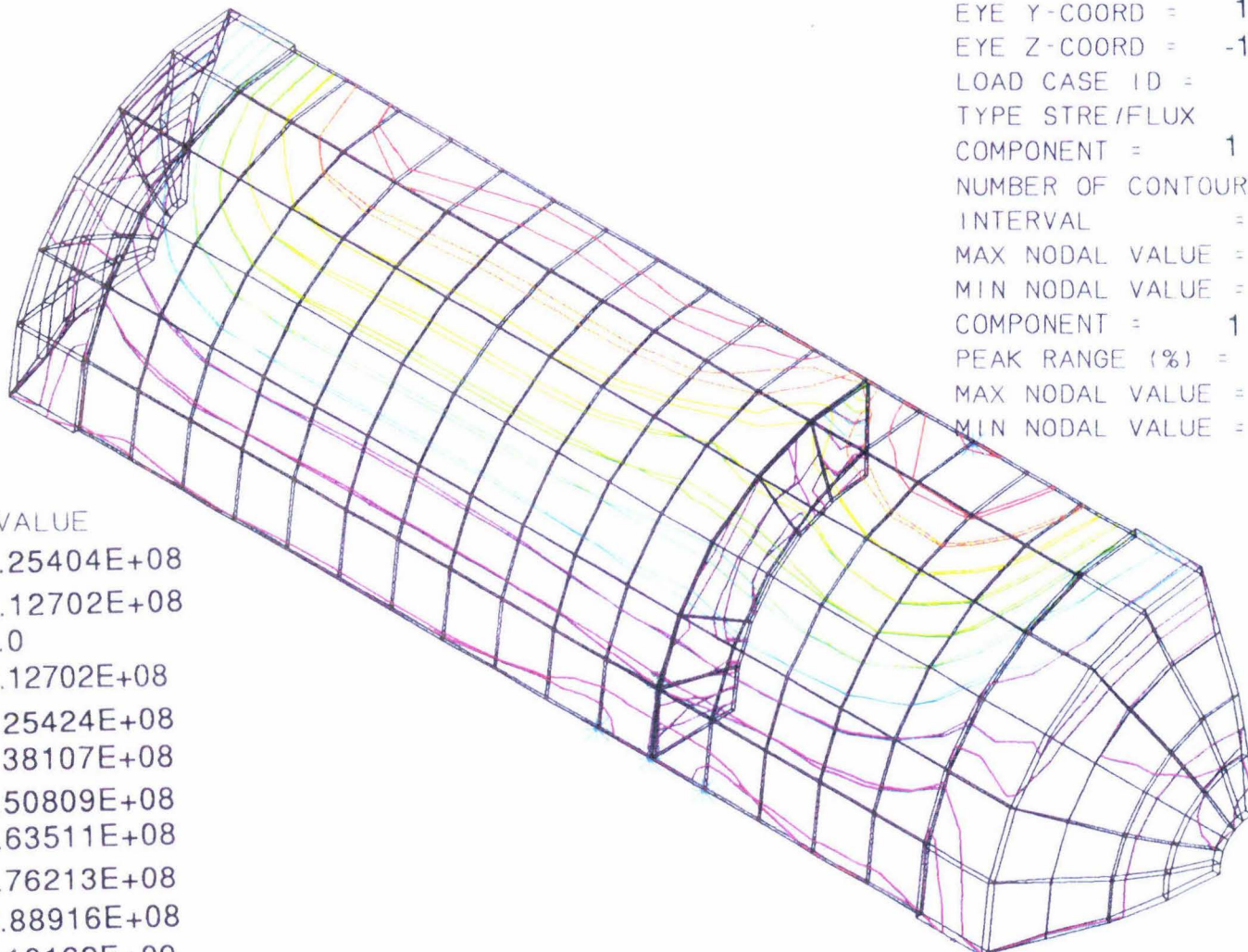
MYSSTRO: 10.1-2

DATE: 5- 2-93

Fig. 6.2

CONTOUR VALUE

A	-0.25404E+08
B	-0.12702E+08
C	0.0
D	0.12702E+08
E	0.25424E+08
F	0.38107E+08
G	0.50809E+08
H	0.63511E+08
I	0.76213E+08
J	0.88916E+08
K	0.10162E+09
L	0.11432E+09

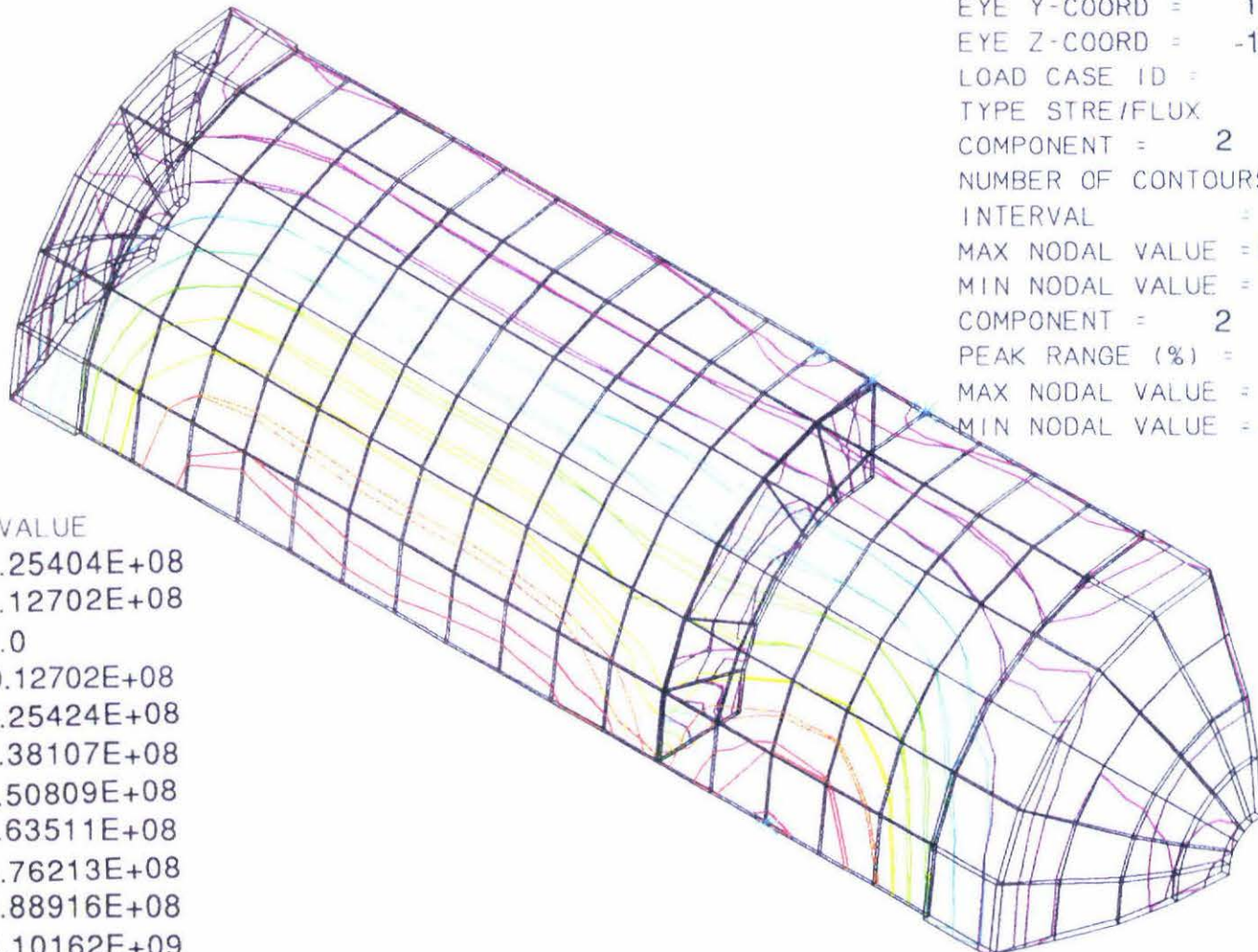


MYSTRO: 10.1-2

DATE: 5- 2-93

Fig.6.3

	CONTOUR VALUE
A	-0.25404E+08
B	-0.12702E+08
C	0.0
D	0.12702E+08
E	0.25424E+08
F	0.38107E+08
G	0.50809E+08
H	0.63511E+08
I	0.76213E+08
J	0.88916E+08
K	0.10162E+09
L	0.11432E+09



MYSTRO: 10.1-2

DATE: 5- 2-93

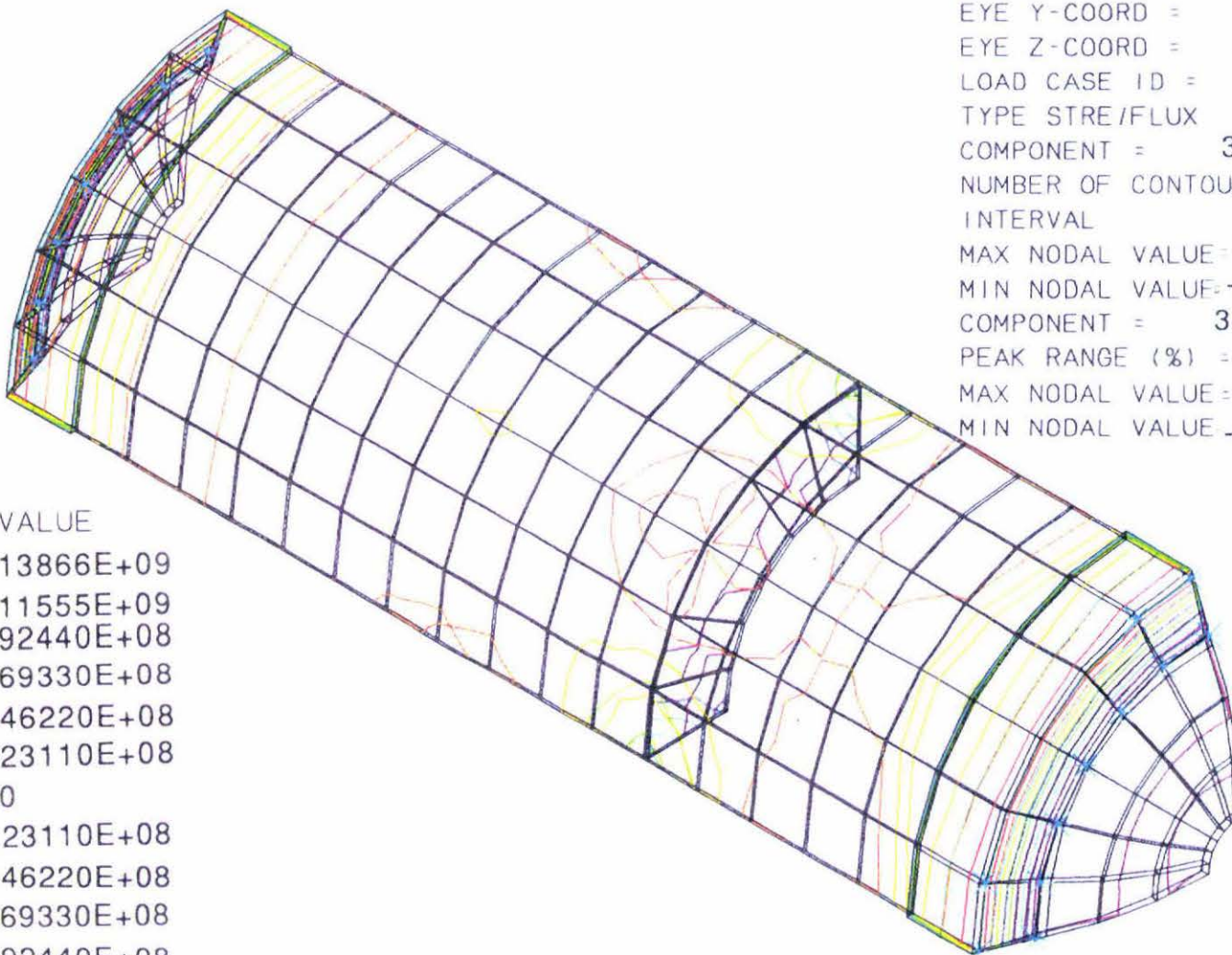
SCALE 1/ 2.071
EYE X-COORD = 1.000
EYE Y-COORD = 1.000
EYE Z-COORD = -1.000
LOAD CASE ID = 1
TYPE STRE/FLUX
COMPONENT = 3
NUMBER OF CONTOURS = 12
INTERVAL 0.23110E+08
MAX NODAL VALUE= 0.11274E+09
MIN NODAL VALUE= -0.11275E+09
COMPONENT = 3
PEAK RANGE (%) = 1.000
MAX NODAL VALUE= 0.11274E+09
MIN NODAL VALUE= -0.11275E+09

Fig. 6.4

67

CONTOUR VALUE

- A -0.13866E+09
- B -0.11555E+09
- C -0.92440E+08
- D -0.69330E+08
- E -0.46220E+08
- F -0.23110E+08
- G 0.0
- H 0.23110E+08
- I 0.46220E+08
- J 0.69330E+08
- K 0.92440E+08
- L 0.11555E+09



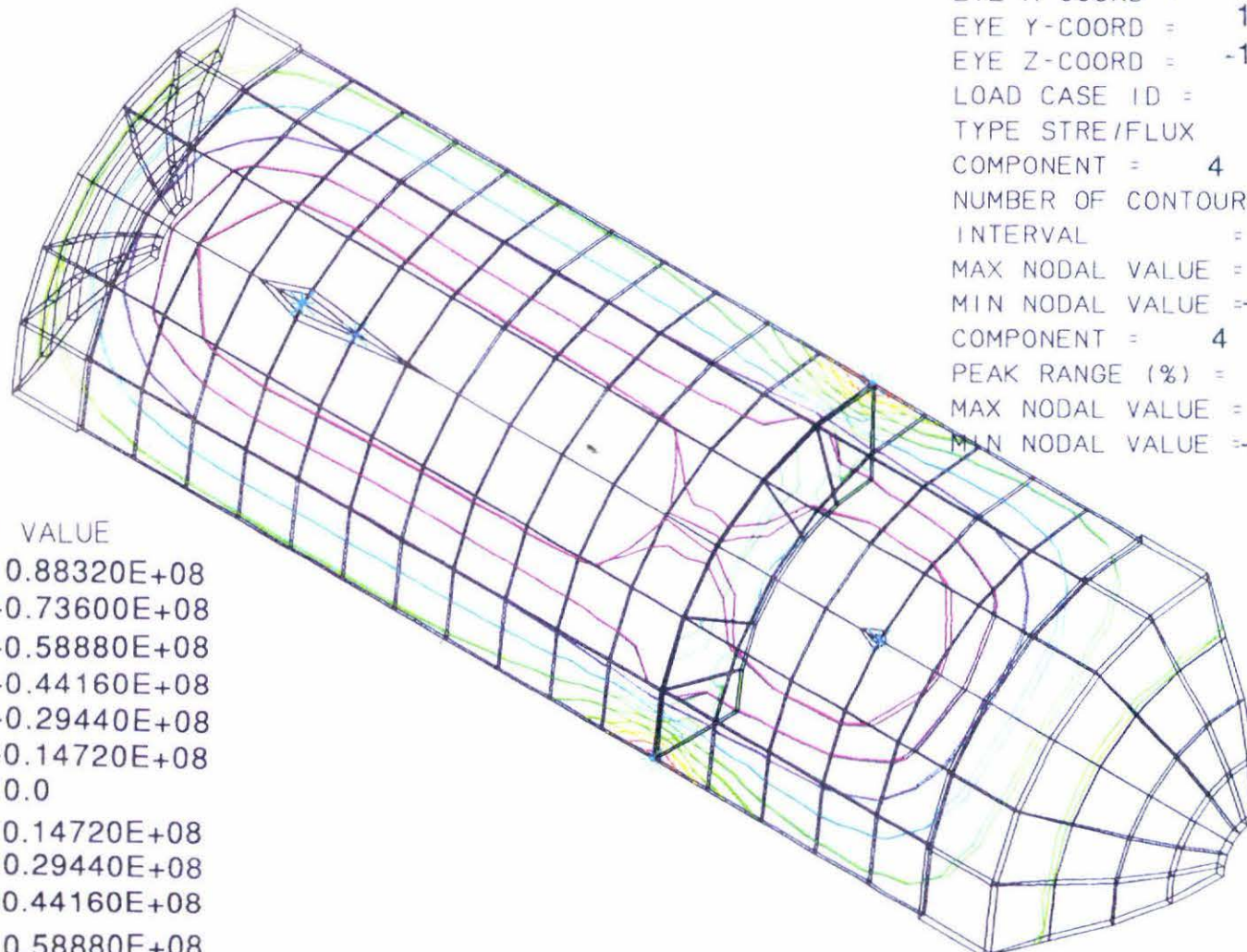
MYSTRO: 10.1-2

DATE: 5- 2-93

Fig. 6.5

68

	CONTOUR VALUE
A	-0.88320E+08
B	-0.73600E+08
C	-0.58880E+08
D	-0.44160E+08
E	-0.29440E+08
F	-0.14720E+08
G	0.0
H	0.14720E+08
I	0.29440E+08
J	0.44160E+08
K	0.58880E+08
L	0.73600E+08



SCALE 1/ 2.071
EYE X-COORD = 1.000
EYE Y-COORD = 1.000
EYE Z-COORD = -1.000
LOAD CASE ID = 1
TYPE STRE/FLUX
COMPONENT = 4
NUMBER OF CONTOURS = 12
INTERVAL = 0.14720E+08
MAX NODAL VALUE = 0.71880E+08
MIN NODAL VALUE = -0.72790E+08
COMPONENT = 4
PEAK RANGE (%) = 1.000
MAX NODAL VALUE = 0.71880E+08
MIN NODAL VALUE = -0.72790E+08

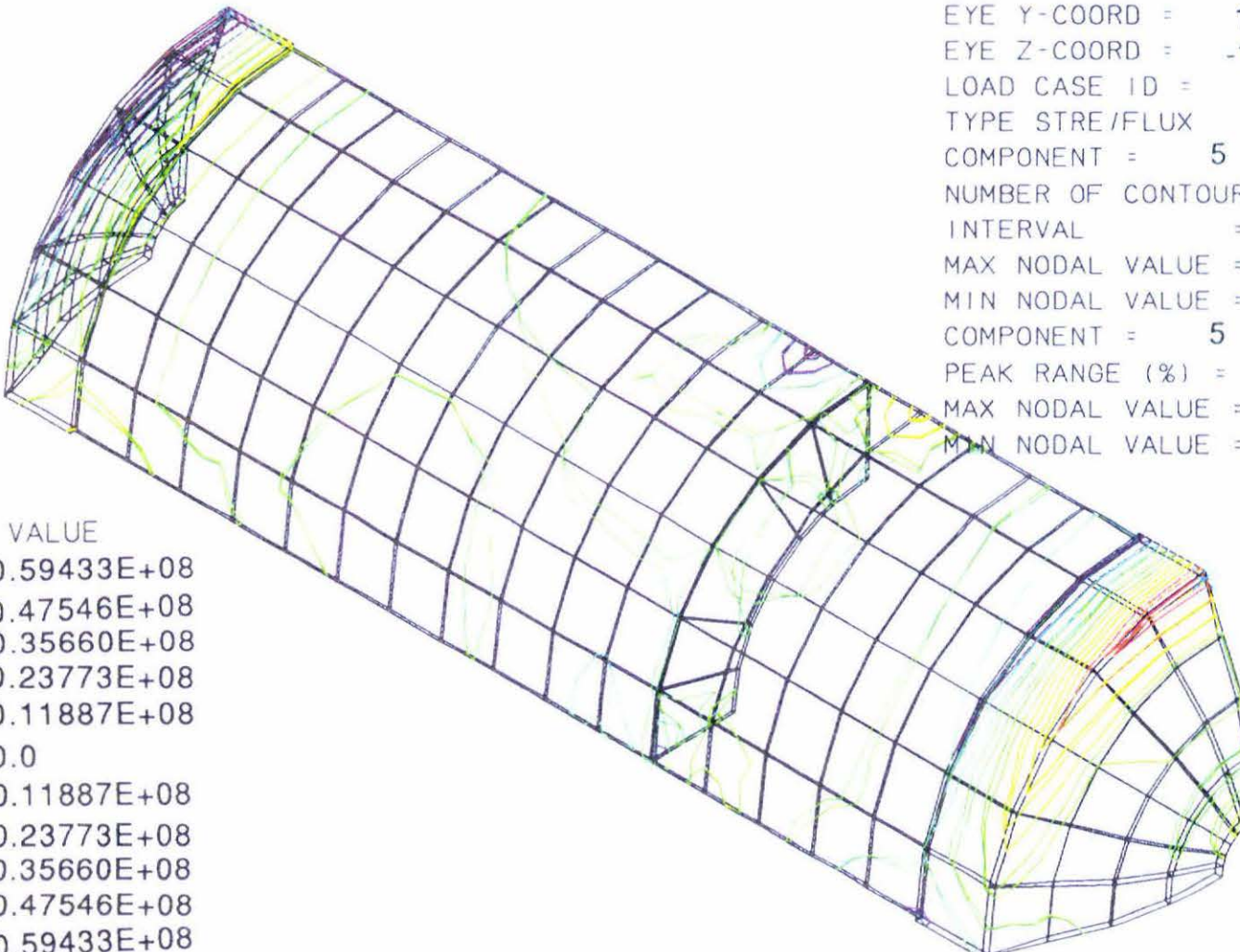
TITLE: Shear Stress in XY Direction

MYSTRO: 10.1-2

DATE: 5- 2-93

Fig. 6.6

CONTOUR VALUE	
A	-0.59433E+08
B	-0.47546E+08
C	-0.35660E+08
D	-0.23773E+08
E	-0.11887E+08
F	0.0
G	0.11887E+08
H	0.23773E+08
I	0.35660E+08
J	0.47546E+08
K	0.59433E+08
L	0.71320E+08



SCALE 1 / 2.071
EYE X-COORD = 1.000
EYE Y-COORD = 1.000
EYE Z-COORD = -1.000
LOAD CASE ID = 1
TYPE STRE/FLUX
COMPONENT = 5
NUMBER OF CONTOURS = 12
INTERVAL = 0.11887E+08
MAX NODAL VALUE = 0.69400E+08
MIN NODAL VALUE = -0.70390E+08
COMPONENT = 5
PEAK RANGE (%) = 1.000
MAX NODAL VALUE = 0.69400E+08
MIN NODAL VALUE = -0.70390E+08

MYSSTRO: 10.1-2

DATE: 5-2-93

SCALE 1/ 2.071
EYE X-COORD = 1.000
EYE Y-COORD = 1.000
EYE Z-COORD = -1.000
LOAD CASE ID = 1
TYPE STRE/FLUX
COMPONENT = 6
NUMBER OF CONTOURS = 12
INTERVAL = 0.11887E+08
MAX NODAL VALUE = 0.69400E+08
MIN NODAL VALUE = -0.70390E+08
COMPONENT = 6
PEAK RANGE (%) = 1.000
MAX NODAL VALUE = 0.69400E+08
MIN NODAL VALUE = -0.70390E+08

70

CONTOUR VALUE
A -0.59433E+08
B -0.47546E+08
C -0.35660E+08
D -0.23773E+08
E -0.11887E+08
F 0.0
G 0.11887E+08
H 0.23773E+08
I 0.35660E+08
J 0.47546E+08
K 0.59433E+08
L 0.71320E+08

TITLE: Shear Stress in XZ Direction

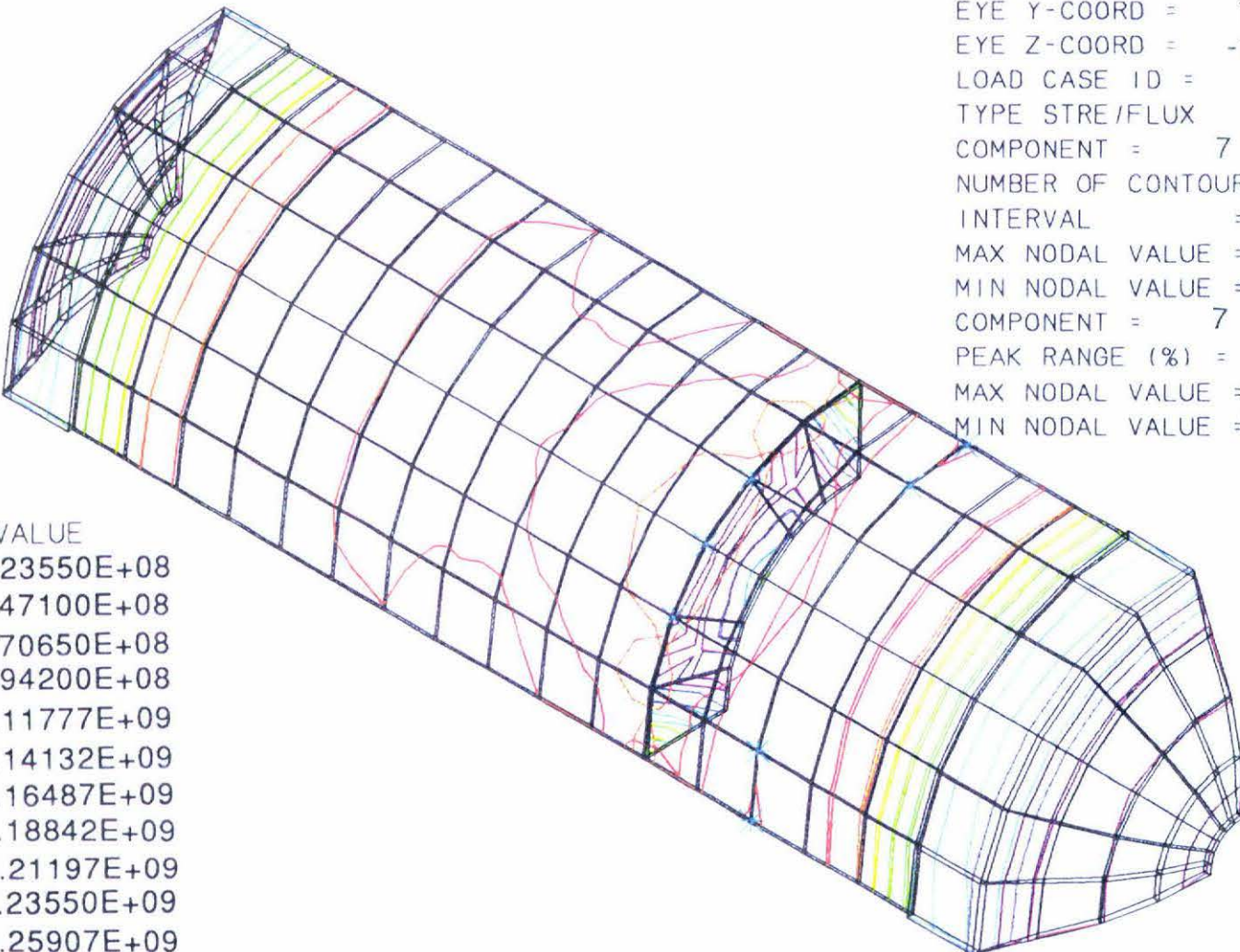
EYE
6.7

MYSSTRO: 10.1-2

DATE: 5- 2-93

Fig.6.8

	CONTOUR VALUE
A	0.23550E+08
B	0.47100E+08
C	0.70650E+08
D	0.94200E+08
E	0.11777E+09
F	0.14132E+09
G	0.16487E+09
H	0.18842E+09
I	0.21197E+09
J	0.23550E+09
K	0.25907E+09
L	0.28264E+09



MYSTRO: 10.1-2

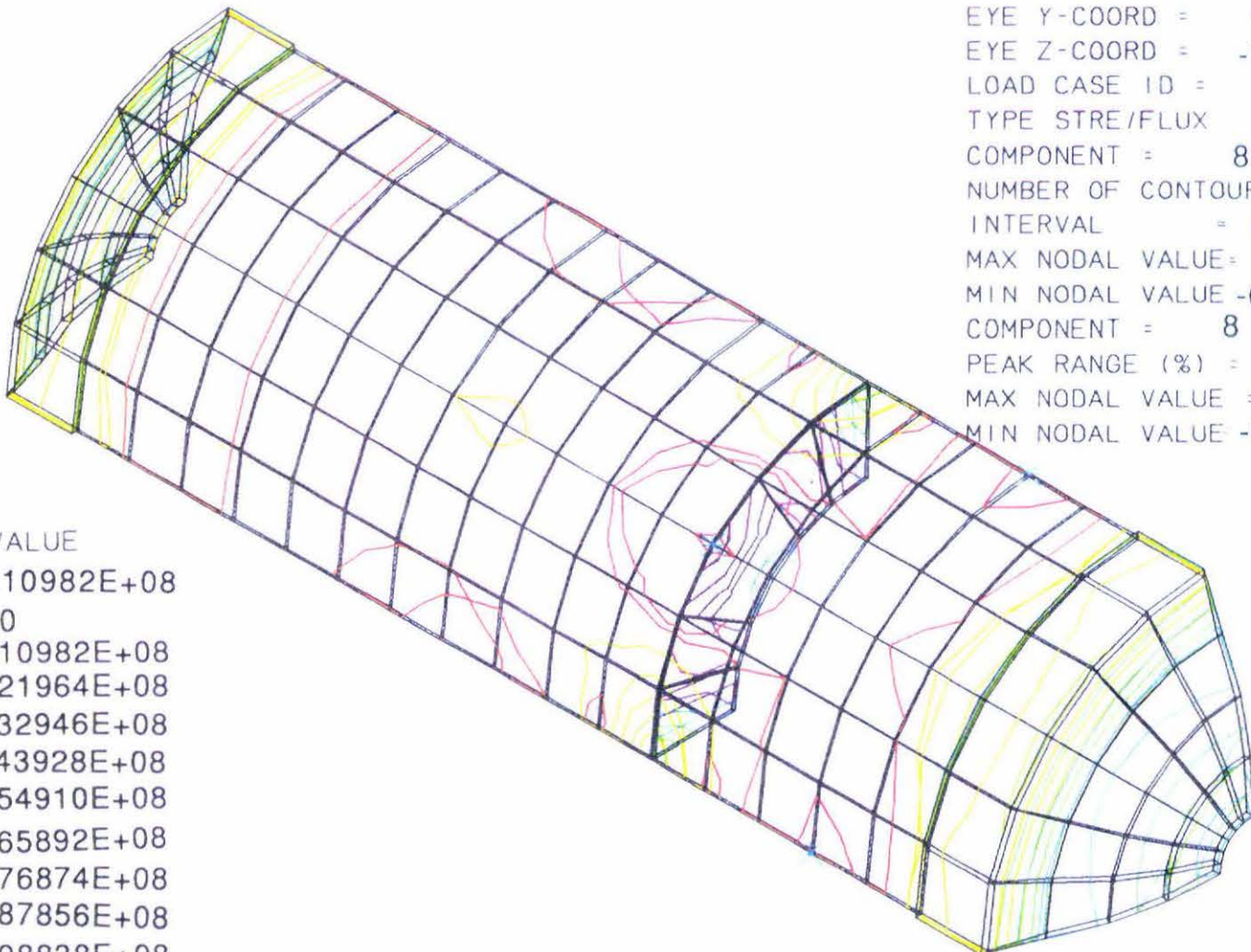
DATE: 5-2-93

SCALE 1 / 2.071
EYE X-COORD = 1.000
EYE Y-COORD = 1.000
EYE Z-COORD = -1.000
LOAD CASE ID = 1
TYPE STRE/FLUX
COMPONENT = 8
NUMBER OF CONTOURS = 12
INTERVAL = 0.10982E+08
MAX NODAL VALUE = 0.10917E+09
MIN NODAL VALUE = -0.18684E+08
COMPONENT = 8
PEAK RANGE (%) = 1.000
MAX NODAL VALUE = 0.10917E+09
MIN NODAL VALUE = -0.18684E+08

Fig.6.9

CONTOUR VALUE

- A -0.10982E+08
- B 0.0
- C 0.10982E+08
- D 0.21964E+08
- E 0.32946E+08
- F 0.43928E+08
- G 0.54910E+08
- H 0.65892E+08
- I 0.76874E+08
- J 0.87856E+08
- K 0.98838E+08
- L 0.10982E+09



MYSSTRO: 10.1-2

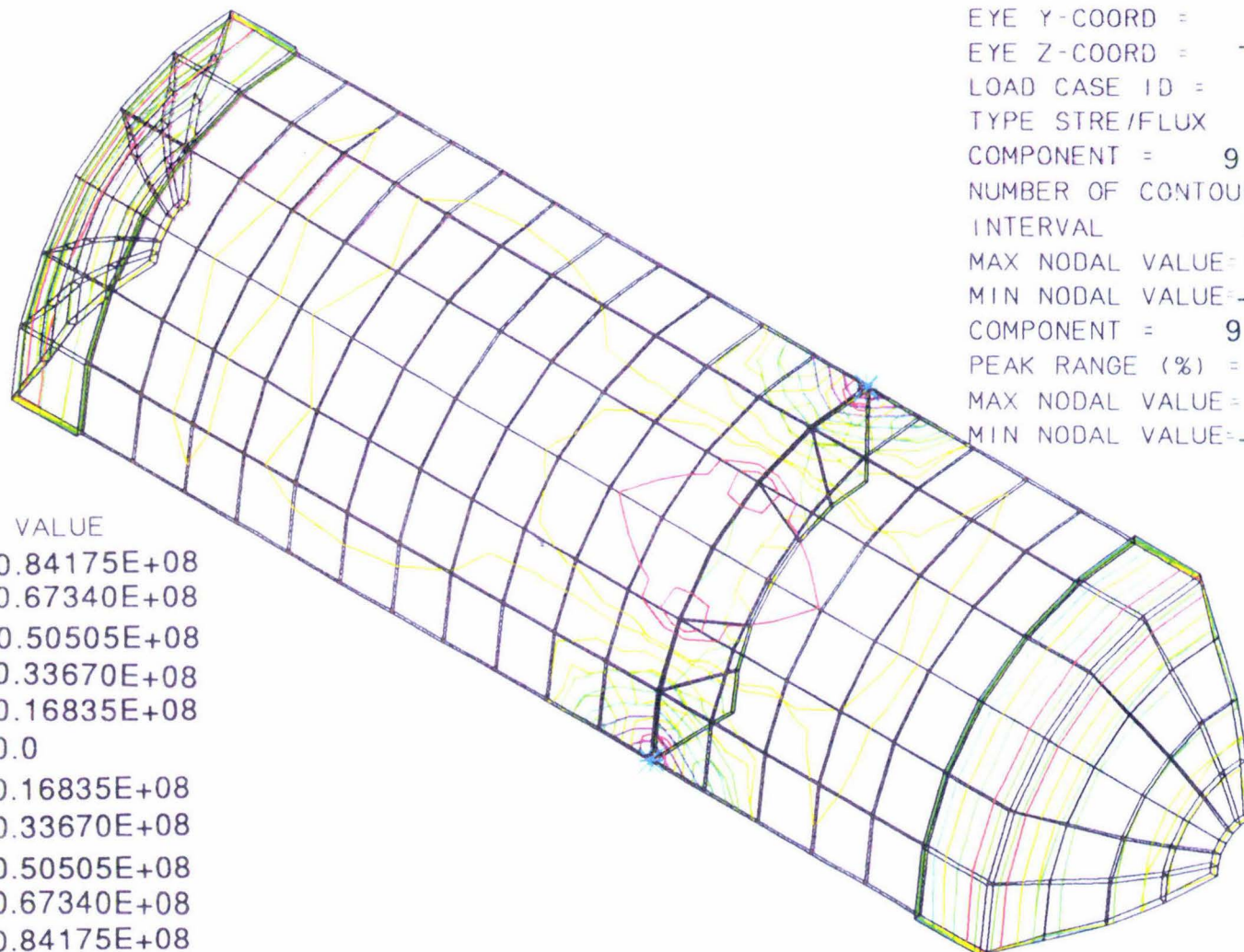
DATE: 5- 2-93

Fig. 6.10

73

CONTOUR VALUE

A	-0.84175E+08
B	-0.67340E+08
C	-0.50505E+08
D	-0.33670E+08
E	-0.16835E+08
F	0.0
G	0.16835E+08
H	0.33670E+08
I	0.50505E+08
J	0.67340E+08
K	0.84175E+08
L	0.10101E+09



SCALE 1/ 2.071
EYE X-COORD = 1.000
EYE Y-COORD = 1.000
EYE Z-COORD = -1.000
LOAD CASE ID = 1
TYPE STRE/FLUX
COMPONENT = 9
NUMBER OF CONTOURS = 12
INTERVAL 0.16835E+08
MAX NODAL VALUE= 0.98460E+08
MIN NODAL VALUE=-0.86100E+08
COMPONENT = 9
PEAK RANGE (%) = 1.000
MAX NODAL VALUE= 0.98460E+08
MIN NODAL VALUE=-0.86100E+08

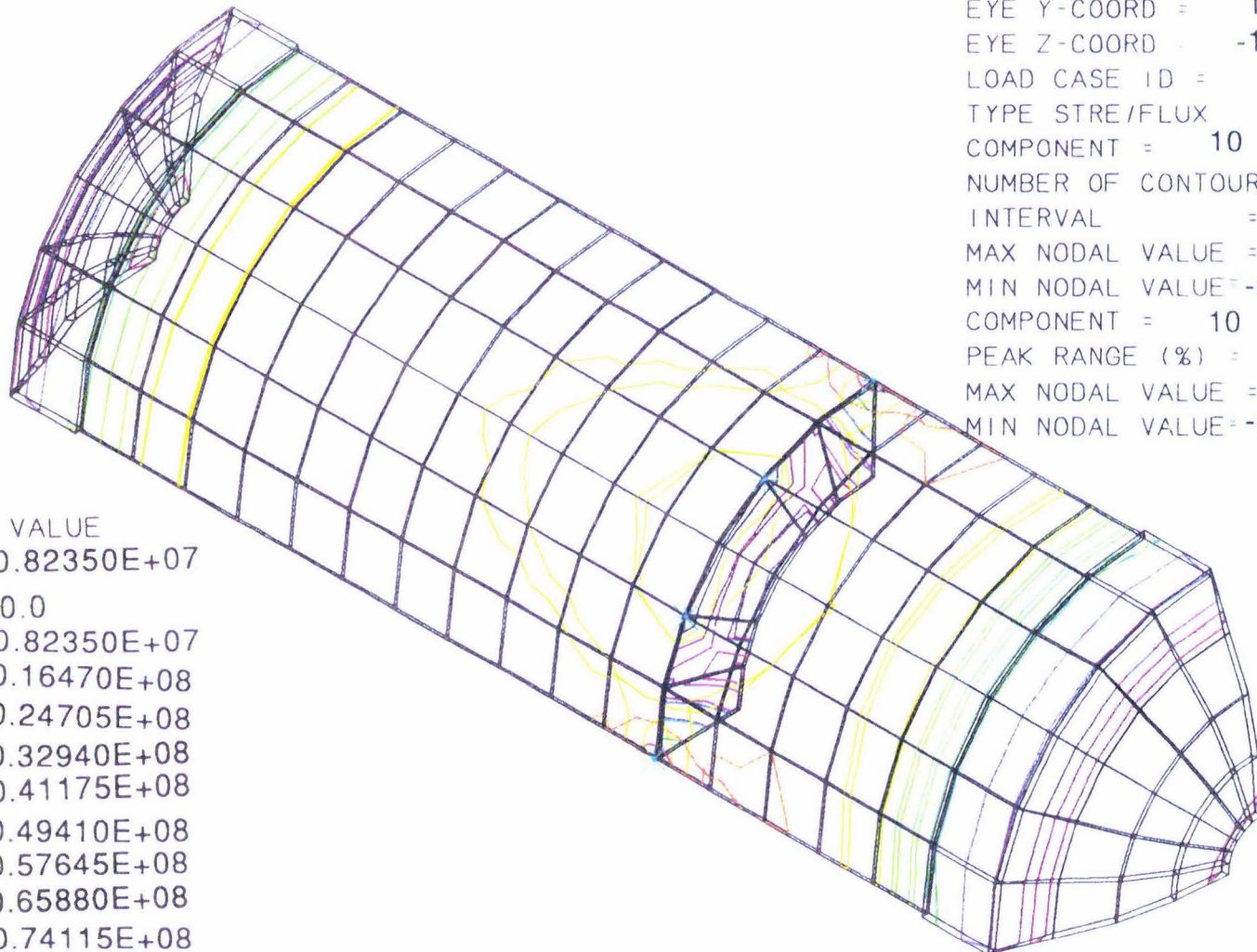
MYSSTRO: 10.1-2

DATE: 5- 2-93

Fig.6.11

74

	CONTOUR VALUE
A	-0.82350E+07
B	0.0
C	0.82350E+07
D	0.16470E+08
E	0.24705E+08
F	0.32940E+08
G	0.41175E+08
H	0.49410E+08
I	0.57645E+08
J	0.65880E+08
K	0.74115E+08
L	0.82350E+08

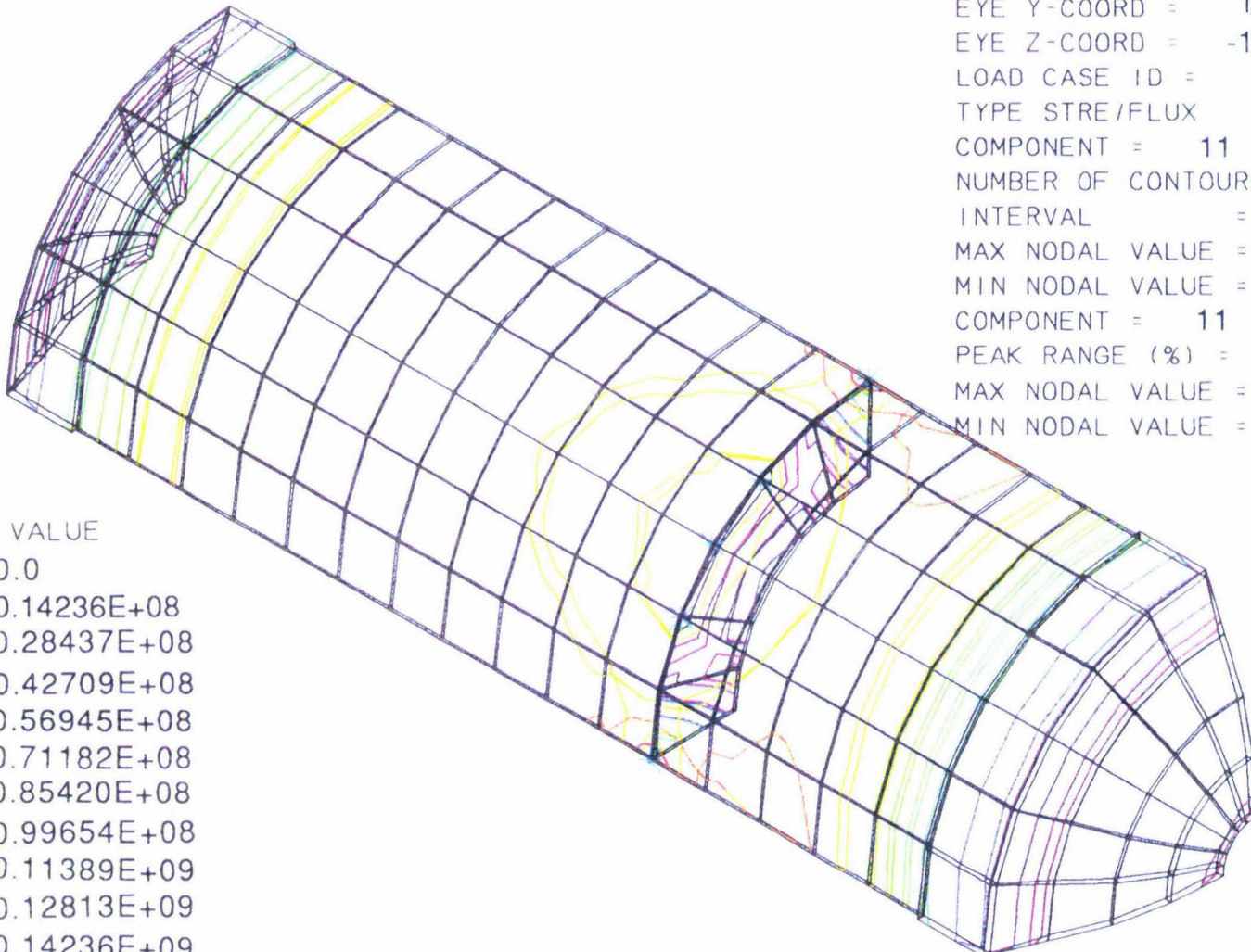


SCALE 1/ 2.071
EYE X-COORD = 1.000
EYE Y-COORD = 1.000
EYE Z-COORD = -1.000
LOAD CASE ID = 1
TYPE STRE/FLUX
COMPONENT = 10
NUMBER OF CONTOURS = 12
INTERVAL = 0.82350E+07
MAX NODAL VALUE = 0.80865E+08
MIN NODAL VALUE = -0.10035E+07
COMPONENT = 10
PEAK RANGE (%) = 1.000
MAX NODAL VALUE = 0.82350E+07
MIN NODAL VALUE = -0.10035E+07

MYSTRO: 10.1-2

DATE: 5- 2-93

SCALE 1/ 2.071
EYE X-COORD = 1.000
EYE Y-COORD = 1.000
EYE Z-COORD = -1.000
LOAD CASE ID = 1
TYPE STRE/FLUX
COMPONENT = 11
NUMBER OF CONTOURS = 12
INTERVAL = 0.14236E+08
MAX NODAL VALUE = 0.15636E+09
MIN NODAL VALUE = 0.17478E+07
COMPONENT = 11
PEAK RANGE (%) = 1.000
MAX NODAL VALUE = 0.15636E+09
MIN NODAL VALUE = 0.17478E+07



CONTOUR VALUE

A	0.0
B	0.14236E+08
C	0.28437E+08
D	0.42709E+08
E	0.56945E+08
F	0.71182E+08
G	0.85420E+08
H	0.99654E+08
I	0.11389E+09
J	0.12813E+09
K	0.14236E+09
L	0.15660E+09

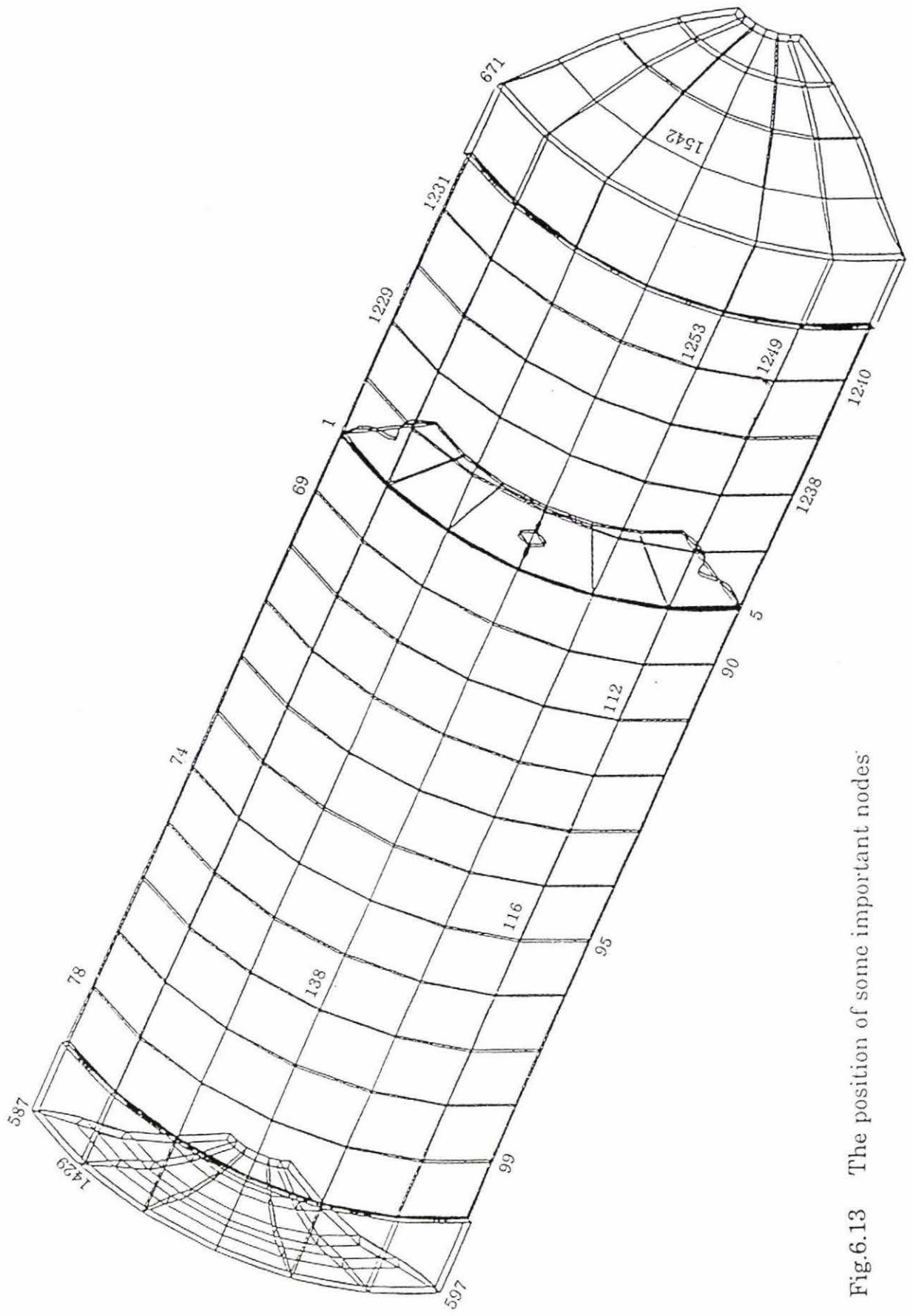


Fig.6.13 The position of some important nodes

6.5 Results from the pressure vessel design formulas

The results from the pressure vessel design formulas were calculated by hand to verify the results from Finite Element Method.

According to design formula, Presented in (37)

CYLINDRICAL SHELL:

$$P = \frac{\sigma J t}{R + 0.6t}$$

where

P: Design pressure or max. allowable working pressure.

σ : Axial stress value of material.

J: Joint efficiency.

R: Inside radius.

t: Wall thickness.

when J=0.65

take P=1.3Mpa

$$\sigma = \frac{P(R + 0.6t)}{Jt} = \frac{1300000(0.128 + 0.6 \times 0.0016)}{0.65 \times 0.0016} = 161.2 \times 10^6 N/m^2$$

ASME FLANGED AND DISHED HEAD:

$$P = \frac{\sigma J t}{0.885L + 0.1t}$$

where

P: Design pressure or max. allowable working pressure.

σ : Axial stress value of material.

J: Joint efficiency.

R: Inside radius.

L: Inside radius of dish.

t: Wall thickness.

when $J=0.65$

$$\sigma = \frac{P(0.885L + 0.1t)}{Jt} = \frac{1300000(0.885 \times 0.42 + 0.1 \times 0.004)}{0.65 \times 0.004} = 186.05 \times 10^6 N/m^2$$

6.6 Results from Laser Speckle Photography experiment (35)

The results from the Laser Speckle Photography are simple displacements. They are as follows:

Fringe Pattern No.	Fringe Spacing Δ	Distance of point from fixed end (x)	Distance of point from central axis (y)	Actual δ (from Young's Equation) (meters)	Predicted δ (meters)
1	4.16 mm	21.25 mm	50.0 mm	5.29×10^{-5}	4.41×10^{-5}
2	4.13 mm	102.5 mm	47.5 mm	5.33×10^{-5}	4.76×10^{-5}
3	4.43 mm	105.0 mm	8.75 mm	4.96×10^{-5}	2.48×10^{-5}
4	5.0 mm	102.5 mm	- 45.0 mm	4.40×10^{-5}	4.57×10^{-5}

Table.6.3 The displacements from Laser Speckle Photography

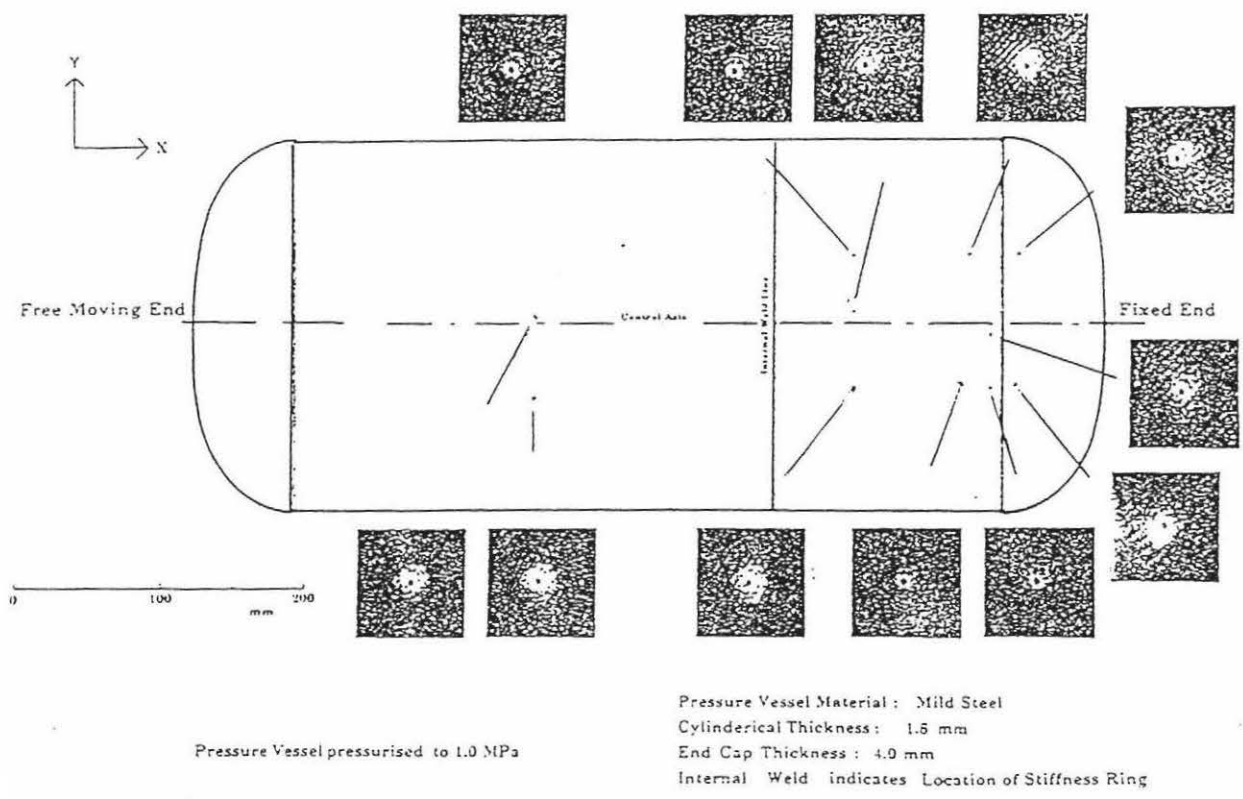


Fig.6.14 Fringe patterns from Laser speckle Photography

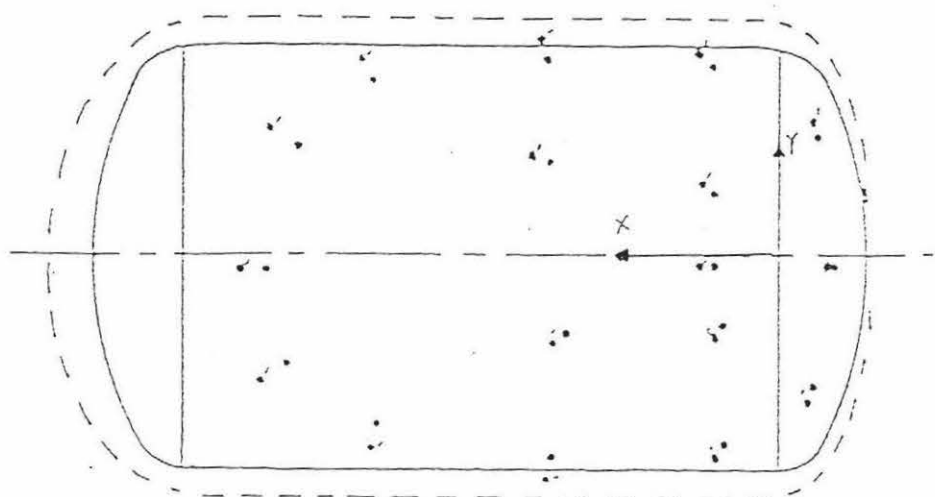


Fig.6.15 Expected displacement directions for speckle pairs

These results have been calculated

using the following formulas:

$$\delta = \frac{D\lambda}{\Delta} \quad (47)$$

$$D = 348 \text{ mm}$$

$$\lambda = 6320 \times 10^{-10} \text{ mm}$$

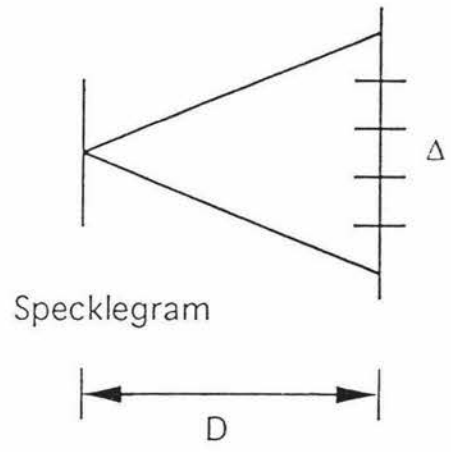


Fig.6.16

where λ is wave length of the coherent light source (He-Ne laser in this case), δ is the principal displacement, D and Δ can be measured.

6.7 Comparison of displacements and stresses determined by FEM , LSP and the pressure vessel design formulas

1. Comparison of displacements determined by Finite Element Method and Laser Speckle Photography

The node No.1 from the LSP has data as follows:

Fringe spacing $\Delta=4.16 \text{ mm}$

Displacement of point from fixed end $x=21.25 \text{ mm}$

Displacement of point from central axis $y=50.0 \text{ mm}$

Actual displacement $\delta=5.29 \times 10^5 \text{ m}$

The points from FEM that relate to No.1(from LSP) are:

No.1504

Displacement in x-direction $x=6.53188 \times 10^{-3} \text{ mm}$

Displacement in y-direction	$y=3.67331E-3mm$
Displacement in z-direction	$z=63.4507E-3mm$
Actual displacement	$\delta = \sqrt{x^2 + y^2 + z^2} = 6.389 \times 10^{-5} m$

No.1582

Displacement in x-direction	$x=3.14414E-3mm$
Displacement in y-direction	$y=1.78281E-3mm$
Displacement in z-direction	$z=69.2859E-3mm$
Actual displacement	$\delta = \sqrt{x^2 + y^2 + z^2} = 6.938 \times 10^{-5} m$

No. 1586

Displacement in x-direction	$x=2.05417E-3mm$
Displacement in y-direction	$y=2.05417E-3mm$
Displacement in z-direction	$z=68.3227E-3mm$
Actual displacement	$\delta = \sqrt{x^2 + y^2 + z^2} = 6.834 \times 10^{-5} m$

No.1646

Displacement in x-direction	$x=3.29072E-3mm$
Displacement in y-direction	$y=1.90765E-3mm$
Displacement in z-direction	$z=69.3958E-3mm$
Actual displacement	$\delta = \sqrt{x^2 + y^2 + z^2} = 6.949 \times 10^{-5} m$

The node **No.2** from LSP has the data as follows:

Fringe spacing	$\Delta=4.13mm$
Displacement of point from fixed end	$x=102.5mm$

Displacement of point from central axis	$y=47.5\text{mm}$
Actual displacement	$\delta=5.33\times10^{-5}\text{m}$

The points from FEM that relate to No.2 (from LSP) are:

No.1253

Displacement in x-direction	$x=48.0760\text{E-3mm}$
Displacement in y-direction	$y=27.7416\text{E-3mm}$
Displacement in z-direction	$z=66.4185\text{E-3mm}$
Actual displacement	$\delta = \sqrt{x^2 + y^2 + z^2} = 8.655 \times 10^{-5}\text{m}$

No. 1340

Displacement in x-direction	$x=47.8214\text{E-3mm}$
Displacement in y-direction	$y=27.5781\text{E-3mm}$
Displacement in z-direction	$z=65.4716\text{E-3mm}$
Actual displacement	$\delta = \sqrt{x^2 + y^2 + z^2} = 8.536 \times 10^{-5}\text{m}$

The node **No. 3** from the LSP has the data as follows:

Fringe spacing	$\Delta=4.43\text{mm}$
Displacement of point from fixed end	$x=105.0\text{mm}$
Displacement of point from central axis	$y=8.75\text{mm}$
Actual displacement	$\delta=4.96 \times 10^{-5}\text{m}$

The points from FEM that relate to No.3 (from LSP) are:

No.1240

Displacement in x-direction	$x=55.3683\text{E-3mm}$
Displacement in y-direction	$y=0\text{mm}$

Displacement in z-direction	$z=67.2497E-3mm$
Actual displacement	$\delta = \sqrt{x^2 + y^2 + z^2} = 8.711 \times 10^{-5} m$

No.1327

Displacement in x-direction	$x=55.0567E-3mm$
Displacement in y-direction	$y=0mm$
Displacement in z-direction	$z=66.3758E-3mm$
Actual displacement	$\delta = \sqrt{x^2 + y^2 + z^2} = 8.623 \times 10^{-5} m$

The Node **No.4** from the LSP has the data as follows:

Fringe spacing	$\Delta = 5.0mm$
Displacement of point from fixed end	$x=102.5mm$
Displacement of point from central axis	$y=-45.0mm$
Actual displacement	$\delta = 4.40 \times 10^{-5} m$

The model in Finite Element Method only considered 1/4 of the model in Laser Speckle Photography, so it can't include the same point (No.4). Therefore, the points whose co-ordinates are $x=102.5mm$, $y=45.0mm$ is taken as relative points.

No.1249

Displacement in x-direction	$x=53.4644E-3mm$
Displacement in y-direction	$y=14.3087E-3mm$
Displacement in z-direction	$z=66.9258E-3mm$
Actual displacement	$\delta = \sqrt{x^2 + y^2 + z^2} = 8.684 \times 10^{-5} m$

No.1336

Displacement in x-direction	x=53.1656E-3mm
Displacement in y-direction	y=14.2289E-3mm
Displacement in z-direction	z=66.0276E-3mm
Actual displacement	$\delta = \sqrt{x^2 + y^2 + z^2} = 8.594 \times 10^{-5} \text{m}$

2. Comparison of stresses determined by Finite Element Method and the pressure vessel design formulas

The maximum axial stress determined from Finite Element Method is:

For CYLINDRICAL SHELL

$$\sigma_{x(\max.)} = 114.32E + 06N/m^2$$

$$\sigma_{y(\max.)} = 114.32E + 06N/m^2$$

$$\sigma_{axial(\max.)} = \sqrt{\sigma_{x(\max.)}^2 + \sigma_{y(\max.)}^2} = \sqrt{(114.32 \times 10^6)^2 + (114.32 \times 10^6)^2} = 161.67 \times 10^6 N/m^2$$

The maximum stress determined from pressure vessel design formulas are:

For CYLINDRICAL SHELL:

$$\sigma_1 = \frac{P(R + 0.6t)}{Jt} = \frac{1300000(0.128 + 0.6 \times 0.0016)}{0.65 \times 0.0016} = 161.2 \times 10^6 N/m^2$$

for ASME FLANGED AND DISHED HEAD:

$$\sigma_2 = \frac{P(0.885L + 0.1t)}{Jt} = \frac{1300000(0.885 \times 0.42 + 0.1 \times 0.004)}{0.65 \times 0.004} = 186.05 \times 10^6 N/m^2$$

7 Conclusion

The results from the Finite Element Method have been compared with results from Laser Speckle Photography and pressure vessel design formulas.

From the comparison of displacements, it was found that the displacements from Finite Element Method are slightly larger than from Laser Speckle Photography. The reason is that the displacements from Laser Speckle Photography were calculated on a 2-dimensional coordinate system and the displacements from Finite Element Method were on a 3-dimensional system. They are still quite similar.

From the comparison of stresses, it was found that the stresses from Finite Element Method and from pressure vessel design formulas are in good agreement.

From Figure 6.1, It was found that the deformation of the pressure vessel follows that expected from the design calculations.

The results from FEM, LSP and pressure vessel design formulas are in good agreement. Thus it is reasonable to believe that results from the Finite Element Method are realistic for the pressure vessel.

The Finite Element Method , in conjunction with automatic computation, constitutes a very effective and elegant device for accurately solving

complex physical and engineering problems. Its advantageous properties as compared with other methods are as follows:

1. Any continuous quantity such as pressure, displacements, stresses, strain etc. can be approximated by a discrete model composed of a set of piecewise continuous functions defined over a finite number of subdomains.
2. Solution of the stresses, deformation and displacements can be obtained directly at any continuous point, and the distribution of stresses and deformation can be shown directly by contour plotting and deformation graphs.
3. The Finite Element Method, as compared with Laser Speckle Photography, can provide a more complete representation of 3-Dimensional displacement and stress components as well as deformation shape.
4. However the Finite Element Method requires experimental confirmation and Laser Speckle Photography is an ideal technique for providing them.

8 Thoughts on further work

Finite Element Method was used to solve the Stress/strain situation in a small pressure vessel. It was an example of how the method can be implemented . A linear static analysis was made. The results from Finite Element Method were compared with the results from Speckle Photography Method and this is where future work should lie. Both Holographic Interferometry and Speckle Photography need some form of theoretical back-up.

The Finite Element Method is a powerful technique for obtaining numerical solutions to engineering and physics related problems. Since its appearance, it has been applied to many areas, such as linear static, linear dynamic, nonlinear and heat transfer analysis on two-, and three-dimensional structural and thermal models, etc.

Finite element analysis by computer may encompass many applications. The LUSAS program is highly interactive. Its application in the Department of Production Technology has showed that its results are an approximation to the real case. Advanced studies of the finite element technique are required to give more confidant results.

Research and development in both the theory and application of the finite element technique are continually ongoing. The current research is focused on developing the nonlinear analysis, dynamic's response, etc. Further research into respective areas will reveal significantly more complex and difficult problems . The present work highlights a different

area that is the application of fea and its comparison with practical techniques.

The pressure vessel has been analysed by means of the Finite Element Method and Laser Speckle Photography. The application of Laser and White-light Speckle Photography in the Department of Production Technology has been ongoing for a few years and this work has proven that the method of Finite Element Analysis can be used to establish the applicability of other practical methods. However, research work is needed to involve different light sources. For solving three-dimensional displacement, it is necessary to introduce the Holographic technique. It is also felt that both fea and the optical method can be used to extend research to more complex and particular problems.

9 References:

- (1) Clough, R. W. "*The finite element method in plane stress analysis.*" Proc. 2nd ASCE conf. Electronic computations, ASCE. Pittsburgh, P.A. (1960)
- (2) Argyris, J. H. "*Recent Advances in Matrix Methods of Structural Analysis.*" Pergamon Press. Elmsford, N.Y. (1954)
- (3) Turner, M., Clough, R. W., Martin, H., & Topp, L. "*Stiffness and Deflection of Complex Structures.*" J. Aero Sci. 23 (1956), pp.805-823
- (4) Melosh, R. J. "*Basis for derivation of Matrices for the Direct Stiffness Method.*" Journal American Institute for Aeronautics and Astronautics, 1 (1965), pp. 1631-1637
- (5) Zienkiewicz, O. C ., & Cheung, Y. K. "*Finite Elements in the Solution of Field Problems.*" The Engineer 220 (1965), pp.507-510
- (6) Huebner, K. H. "*Finite Element Method for engineers.*" John Wiley & Sons, New York. (1975)
- (7) Heuser, J. "*Finite Element Method for Thermal Analysis.*" NASA Technical Note Goddard Space Flight Center, Greenbelt, Md. TN. (1972)
- (8) Martin, H. C. "*Finite Element Analysis of Fluid Flow.*" Proc. 2nd Conf. Matrix Methods in Structural Mechanics, Wright Pattern Air Force Base, Dayton, Ohio. (1968)
- (9) Finlayson, B. A. "*The Method of Weighted Residuals and Variational Principles.*" Academic Press, New York. (1972)
- (10) Desai, C. S. "*Elementary Finite Element Method.*" Prentice-hall, Inc. Englewood Cliffs, N.J.(1979)
- (11) Becker, E. G., Carey, G. F., & Oden, J. T. "*Finite Elements, An Introduction.*" Prentice-Hall, Inc. Englewood Cliffs, N.J. (1981)
- (12) Flecher, C. A. J. "Computational Galerkin Methods. ' Springer-Verlag, Berlin. (1984)
- (13) Reddy, J.N. " *An Introduction to the Finite Element Method.*" McGraw-Hill Book Company, New York. (1984)
- (14) Segerlind, L.J. "*Applied Finite Element Analysis.*" John Wiley & Sons, New York. (1984)
- (15) Hughes, T. J. R. "*The Finite Element Method .*" Prentice-Hill, Inc., Englewood Cliffs, N.J. (1987)

- (16) Bickford, W. B. " *A First course in the Finite Element Method.* " Richard D. Irwin, Inc., Homewood, Ill. (1990)
- (17) Zienkiewicz, O. C. & Taylor, R. L. " *The Finite Element Method.* " McGraw-Hill Book Company. Maidenhead, Uk. (1989)
- (18) Johnson, C. " *Numerical Solution of Partial Differential Equations by the Finite Element Method.*" Cambridge University Press. Cambridge, UK. (1987)
- (19) Smith, I. M. " *Programming the Finite Element Method.* " John Wiley & Sons, New York. (1982)
- (20) Owen, D. R. J., & Hinton, E. " *A Simple Guide for Finite Elements.*" Prineridge Press Limited . Swansea, UK. (1980)
- (21) Rayleigh, J. W. S. " *Theory of Sound, 1st rev. ed.* " Dover Publishers. N.Y. (1877)
- (22) Ritz, W. " *Über eine Neue Methode zur Lösung Gewisses Variations-Probleme der Mathematischen Physik.*" J. Reine Angew. Math. 135 (1909), pp.1-61
- (23) Galerkin, B. G. " *Series Occurring in Some Problems of Elastic Stability of Rods and Plates.*" Eng. Bull. 19 (1915), pp.897-908
- (24) Burch, J. M. & Tokarski, T. M. J. " *Production of multiple beam fringes from photographic scatters.*" Opt Acta, 15 (1968), pp.101-111
- (25) Archbold, E. & Ennos, A. E. " *Displacement measurement from double-exposure laser photographys.* " Opt Acta, 19 (1972), pp.253-271
- (26) Leendertz, J.A. " *A double exposure technique for speckle pattern interferometry*". J.Phys. E 4 (1971), pp.277
- (27) Burch, J. M. & Forno, C. " *A High Sensitivity More Grid Technique for Studing Deformation in Lager Objects.* " Opt Engin, 14 (1975), pp. 178-185
- (28) Boone, P. M., & De Backer, L. C. " *Speckle methods using photography and reconstruction in incoherent light.* " Optik, 44 (1976), pp. 343-355
- (29) Asundi, a., & Chiang, F. P. " *Theory and applications of the white light speckle method for strain analysis.* " Opt Engin, 21 (1982), pp.570-580
- (30) Verdet, E: Ann. scientif. 1' Ecole Normale Supérieure 2 (1865), pp.291; Strutt, J.W. (Lord Rayleigh): Phil. Mag. 10 (1880) ,pp.73

- (31) Laue, M. von: Sitzungsber.Akad.Wiss. 44 (1914), pp.1144; Laue, M. von: Mitt.Physik Ges. 18 (1916), pp.90; Laue, M. von: Verhandl. Deut. Phys. Ges. 19 (1917), pp.19
- (32) Cloud, G., & Conley, E. "A whole-field interferometric scheme for measuring strain and flow rates of Glacier and other natural surface." J Glaciol, 29 (1983), pp.492-497
- (33) Smith, E. W., & North, H. " Sunlight Speckle Phitography." 4th International Conf. on Holographic Systems. Neuchatel, Switzerland. (1993)
- (34) Hinton, E., & Owen, D. R. J. " An Introduction to Finite Element Computations. " Pineridge Press Limited. Swansea, UK. (1979)
- (35) Hendel, H. " Laser Speckle Photography applied to Stress Analysis." M. Tech Thesis, Massey university, Palmerston North. (1992)
- (36) Zienkiewicz, O. C. " The Finite Element method. " McGraw-Hill Book Company. UK. (1988)
- (37) Megyesy, E. F. " Pressure Vessel Handbook. ' Publishing Inc. Tulsa, Oklahpma. (1973)

10 Index

Fig.1.1 Optical arrangement for double exposure Laser Speckle Photography	5
Fig.1.2 Example of an enlarge speckle pattern	5
Fig.1.3 Point-by-Point filtering set-up	6
Fig.1.4 Full field filtering set-up	7
Fig.3.1 A finite element computational model	12
Fig.3.2 The relationship between MYSTRO and LUSAS	17
Fig.4.1 Pressure vessel model	18
Fig.4.2.1 Lines	20
Fig.4.2.2 Surfaces	21
Fig.4.2.3 Volumes	22
Fig.4.3 A quarter of the stiffness ring	23
Fig.4.4 Local and global co-ordinates	24
Fig.4.5.1 Side view mesh of a quarter of the pressure vessel	29
Fig.4.5.2 End view mesh of a quarter of the pressure vessel	30
Fig.4.6 Loading at two end sides	40
Fig.4.7 Mesh, support and loading	43
Fig.6.1 The deformed mesh is superimposed over the original mesh	57
Fig.6.2 Direct stress in x direction	65
Fig.6.3 Direct stress in y direction	66
Fig.6.4 Direct stress in z direction	67
Fig.6.5 Shear stress in xy direction	68
Fig.6.6 Shear stress in yz direction	69
Fig.6.7 Shear stress in xz direction	70
Fig.6.8 Major principal stress	71
Fig.6.9 Intermediate principal stress	72
Fig.6.10 Minor principal stress	73
Fig.6.11 Maximum shear stress	74
Fig.6.12 Equivalent stress	75
Fig.6.13 The position of some important nodes	76

Fig.6.15 Expected displacement directions for speckle pairs	79
Fig.6.16 The relationship between D and	80
Table 4.1 Summary of loading types and components	32
Table 4.2 Material property type numbers	33
Table 5.1 A example of CONFIG.FIL	48
Table 5.2 MYSTRO plotsize	50
Table 6.1 Displacements at nodes	55
Table 6.2 Direct and shear stresses in element	62
Table 6.3 The displacements from Laser Speckle Photography	78

APPENDICES

Appendix I

EQUILIBRIUM

Equilibrium arguments are used to relate the stresses in the structure to applied forces.

Generally, the internal stresses in a structure are integrated to form internal forces at discrete points or nodes.

Similarly, the applied loading is converted to external forces applied at the same discrete points.

Then for equilibrium, the sum of the internal and external forces must be zero.

In dynamic analyses, the internal force due to the stresses will be supplemented by the inertia and damping forces.

COMPATABILITY

Compatibility arguments are used to relate strains to displacements and also displacements between discrete sections of the structure i.e. members or elements.

The strain-displacement relationship is dependent upon the definition of strain and on the type of deformation and geometry of a particular structure.

The inter-element compatibility condition ensures that all sections of a structure connected to a discrete point deform by the correct amount, so that no gaps appear in the structure.

STRESS STRAIN LAW

A 'constitutive relationship' that relates the stress to the strain is required.

The constitutive relationship may often be approximated as being linear for many structural materials within their useful working range e.g. ferrous materials.

Nonlinear constitutive relationships may be required for some materials e.g. creep analysis, or for ultimate load analysis of structures e.g. plastic collapse loads of frame structures.

Appendix II

N O D E C O O R D I N A T E S

NODE NO.	COORDINATE IN X-DIRECTION	COORDINATE IN Y-DIRECTION	COORDINATE IN Z-DIRECTION
1	0.228879E-13	128.000	-0.228879E-13
2	0.246227E-13	129.600	-0.246227E-13
5	128.000	0.228879E-13	0.299760E-14
6	33.1288	123.639	-0.235124E-13
7	64.0000	110.851	-0.217673E-13
8	90.5097	90.5097	-0.128439E-13
9	110.851	64.0000	-0.792422E-14
10	123.639	33.1288	0.209555E-14
17	129.600	0.246227E-13	0.658848E-14
19	33.5429	125.184	-0.208306E-13
20	64.8000	112.237	-0.119384E-13
21	91.6410	91.6410	-0.183083E-13
22	112.237	64.8000	-0.336189E-14
23	125.184	33.5429	-0.207126E-14
35	0.258543E-13	128.000	340.000
36	0.275890E-13	129.600	340.000
39	128.000	-0.320299E-13	340.000
40	33.1288	123.639	340.000
41	64.0000	110.851	340.000
42	90.5097	90.5097	340.000
43	110.851	64.0000	340.000
44	123.639	33.1288	340.000
51	129.600	-0.418970E-13	340.000
53	33.5429	125.184	340.000
54	64.8000	112.237	340.000
55	91.6410	91.6410	340.000
56	112.237	64.8000	340.000
57	125.184	33.5429	340.000
69	0.240676E-13	128.000	30.9091
70	0.269472E-13	128.000	61.8182
71	0.235645E-13	128.000	92.7273
72	0.213594E-13	128.000	123.636
73	0.245828E-13	128.000	154.545
74	0.300419E-13	128.000	185.455
75	0.236824E-13	128.000	216.364
76	0.330257E-13	128.000	247.273
77	0.147833E-13	128.000	278.182
78	0.364361E-13	128.000	309.091
90	128.000	0.183291E-13	30.9091
91	128.000	0.125750E-13	61.8182
92	128.000	0.741854E-14	92.7273
93	128.000	0.772319E-15	123.636
94	128.000	-0.504891E-14	154.545
95	128.000	-0.805085E-14	185.455
96	128.000	-0.155067E-13	216.364
97	128.000	-0.217638E-13	247.273
98	128.000	-0.297193E-13	278.182
99	128.000	-0.236651E-13	309.091
111	123.775	33.1260	30.9091
112	123.775	33.1260	61.8182
113	123.775	33.1260	92.7273
114	123.775	33.1260	123.636
115	123.775	33.1260	154.545
116	123.775	33.1260	185.455
117	123.775	33.1260	216.364
118	123.775	33.1260	247.273
119	123.775	33.1260	278.182
120	123.775	33.1260	309.091
121	110.913	63.9936	30.9091
122	110.913	63.9936	61.8182
123	110.913	63.9936	92.7273
124	110.913	63.9936	123.636
125	110.913	63.9936	154.545
126	110.913	63.9936	185.455
127	110.913	63.9936	216.364
128	110.913	63.9936	247.273
129	110.913	63.9936	278.182
130	110.913	63.9936	309.091
131	90.5097	90.5097	30.9091
132	90.5097	90.5097	61.8182
133	90.5097	90.5097	92.7273
134	90.5097	90.5097	123.636
135	90.5097	90.5097	154.545
136	90.5097	90.5097	185.455
137	90.5097	90.5097	216.364
138	90.5097	90.5097	247.273

139	90.5097	90.5097	278.182
140	90.5097	90.5097	309.091
141	63.9936	110.913	30.9091
142	63.9936	110.913	61.8182
143	63.9936	110.913	92.7273
144	63.9936	110.913	123.636
145	63.9936	110.913	154.545
146	63.9936	110.913	185.455
147	63.9936	110.913	216.364
148	63.9936	110.913	247.273
149	63.9936	110.913	278.182
150	63.9936	110.913	309.091
151	33.1260	123.775	30.9091
152	33.1260	123.775	61.8182
153	33.1260	123.775	92.7273
154	33.1260	123.775	123.636
155	33.1260	123.775	154.545
156	33.1260	123.775	185.455
157	33.1260	123.775	216.364
158	33.1260	123.775	247.273
159	33.1260	123.775	278.182
160	33.1260	123.775	309.091
276	0.258057E-13	129.600	30.9091
277	0.286837E-13	129.600	61.8182
278	0.253001E-13	129.600	92.7273
279	0.241204E-13	129.600	123.636
280	0.273444E-13	129.600	154.545
281	0.201748E-13	129.600	185.455
282	0.254172E-13	129.600	216.364
283	0.231620E-13	129.600	247.273
284	0.247233E-13	129.600	278.182
285	0.381709E-13	129.600	309.091
297	129.600	0.200708E-13	30.9091
298	129.600	0.114110E-13	61.8182
299	129.600	0.625368E-14	92.7273
300	129.600	0.117712E-14	123.636
301	129.600	-0.518856E-14	154.545
302	129.600	-0.921659E-14	185.455
303	129.600	-0.137720E-13	216.364
304	129.600	-0.258266E-13	247.273
305	129.600	-0.255802E-13	278.182
306	129.600	-0.335322E-13	309.091
318	125.323	33.5401	30.9091
319	125.323	33.5401	61.8182
320	125.323	33.5401	92.7273
321	125.323	33.5401	123.636
322	125.323	33.5401	154.545
323	125.323	33.5401	185.455
324	125.323	33.5401	216.364
325	125.323	33.5401	247.273
326	125.323	33.5401	278.182
327	125.323	33.5401	309.091
328	112.300	64.7936	30.9091
329	112.300	64.7936	61.8182
330	112.300	64.7936	92.7273
331	112.300	64.7936	123.636
332	112.300	64.7936	154.545
333	112.300	64.7936	185.455
334	112.300	64.7936	216.364
335	112.300	64.7936	247.273
336	112.300	64.7936	278.182
337	112.300	64.7936	309.091
338	91.6410	91.6410	30.9091
339	91.6410	91.6410	61.8182
340	91.6410	91.6410	92.7273
341	91.6410	91.6410	123.636
342	91.6410	91.6410	154.545
343	91.6410	91.6410	185.455
344	91.6410	91.6410	216.364
345	91.6410	91.6410	247.273
346	91.6410	91.6410	278.182
347	91.6410	91.6410	309.091
348	64.7936	112.300	30.9091
349	64.7936	112.300	61.8182
350	64.7936	112.300	92.7273
351	64.7936	112.300	123.636
352	64.7936	112.300	154.545
353	64.7936	112.300	185.455
354	64.7936	112.300	216.364
355	64.7936	112.300	247.273
356	64.7936	112.300	278.182
357	64.7936	112.300	309.091
358	33.5401	123.323	30.9091
359	33.5401	123.323	61.8182

360	33.5401	125.323	92.7273
361	33.5401	125.323	123.636
362	33.5401	125.323	154.545
363	33.5401	125.323	185.455
364	33.5401	125.323	216.364
365	33.5401	125.323	247.273
366	33.5401	125.323	278.182
367	33.5401	125.323	309.091
503	0.270894E-13	128.000	-160.000
504	0.259237E-13	129.600	-160.000
513	128.000	0.533046E-13	-160.000
521	129.600	0.550393E-13	-160.000
564	0.267911E-13	132.000	340.000
572	132.000	-0.310932E-13	340.000
587	0.248898E-13	128.000	379.000
588	0.292266E-13	132.000	379.000
597	132.000	-0.428060E-13	379.000
605	128.000	-0.355480E-13	379.000
648	0.198175E-13	132.000	-160.000
656	132.000	0.460326E-13	-160.000
671	0.251466E-13	128.000	-199.000
673	128.000	0.568157E-13	-199.000
681	0.178746E-13	132.000	-199.000
689	132.000	0.611525E-13	-199.000
732	-0.228983E-14	20.0000	408.500
745	0.252159E-13	20.0000	404.500
765	20.0000	-0.841549E-13	408.500
778	20.0000	-0.633937E-13	404.500
814	0.140651E-13	20.0000	-228.500
827	0.839606E-15	20.0000	-224.500
847	20.0000	0.526384E-13	-228.500
860	20.0000	0.434999E-13	-224.500
896	0.121275E-13	79.6000	0.800000
898	56.3000	56.3000	0.800000
945	79.6000	0.144017E-13	0.800000
968	91.6400	91.6400	0.800000
1004	0.167123E-13	79.6000	-0.800000
1006	56.3000	56.3000	-0.800000
1030	0.175693E-13	129.000	-1.60000
1039	91.6400	91.6400	-0.800000
1125	128.000	0.188217E-13	-1.60000
1149	79.6000	0.144381E-13	-0.800000
1200	33.1288	123.639	-160.000
1201	64.0000	110.851	-160.000
1202	90.5097	90.5097	-160.000
1203	110.851	64.0000	-160.000
1204	123.639	33.1288	-160.000
1212	33.5429	125.184	-160.000
1213	64.8000	112.237	-160.000
1214	91.6410	91.6410	-160.000
1215	112.237	64.8000	-160.000
1216	125.184	33.5429	-160.000
1228	0.222634E-13	128.000	-32.0000
1229	0.240433E-13	128.000	-64.0000
1230	0.126982E-13	128.000	-96.0000
1231	0.270339E-13	128.000	-128.000
1237	128.000	0.280080E-13	-32.0000
1238	128.000	0.355341E-13	-64.0000
1239	128.000	0.332541E-13	-96.0000
1240	128.000	0.457759E-13	-128.000
1246	123.775	33.1260	-32.0000
1247	123.775	33.1260	-64.0000
1248	123.775	33.1260	-96.0000
1249	123.775	33.1260	-128.000
1250	110.913	63.9936	-32.0000
1251	110.913	63.9936	-64.0000
1252	110.913	63.9936	-96.0000
1253	110.913	63.9936	-128.000
1254	90.5097	90.5097	-32.0000
1255	90.5097	90.5097	-64.0000
1256	90.5097	90.5097	-96.0000
1257	90.5097	90.5097	-128.000
1258	63.9936	110.913	-32.0000
1259	63.9936	110.913	-64.0000
1260	63.9936	110.913	-96.0000
1261	63.9936	110.913	-128.000
1262	33.1260	123.775	-32.0000
1263	33.1260	123.775	-64.0000
1264	33.1260	123.775	-96.0000
1265	33.1260	123.775	-128.000
1315	0.181972E-13	129.600	-32.0000
1316	0.257780E-13	129.600	-64.0000
1317	0.363198E-14	129.600	-96.0000
1318	0.258682E-13	129.600	-128.000

1324	129.600	0.297436E-13	-32.0000
1325	129.600	0.372688E-13	-64.0000
1326	129.600	0.283801E-13	-96.0000
1327	129.600	0.475106E-13	-128.000
1333	125.323	33.5401	-32.0000
1334	125.323	33.5401	-64.0000
1335	125.323	33.5401	-96.0000
1336	125.323	33.5401	-128.000
1337	112.300	64.7936	-32.0000
1338	112.300	64.7936	-64.0000
1339	112.300	64.7936	-96.0000
1340	112.300	64.7936	-128.000
1341	91.6410	91.6410	-32.0000
1342	91.6410	91.6410	-64.0000
1343	91.6410	91.6410	-96.0000
1344	91.6410	91.6410	-128.000
1345	64.7936	112.300	-32.0000
1346	64.7936	112.300	-64.0000
1347	64.7936	112.300	-96.0000
1348	64.7936	112.300	-128.000
1349	33.5401	125.323	-32.0000
1350	33.5401	125.323	-64.0000
1351	33.5401	125.323	-96.0000
1352	33.5401	125.323	-128.000
1411	34.1641	127.502	340.000
1412	66.0000	114.315	340.000
1413	93.3381	93.3381	340.000
1414	114.315	66.0000	340.000
1415	127.502	34.1641	340.000
1429	34.1641	127.502	379.000
1430	66.0000	114.315	379.000
1431	93.3381	93.3381	379.000
1432	114.315	66.0000	379.000
1433	127.502	34.1641	379.000
1441	33.1288	123.639	379.000
1442	64.0000	110.851	379.000
1443	90.5097	90.5097	379.000
1444	110.851	64.0000	379.000
1445	123.639	33.1288	379.000
1472	34.1641	127.502	-160.000
1473	66.0000	114.315	-160.000
1474	93.3381	93.3381	-160.000
1475	114.315	66.0000	-160.000
1476	127.502	34.1641	-160.000
1489	33.1288	123.639	-199.000
1490	64.0000	110.851	-199.000
1491	90.5097	90.5097	-199.000
1492	110.851	64.0000	-199.000
1493	123.639	33.1288	-199.000
1501	34.1641	127.502	-199.000
1502	66.0000	114.315	-199.000
1503	93.3381	93.3381	-199.000
1504	114.315	66.0000	-199.000
1505	127.502	34.1641	-199.000
1532	0.150435E-13	49.1412	-226.555
1533	0.738298E-14	77.8254	-220.756
1534	0.819483E-14	104.787	-209.658
1540	0.909689E-14	47.8964	-222.741
1541	0.954792E-14	75.3306	-217.299
1542	0.112965E-13	101.262	-207.030
1550	47.8964	0.463726E-13	-222.741
1551	75.3306	0.563716E-13	-217.299
1552	101.262	0.571973E-13	-207.030
1558	49.1412	0.473649E-13	-226.555
1559	77.8254	0.445338E-13	-220.756
1560	104.787	0.445963E-13	-209.658
1568	5.16384	19.3060	-228.165
1569	9.97958	17.3001	-227.954
1570	14.1190	14.1190	-227.862
1571	17.3001	9.97958	-227.954
1572	19.3060	5.16384	-228.165
1579	27.0420	101.219	-209.574
1580	52.2504	90.6346	-209.521
1581	73.9248	73.9248	-209.504
1582	90.6346	58.2204	-209.521
1583	101.219	12.1420	-209.574
1584	19.9704	7.91.21.22	-220.588
1585	38.6016	36.10.0699	-220.483
1586	54.6501	19.4.6501	-220.447
1587	67.0699	36.6016	-220.483
1588	75.0122	19.9704	-220.588
1589	12.6024	41.3564	-226.302
1590	24.3616	42.3365	-226.145
1591	34.4930	34.4930	-226.091

1592	42.3365	24.3616	-226.145
1593	47.3564	12.6024	-226.302
1632	5.16384	19.3060	-224.165
1633	9.97958	17.3001	-223.954
1634	14.1190	14.1190	-223.882
1635	17.3001	9.97958	-223.954
1636	19.3060	5.16384	-224.165
1643	26.1802	97.3831	-206.945
1644	50.5793	87.6893	-206.893
1645	71.5456	71.5456	-206.875
1646	87.6893	50.5793	-206.893
1647	97.3831	26.1802	-206.945
1648	19.3765	72.6867	-217.132
1649	37.4485	65.0265	-217.027
1650	53.0048	53.0048	-216.991
1651	65.0265	37.4485	-217.027
1652	72.6867	19.3765	-217.132
1653	12.3052	46.1890	-222.489
1654	23.7843	41.3120	-222.331
1655	33.6688	33.6688	-222.278
1656	41.3120	23.7843	-222.331
1657	46.1890	12.3052	-222.489
1701	-0.138778E-15	49.1412	406.555
1702	0.260625E-13	77.8254	400.756
1703	0.435138E-13	104.787	389.658
1708	0.112410E-14	47.8964	402.741
1709	0.727890E-14	75.3506	397.299
1710	0.310169E-13	101.262	387.030
1719	5.16384	19.3060	408.165
1720	9.97958	17.3001	407.954
1721	14.1190	14.1190	407.882
1722	17.3001	9.97958	407.954
1723	19.3060	5.16384	408.165
1731	5.16384	19.3060	404.165
1732	9.97958	17.3001	403.954
1733	14.1190	14.1190	403.882
1734	17.3001	9.97958	403.954
1735	19.3060	5.16384	404.165
1747	49.1412	-0.813238E-13	406.555
1748	77.8254	-0.674183E-13	400.756
1749	104.787	-0.4556718E-13	389.658
1754	47.8964	-0.622211E-13	402.741
1755	75.3506	-0.5554626E-13	397.299
1756	101.262	-0.448322E-13	387.030
1764	27.0420	101.219	389.574
1765	52.2504	90.6346	389.521
1766	73.9248	73.9248	389.504
1767	90.6346	52.2504	389.521
1768	101.219	27.0420	389.574
1769	19.9704	75.3122	400.588
1770	38.6016	67.0699	400.483
1771	54.6501	54.6501	400.447
1772	67.0699	38.6016	400.483
1773	75.0122	19.9704	400.588
1774	12.6024	47.3564	406.302
1775	24.3616	42.3365	406.145
1776	34.4930	34.4930	406.091
1777	42.3365	24.3616	406.145
1778	47.3564	12.6024	406.302
1817	12.3052	46.1890	402.489
1818	23.7843	41.3120	402.331
1819	33.6688	33.6688	402.278
1820	41.3120	23.7843	402.331
1821	46.1890	12.3052	402.489
1822	19.3765	72.6867	397.132
1823	37.4485	65.0265	397.027
1824	53.0048	53.0048	396.991
1825	65.0265	37.4485	397.027
1826	72.6867	19.3765	397.132
1827	26.1802	97.3831	386.945
1828	50.5793	87.6893	386.893
1829	71.5456	71.5456	386.875
1830	87.6893	50.5793	386.893
1831	97.3831	26.1802	386.945
1927	111.657	64.6334	0.414812
1928	124.055	33.3858	0.142027
2009	20.6057	76.3944	0.300000
2010	33.3087	68.3471	0.300000
2015	33.3858	124.055	0.142027
2016	64.6334	111.657	0.414812
2045	20.6057	76.3944	-0.300000
2047	33.3087	68.3471	-0.300000
2052	33.3858	124.055	-1.45797
2053	64.6334	111.657	-1.18519

2074	68.9471	39.3087	0.800000
2075	76.8944	20.6057	0.800000
2082	111.657	64.6334	-1.18519
2083	124.055	33.3358	-1.45797
2088	68.9471	39.3087	-0.800000
2089	76.8944	20.6057	-0.800000

MATERIAL PROPERTIES

MATERIAL

$E = 0.2000E+06$ $\nu = 0.3000$ $\rho = 7.7028E-05$ $\alpha = 1.1000E-05$
 $\text{ARAYL} = 0.0000E+00$ $\text{BRAYL} = 0.0000E+00$
 $\text{TEMP} = 17$

DATA STORAGE LOCATIONS USED = 13

MATERIAL ASSIGNMENTS

FIRST ELEMENT	LAST ELEMENT	DIFFERENCE	MATERIAL SET
---------------	--------------	------------	--------------

239	304	1	1
759	788	1	1
841	846	1	1
899	904	1	1
1113	1136	1	1
997	1020	1	1
1285	1287	1	1
1319	1321	1	1

TOTAL NUMBER OF MATERIAL ASSIGNMENT SETS = 8
 TOTAL NUMBER OF ELEMENTS = 162
 LARGEST ELEMENT NUMBER = 1321
 LARGEST MATERIAL ASSIGNMENT SET NUMBER = 1

DATA STORAGE LOCATIONS USED = 33

SUPPORT NODES

F=FREE

R=RESTRAINED OR RESTRAINED WITH PRESCRIBED DISPLACEMENT

S=SPRING

FIRST NODE	LAST NODE	DIFF R NCE	SUPPORT	SUPPORT	SUPPORT	SUPPORT
			CONDITION	CONSTANT	CONSTANT	CONSTANT
			/	/	/	/
1	0	0	R F F	0.000000E+00	0.000000E+00	0.000000E+00
2	0	0	R F F	0.000000E+00	0.000000E+00	0.000000E+00
5	0	0	R R R	0.000000E+00	0.000000E+00	0.000000E+00
17	0	0	R R R	0.000000E+00	0.000000E+00	0.000000E+00
35	0	0	R R R	0.000000E+00	0.000000E+00	0.000000E+00
36	0	0	R R R	0.000000E+00	0.000000E+00	0.000000E+00
39	0	0	R R R	0.000000E+00	0.000000E+00	0.000000E+00
51	0	0	R R R	0.000000E+00	0.000000E+00	0.000000E+00
69	0	0	R R R	0.000000E+00	0.000000E+00	0.000000E+00
70	0	0	R R R	0.000000E+00	0.000000E+00	0.000000E+00
71	0	0	R R R	0.000000E+00	0.000000E+00	0.000000E+00
72	0	0	R R R	0.000000E+00	0.000000E+00	0.000000E+00
73	0	0	R R R	0.000000E+00	0.000000E+00	0.000000E+00
74	0	0	R R R	0.000000E+00	0.000000E+00	0.000000E+00
0.000000E+00	0.000000E+00		R R R	0.000000E+00	0.000000E+00	0.000000E+00
75	0	0	R R R	0.000000E+00	0.000000E+00	0.000000E+00
76	0	0	R R R	0.000000E+00	0.000000E+00	0.000000E+00
77	0	0	R R R	0.000000E+00	0.000000E+00	0.000000E+00
78	0	0	R R R	0.000000E+00	0.000000E+00	0.000000E+00
90	0	0	R R R	0.000000E+00	0.000000E+00	0.000000E+00
91	0	0	R R R	0.000000E+00	0.000000E+00	0.000000E+00
92	0	0	R R R	0.000000E+00	0.000000E+00	0.000000E+00
93	0	0	R R R	0.000000E+00	0.000000E+00	0.000000E+00
94	0	0	R R R	0.000000E+00	0.000000E+00	0.000000E+00
95	0	0	R R R	0.000000E+00	0.000000E+00	0.000000E+00
96	0	0	R R R	0.000000E+00	0.000000E+00	0.000000E+00
97	0	0	R R R	0.000000E+00	0.000000E+00	0.000000E+00

1701	0	0	R F F	0.000000E+00	0.000000E+00	0.000000E+00
1702	0	0	R F F	0.000000E+00	0.000000E+00	0.000000E+00
1703	0	0	R F F	0.000000E+00	0.000000E+00	0.000000E+00
1708	0	0	R F F	0.000000E+00	0.000000E+00	0.000000E+00
1709	0	0	R F F	0.000000E+00	0.000000E+00	0.000000E+00
1710	0	0	R F F	0.000000E+00	0.000000E+00	0.000000E+00
1719	0	0	R R F	0.000000E+00	0.000000E+00	0.000000E+00
1720	0	0	R R F	0.000000E+00	0.000000E+00	0.000000E+00
1721	0	0	R R F	0.000000E+00	0.000000E+00	0.000000E+00
1722	0	0	R R F	0.000000E+00	0.000000E+00	0.000000E+00
1723	0	0	R R F	0.000000E+00	0.000000E+00	0.000000E+00
1731	0	0	R R F	0.000000E+00	0.000000E+00	0.000000E+00
1732	0	0	R R F	0.000000E+00	0.000000E+00	0.000000E+00
1733	0	0	R R F	0.000000E+00	0.000000E+00	0.000000E+00
1734	0	0	R R F	0.000000E+00	0.000000E+00	0.000000E+00
1735	0	0	R R F	0.000000E+00	0.000000E+00	0.000000E+00
1747	0	0	F R F	0.000000E+00	0.000000E+00	0.000000E+00
1748	0	0	F R F	0.000000E+00	0.000000E+00	0.000000E+00
1749	0	0	F R F	0.000000E+00	0.000000E+00	0.000000E+00
1754	0	0	F R F	0.000000E+00	0.000000E+00	0.000000E+00
1755	0	0	F R F	0.000000E+00	0.000000E+00	0.000000E+00
1756	0	0	F R F	0.000000E+00	0.000000E+00	0.000000E+00

TOTAL NUMBER OF SUPPORT NODES = 132
 LARGEST NODE NUMBER = 1756

DATA STORAGE LOCATIONS USED = 924

LOAD CASE 1

FLD LOAD INPUT

NUMBER OF VALUES = 3 START LOCATION = 1

NOTE: ZERO NODE NUMBER INDICATES UNIFORM LOADING FOR ALL THE NODES OF THE SPECIFIED FACE

4	ELEMENT VALUE 5	FACE NODE VALUE 6	VALUE 1	VALUE 2	VALUE 3	VALUE
239	4	1	0.000000E+00	0.000000E+00	-1346.52	-1346.52
239	4	69	0.000000E+00	0.000000E+00	-1346.52	-1346.52
239	4	151	0.000000E+00	0.000000E+00	-1346.52	-1346.52
239	4	6	0.000000E+00	0.000000E+00	-1346.52	-1346.52
240	4	6	0.000000E+00	0.000000E+00	-1346.52	-1346.52
240	4	151	0.000000E+00	0.000000E+00	-1346.52	-1346.52
240	4	141	0.000000E+00	0.000000E+00	-1346.52	-1346.52
240	4	7	0.000000E+00	0.000000E+00	-1346.52	-1346.52
241	4	7	0.000000E+00	0.000000E+00	-1346.52	-1346.52
241	4	141	0.000000E+00	0.000000E+00	-1346.52	-1346.52
241	4	131	0.000000E+00	0.000000E+00	-1346.52	-1346.52
241	4	8	0.000000E+00	0.000000E+00	-1346.52	-1346.52
242	4	8	0.000000E+00	0.000000E+00	-1346.52	-1346.52
242	4	131	0.000000E+00	0.000000E+00	-1346.52	-1346.52
242	4	121	0.000000E+00	0.000000E+00	-1346.52	-1346.52
242	4	9	0.000000E+00	0.000000E+00	-1346.52	-1346.52
243	4	9	0.000000E+00	0.000000E+00	-1346.52	-1346.52
243	4	121	0.000000E+00	0.000000E+00	-1346.52	-1346.52
243	4	111	0.000000E+00	0.000000E+00	-1346.52	-1346.52
243	4	10	0.000000E+00	0.000000E+00	-1346.52	-1346.52
244	4	10	0.000000E+00	0.000000E+00	-1346.52	-1346.52
244	4	111	0.000000E+00	0.000000E+00	-1346.52	-1346.52
244	4	90	0.000000E+00	0.000000E+00	-1346.52	-1346.52
244	4	5	0.000000E+00	0.000000E+00	-1346.52	-1346.52
245	4	69	0.000000E+00	0.000000E+00	-1346.52	-1346.52
245	4	70	0.000000E+00	0.000000E+00	-1346.52	-1346.52
245	4	152	0.000000E+00	0.000000E+00	-1346.52	-1346.52
245	4	151	0.000000E+00	0.000000E+00	-1346.52	-1346.52
246	4	151	0.000000E+00	0.000000E+00	-1346.52	-1346.52
246	4	152	0.000000E+00	0.000000E+00	-1346.52	-1346.52
246	4	142	0.000000E+00	0.000000E+00	-1346.52	-1346.52
246	4	141	0.000000E+00	0.000000E+00	-1346.52	-1346.52
247	4	141	0.000000E+00	0.000000E+00	-1346.52	-1346.52
247	4	142	0.000000E+00	0.000000E+00	-1346.52	-1346.52
247	4	132	0.000000E+00	0.000000E+00	-1346.52	-1346.52
247	4	131	0.000000E+00	0.000000E+00	-1346.52	-1346.52
248	4	131	0.000000E+00	0.000000E+00	-1346.52	-1346.52
248	4	132	0.000000E+00	0.000000E+00	-1346.52	-1346.52
248	4	122	0.000000E+00	0.000000E+00	-1346.52	-1346.52
248	4	121	0.000000E+00	0.000000E+00	-1346.52	-1346.52
249	4	121	0.000000E+00	0.000000E+00	-1346.52	-1346.52
249	4	122	0.000000E+00	0.000000E+00	-1346.52	-1346.52
249	4	112	0.000000E-00	0.000000E+00	-1346.52	-1346.52
249	4	111	0.000000E-00	0.000000E+00	-1346.52	-1346.52
250	4	111	0.000000E-00	0.000000E+00	-1346.52	-1346.52
250	4	112	0.000000E+00	0.000000E+00	-1346.52	-1346.52
250	4	91	0.000000E+00	0.000000E+00	-1346.52	-1346.52
250	4	90	0.000000E+00	0.000000E+00	-1346.52	-1346.52
251	4	70	0.000000E-00	0.000000E+00	-1346.52	-1346.52
251	4	71	0.000000E+00	0.000000E+00	-1346.52	-1346.52
251	4	153	0.000000E-00	0.000000E+00	-1346.52	-1346.52
251	4	152	0.000000E-00	0.000000E+00	-1346.52	-1346.52
252	4	152	0.000000E-00	0.000000E+00	-1346.52	-1346.52
252	4	153	0.000000E+00	0.000000E+00	-1346.52	-1346.52
252	4	143	0.000000E+00	0.000000E+00	-1346.52	-1346.52
252	4	142	0.000000E-00	0.000000E+00	-1346.52	-1346.52
253	4	142	0.000000E-00	0.000000E+00	-1346.52	-1346.52
253	4	143	0.000000E-00	0.000000E+00	-1346.52	-1346.52
253	4	133	0.000000E-00	0.000000E+00	-1346.52	-1346.52
253	4	132	0.000000E-00	0.000000E+00	-1346.52	-1346.52
254	4	132	0.000000E+00	0.000000E+00	-1346.52	-1346.52
254	4	133	0.000000E-00	0.000000E+00	-1346.52	-1346.52
254	4	123	0.000000E-00	0.000000E+00	-1346.52	-1346.52
254	4	122	0.000000E+00	0.000000E+00	-1346.52	-1346.52
255	4	122	0.000000E+00	0.000000E+00	-1346.52	-1346.52
255	4	123	0.000000E-00	0.000000E+00	-1346.52	-1346.52
255	4	113	0.000000E+00	0.000000E+00	-1346.52	-1346.52

1007	3	1654	0.000000E+00	0.000000E+00	-742.500
1008	3	1654	0.000000E+00	0.000000E+00	-742.500
1008	3	1655	0.000000E+00	0.000000E+00	-742.500
1008	3	1634	0.000000E+00	0.000000E+00	-742.500
1008	3	1633	0.000000E+00	0.000000E+00	-742.500
1009	3	1491	0.000000E+00	0.000000E+00	-742.500
1009	3	1492	0.000000E+00	0.000000E+00	-742.500
1009	3	1646	0.000000E+00	0.000000E+00	-742.500
1009	3	1645	0.000000E+00	0.000000E+00	-742.500
1010	3	1645	0.000000E+00	0.000000E+00	-742.500
1010	3	1646	0.000000E+00	0.000000E+00	-742.500
1010	3	1651	0.000000E+00	0.000000E+00	-742.500
1010	3	1650	0.000000E+00	0.000000E+00	-742.500
1011	3	1650	0.000000E+00	0.000000E+00	-742.500
1011	3	1651	0.000000E+00	0.000000E+00	-742.500
1011	3	1656	0.000000E+00	0.000000E+00	-742.500
1011	3	1655	0.000000E+00	0.000000E+00	-742.500
1012	3	1655	0.000000E+00	0.000000E+00	-742.500
1012	3	1656	0.000000E+00	0.000000E+00	-742.500
1012	3	1635	0.000000E+00	0.000000E+00	-742.500
1012	3	1634	0.000000E+00	0.000000E+00	-742.500
1013	3	1492	0.000000E+00	0.000000E+00	-742.500
1013	3	1493	0.000000E+00	0.000000E+00	-742.500
1013	3	1647	0.000000E+00	0.000000E+00	-742.500
1013	3	1646	0.000000E+00	0.000000E+00	-742.500
1014	3	1646	0.000000E+00	0.000000E+00	-742.500
1014	3	1647	0.000000E+00	0.000000E+00	-742.500
1014	3	1652	0.000000E+00	0.000000E+00	-742.500
1014	3	1651	0.000000E+00	0.000000E+00	-742.500
1015	3	1651	0.000000E+00	0.000000E+00	-742.500
1015	3	1652	0.000000E+00	0.000000E+00	-742.500
1015	3	1657	0.000000E+00	0.000000E+00	-742.500
1015	3	1656	0.000000E+00	0.000000E+00	-742.500
1016	3	1656	0.000000E+00	0.000000E+00	-742.500
1016	3	1657	0.000000E+00	0.000000E+00	-742.500
1016	3	1636	0.000000E+00	0.000000E+00	-742.500
1016	3	1635	0.000000E+00	0.000000E+00	-742.500
1017	3	1493	0.000000E+00	0.000000E+00	-742.500
1017	3	673	0.000000E+00	0.000000E+00	-742.500
1017	3	1552	0.000000E+00	0.000000E+00	-742.500
1017	3	1647	0.000000E+00	0.000000E+00	-742.500
1018	3	1647	0.000000E+00	0.000000E+00	-742.500
1018	3	1552	0.000000E+00	0.000000E+00	-742.500
1018	3	1551	0.000000E+00	0.000000E+00	-742.500
1018	3	1632	0.000000E+00	0.000000E+00	-742.500
1019	3	1632	0.000000E+00	0.000000E+00	-742.500
1019	3	1551	0.000000E+00	0.000000E+00	-742.500
1019	3	1550	0.000000E+00	0.000000E+00	-742.500
1019	3	1550	0.000000E+00	0.000000E+00	-742.500
1019	3	1657	0.000000E+00	0.000000E+00	-742.500
1020	3	1657	0.000000E+00	0.000000E+00	-742.500
1020	3	1550	0.000000E+00	0.000000E+00	-742.500
1020	3	860	0.000000E+00	0.000000E+00	-742.500
1020	3	1636	0.000000E+00	0.000000E+00	-742.500
1285	3	898	0.000000E+00	0.000000E+00	-43.3500
1285	3	1006	0.000000E+00	0.000000E+00	-43.3500
1295	3	2047	0.000000E+00	0.000000E+00	-43.3500
1295	3	2010	0.000000E+00	0.000000E+00	-43.3500
1286	3	2010	0.000000E+00	0.000000E+00	-43.3500
1286	3	2047	0.000000E+00	0.000000E+00	-43.3500
1286	3	2046	0.000000E+00	0.000000E+00	-43.3500
1286	3	2009	0.000000E+00	0.000000E+00	-43.3500
1287	3	2009	0.000000E+00	0.000000E+00	-43.3500
1287	3	2046	0.000000E+00	0.000000E+00	-43.3500
1287	3	1004	0.000000E+00	0.000000E+00	-43.3500
1287	3	896	0.000000E+00	0.000000E+00	-43.3500
1319	3	2074	0.000000E+00	0.000000E+00	-43.3500
1319	3	2088	0.000000E+00	0.000000E+00	-43.3500
1319	3	1036	0.000000E+00	0.000000E+00	-43.3500
1319	3	898	0.000000E+00	0.000000E+00	-43.3500
1320	3	2075	0.000000E+00	0.000000E+00	-43.3500
1320	3	2089	0.000000E+00	0.000000E+00	-43.3500
1320	3	2088	0.000000E+00	0.000000E+00	-43.3500
1320	3	2074	0.000000E+00	0.000000E+00	-43.3500
1321	3	945	0.000000E+00	0.000000E+00	-43.3500
1321	3	1149	0.000000E+00	0.000000E+00	-43.3500
1321	3	2089	0.000000E+00	0.000000E+00	-43.3500
1321	3	2075	0.000000E+00	0.000000E+00	-43.3500

NUMBER OF LOADED NODES OR ELEMENTS = 648
LARGEST NODE OR ELEMENT NUMBER = 2089

Appendix III

D I S P L A C E M E N T S A T N O D E S

IN STRUCTURE GLOBAL AXES

NODAL POINT NO.	DISPLACEMENT IN X-DIRECTION	DISPLACEMENT IN Y-DIRECTION	DISPLACEMENT IN Z-DIRECTION
1	0.000000E+00	23.8238	64.2835
2	0.000000E+00	23.4768	64.3892
5	23.8238	0.000000E+00	64.2835
6	17.1429	43.4860	64.2931
7	39.7814	59.3115	64.3065
8	56.9753	56.9753	64.3131
9	59.3115	39.7814	64.3065
10	43.4860	17.1429	64.2931
17	23.4768	0.000000E+00	64.3892
19	15.7080	43.5456	64.3869
20	38.9554	59.4806	64.3886
21	56.7727	56.7727	64.3923
22	59.4806	38.9554	64.3886
23	43.5456	15.7080	64.3869
35	0.000000E+00	31.0719	60.4942
36	0.000000E+00	30.9804	61.6437
39	31.0719	0.000000E+00	60.4942
40	8.02855	29.9881	60.4960
41	15.4724	26.9166	60.5083
42	21.8578	21.8578	60.5159
43	26.8166	15.4724	60.5083
44	29.9881	8.02855	60.4960
51	30.9804	0.000000E+00	61.6437
53	7.98163	29.8021	61.6416
54	15.3803	26.5486	61.6693
55	21.7224	21.7224	61.6910
56	26.6486	15.3803	61.6693
57	29.8021	7.98163	61.6416
69	0.000000E+00	39.3251	63.9086
70	0.000000E+00	54.5467	63.1879
71	0.000000E+00	51.6583	62.7216
72	0.000000E+00	54.1173	62.4066
73	0.000000E+00	54.4746	62.1430
74	0.000000E+00	54.6071	61.8223
75	0.000000E+00	55.3613	61.3688
76	0.000000E+00	56.1395	60.7377
77	0.000000E+00	57.1526	59.9964
78	0.000000E+00	52.6743	59.6063
90	39.3251	0.100000E+00	63.9086
91	54.5467	0.100000E+00	63.1879
92	51.6583	0.100000E+00	62.7216
93	54.1179	0.100000E+00	62.4066

94	64.4746	0.000000E+00	62.1430
95	64.6071	0.000000E+00	61.8223
96	65.3613	0.000000E+00	61.3688
97	66.1395	0.000000E+00	60.7377
98	63.7826	0.000000E+00	59.9964
99	52.5793	0.000000E+00	59.6063
111	46.5865	16.7223	64.2040
112	55.2649	16.9078	63.6921
113	60.4161	16.8527	63.1339
114	61.8752	16.5797	62.7108
115	61.9985	16.4343	62.3250
116	62.1868	16.5153	61.9078
117	63.0129	16.8133	61.4014
118	63.3314	17.0913	60.7564
119	61.5699	16.5089	60.0315
120	50.7366	13.5977	59.6715
121	57.3657	37.6688	64.5558
122	56.2084	34.9334	64.5123
123	55.9477	33.0363	64.0115
124	55.5710	32.0928	63.3455
125	55.3202	31.7562	62.6929
126	55.5976	31.9522	62.0837
127	56.5252	32.5724	61.4706
128	57.3941	33.1397	60.7760
129	55.4101	32.0220	60.0256
130	45.6212	26.3562	59.6453
131	54.4773	34.4773	64.7425
132	50.1909	50.1909	64.8369
133	46.9066	46.9066	64.4302
134	45.4543	45.4543	63.6716
135	45.0678	45.0678	62.8771
136	45.3543	45.3543	62.1712
137	46.2226	46.2226	61.5044
138	47.0197	47.0197	60.7834
139	45.4332	45.4332	60.0203
140	37.3810	37.3810	59.6302
141	37.6688	37.3657	64.5558
142	34.9334	35.2084	64.5123
143	33.0863	33.9477	64.0115
144	32.0928	33.3710	63.3455
145	31.7562	33.3202	62.6929
146	31.9522	33.5976	62.0837
147	32.5724	33.5252	61.4706
148	33.1397	37.3941	60.7760
149	32.0220	33.4101	60.0256
150	26.3562	45.6212	59.6453
151	16.7223	46.5865	64.2040
152	16.9078	55.2649	63.6921
153	16.8527	60.4161	63.1339
154	16.5797	61.8752	62.7108
155	16.4343	61.9985	62.3250
156	16.5153	62.1868	61.9078
157	16.8133	63.0129	61.4014
158	16.0913	63.3314	60.7564
159	16.5089	61.5699	60.0315

160	13.5977	50.7366	59.6715
276	0.000000E+00	38.9637	62.8384
277	0.000000E+00	54.1970	62.6489
278	0.000000E+00	51.3229	62.4988
279	0.000000E+00	53.7801	62.3525
280	0.000000E+00	54.1420	62.1419
281	0.000000E+00	54.2754	61.8019
282	0.000000E+00	55.0264	61.3158
283	0.000000E+00	55.8007	60.7374
284	0.000000E+00	53.4524	60.2926
285	0.000000E+00	52.2856	60.4907
297	38.9637	0.000000E+00	62.8384
298	54.1970	0.000000E+00	62.6489
299	51.3229	0.000000E+00	62.4988
300	53.7801	0.000000E+00	62.3525
301	54.1420	0.000000E+00	62.1419
302	54.2754	0.000000E+00	61.8019
303	55.0264	0.000000E+00	61.3158
304	55.8007	0.000000E+00	60.7374
305	53.4524	0.000000E+00	60.2926
306	52.2856	0.000000E+00	60.4907
318	46.4752	15.8723	63.8448
319	55.0115	16.5415	63.3032
320	60.1098	16.6866	62.9927
321	61.5507	16.4962	62.6901
322	61.6716	16.3709	62.3254
323	61.8612	16.4467	61.8812
324	62.6864	16.7349	61.3427
325	63.5024	17.0056	60.7533
326	61.2493	16.4234	60.3285
327	50.4513	13.5233	60.5551
328	57.4834	36.8887	64.7118
329	56.1233	34.4567	64.6006
330	55.7200	32.8353	64.0591
331	55.2943	31.9164	63.3804
332	55.0345	31.5920	62.6962
333	55.3129	31.7825	62.0451
334	56.2416	32.3928	61.4006
335	57.1103	32.9520	60.7667
336	55.1346	31.8366	60.3229
337	45.3742	26.1947	60.5385
338	54.2828	54.2828	65.0183
339	49.9841	49.9841	65.1413
340	46.6849	46.6849	64.6010
341	45.2263	45.2263	63.7306
342	44.8371	44.8371	62.8798
343	45.1217	45.1217	62.1273
344	45.9869	45.9869	61.4288
345	46.7810	46.7810	60.7706
346	45.2005	45.2005	60.3179
347	37.1738	37.1738	60.5315
348	36.8887	57.4834	64.7118
349	34.4567	56.1233	64.6006
350	32.8353	55.7200	64.0591

351	31.9164	55.2943	63.3804
352	31.5920	55.0345	62.6962
353	31.7825	55.3129	62.0451
354	32.3928	56.1416	61.4006
355	32.9520	57.1113	60.7667
356	31.8366	55.1346	60.3229
357	26.1947	45.3742	60.5385
358	15.3723	45.4752	63.8448
359	16.5415	55.0115	63.3032
360	16.6866	50.1098	62.9927
361	16.4962	61.3507	62.6901
362	16.3709	61.5716	62.3254
363	16.4467	61.3512	61.8812
364	16.7349	62.6864	61.3427
365	17.0056	63.5024	60.7533
366	16.4234	61.2493	60.3285
367	13.5233	50.4513	60.5551
503	0.000000E+00	32.3816	66.1919
504	0.000000E+00	32.1825	64.9864
513	32.3816	0.000000E+00	66.1919
521	32.1825	0.000000E+00	64.9864
564	0.000000E+00	30.6151	63.5793
572	30.6151	0.000000E+00	63.5793
587	0.000000E+00	7.36415	61.8326
588	0.000000E+00	7.27370	62.9184
597	7.27370	0.000000E+00	62.9184
605	7.36415	0.000000E+00	61.8326
648	0.000000E+00	31.9131	62.9742
656	31.9131	0.000000E+00	62.9742
671	0.000000E+00	7.57035	64.7368
673	7.57235	0.000000E+00	64.7368
681	0.000000E+00	7.48517	63.6268
689	7.48517	0.000000E+00	63.6268
732	0.000000E+00	1.000000E+00	67.2478
745	0.000000E+00	1.000000E+00	67.3639
765	0.000000E+00	1.000000E+00	67.2478
778	0.000000E+00	1.000000E+00	67.3639
814	0.000000E+00	1.000000E+00	0.000000E+00
827	0.000000E+00	1.000000E+00	0.000000E+00
847	0.000000E+00	1.000000E+00	0.000000E+00
860	0.000000E+00	1.000000E+00	0.000000E+00
896	1.44337	16.2431	141.214
898	3.100332	3.000332	96.1925
945	18.1431	1.44337	141.214
968	1.09037	2.19167	74.7939
1004	-0.301416	15.1113	141.240
1006	2.533350	2.000332	96.3512
1030	0.243734	21.1545	64.5003
1039	1.59515	1.600332	74.7569
1125	31.1545	0.049734	64.5003
1149	18.3013	-0.301416	141.240
1200	9.14056	11.0353	66.0722

1201	15.7846	27.5204	65.8247
1202	22.2783	22.2783	65.6999
1203	27.5204	15.7846	65.8247
1204	31.0958	3.24056	66.0722
1212	8.20450	30.9016	64.8654
1213	15.7029	27.3465	64.5924
1214	22.1450	22.1450	64.4525
1215	27.3465	15.7029	64.5924
1216	30.9016	3.20450	64.8654
1228	0.000000E+00	43.2069	64.8469
1229	0.000000E+00	50.3063	65.9390
1230	0.000000E+00	55.0287	66.8666
1231	0.000000E+00	55.3683	67.2497
1237	43.2069	0.000000E+00	64.8469
1238	50.3063	0.000000E+00	65.9390
1239	55.0287	0.000000E+00	66.8666
1240	55.3683	0.000000E+00	67.2497
1246	50.0178	17.5746	64.5519
1247	60.6548	18.2455	65.4414
1248	63.5939	17.6317	66.4513
1249	53.4644	14.3087	66.9258
1250	60.1088	39.1905	64.1929
1251	60.6844	37.4003	64.6285
1252	58.6612	34.5679	65.6385
1253	48.0760	27.7416	66.4185
1254	56.6100	56.6100	64.0066
1255	53.6599	53.6599	64.3082
1256	49.0233	49.0233	65.2501
1257	39.3270	39.3270	66.1588
1258	39.1905	60.1088	64.1929
1259	37.4003	60.6844	64.6285
1260	34.5679	58.6612	65.6385
1261	27.7416	48.0760	66.4185
1262	17.5746	50.0178	64.5519
1263	19.2455	50.6548	65.4414
1264	17.6317	53.5939	66.4513
1265	14.3087	53.4644	66.9258
1315	0.000000E+00	42.8331	66.0363
1316	0.000000E+00	53.9370	66.4782
1317	0.000000E+00	64.6713	66.7740
1318	0.000000E+00	53.0567	66.3758
1324	42.8331	0.000000E+00	66.0363
1325	59.9370	0.000000E+00	66.4782
1326	64.6713	0.000000E+00	66.7740
1327	55.0567	0.000000E+00	66.3758
1333	49.8879	16.7431	65.0501
1334	60.3771	17.8909	65.8452
1335	63.2733	17.4689	66.2845
1336	53.1656	14.2289	66.0276
1337	60.2092	38.4141	64.1808
1338	60.5729	36.9276	64.5787
1339	58.4190	34.3161	65.3046
1340	47.8214	27.5781	65.4716

1341	56.4067	56.4067	63.8726
1342	53.4383	53.4383	64.0500
1343	48.7925	48.7925	64.8050
1344	39.1168	39.1168	65.1882
1345	38.4141	38.2092	64.1808
1346	36.9276	36.5729	64.5787
1347	34.3161	38.4190	65.3046
1348	27.5781	47.8214	65.4716
1349	16.7431	49.8879	65.0501
1350	17.8909	60.3771	65.8452
1351	17.4689	63.2733	66.2845
1352	14.2289	53.1656	66.0276
1411	7.91734	29.5445	63.5797
1412	15.2518	26.4153	63.5864
1413	21.5337	21.5337	63.5903
1414	26.4153	15.2518	63.5864
1415	29.5445	7.91734	63.5797
1429	1.87866	7.03239	62.9219
1430	3.63594	5.30801	62.9205
1431	5.14892	5.14892	62.9206
1432	6.30801	3.63594	62.9205
1433	7.03239	1.87866	62.9219
1441	1.90117	7.11422	61.8412
1442	3.67801	6.37980	61.8553
1443	5.20724	5.20724	61.8631
1444	6.37980	3.67801	61.8553
1445	7.11422	1.90117	61.8412
1472	8.16720	30.6307	62.8832
1473	15.5946	27.0907	62.6942
1474	21.9483	21.9483	62.5983
1475	27.0907	15.5946	62.6942
1476	30.6307	8.16720	62.8832
1489	1.88796	7.33571	64.7145
1490	3.72456	6.60051	64.5724
1491	5.35940	5.35940	64.4999
1492	6.60051	3.72456	64.5724
1493	7.33571	1.88796	64.7145
1501	1.85573	7.25467	63.5656
1502	3.67331	5.53168	63.4507
1503	5.29969	5.29969	63.3915
1504	6.53168	3.67331	63.4507
1505	7.25467	1.85573	63.5656
1532	0.000000E+00	2.39388	63.8581
1533	0.000000E+00	2.79863	68.9129
1534	0.000000E+00	3.52022	69.5891
1540	0.000000E+00	1.65358	63.4533
1541	0.000000E+00	2.40877	69.4177
1542	0.000000E+00	3.72383	69.7320
1550	1.65358	2.000000E+00	63.4533
1551	2.40877	3.000000E+00	69.4177
1552	3.72383	2.000000E+00	69.7320
1558	2.39388	3.000000E+00	63.8581
1559	2.79863	2.000000E+00	68.9129

1560	3.52022	0.000000E+00	69.5891
1568	0.000000E+00	0.000000E+00	0.000000E+00
1569	0.000000E+00	0.000000E+00	0.000000E+00
1570	0.000000E+00	0.000000E+00	0.000000E+00
1571	0.000000E+00	0.000000E+00	0.000000E+00
1572	0.000000E+00	0.000000E+00	0.000000E+00
1579	0.893499	3.44198	69.4934
1580	1.78281	3.14414	69.2858
1581	2.57702	2.57702	69.1782
1582	3.14414	1.78281	69.2858
1583	3.44198	0.893499	69.4934
1584	0.699109	2.73263	68.7444
1585	1.41654	2.50559	68.4551
1586	2.05417	2.05417	68.3227
1587	2.50559	1.41654	68.4551
1588	2.73263	0.699109	68.7444
1589	0.576949	2.29000	63.7191
1590	1.16005	2.05445	63.5069
1591	1.66890	1.66890	63.4188
1592	2.05445	1.16005	63.5069
1593	2.29000	0.576949	63.7191
1632	0.000000E+00	0.000000E+00	0.000000E+00
1633	0.000000E+00	0.000000E+00	0.000000E+00
1634	0.000000E+00	0.000000E+00	0.000000E+00
1635	0.000000E+00	0.000000E+00	0.000000E+00
1636	0.000000E+00	0.000000E+00	0.000000E+00
1643	0.978264	3.62533	69.6208
1644	1.90765	3.29072	69.3958
1645	2.70796	2.70796	69.2817
1646	3.29072	1.90765	69.3958
1647	3.62533	0.978264	69.6208
1648	0.649180	2.34004	68.2565
1649	1.25933	2.14103	67.9734
1650	1.77599	1.77599	67.8446
1651	2.14103	1.25933	67.9734
1652	2.34004	0.649180	68.2565
1653	0.462526	1.56875	63.3257
1654	0.855457	1.41404	63.1254
1655	1.17614	1.17614	63.0422
1656	1.41404	0.855457	63.1254
1657	1.56875	0.462526	63.3257
1701	0.000000E+00	2.42030	63.4735
1702	0.000000E+00	2.83227	58.3149
1703	0.000000E+00	3.49394	57.4015
1708	0.000000E-00	1.66988	63.8829
1709	0.000000E+00	2.42323	58.8228
1710	0.000000E-00	3.66191	57.3016
1719	0.000000E+00	2.000000E+00	67.2629
1720	0.000000E+00	2.000000E+00	67.2773
1721	0.000000E+00	2.000000E+00	67.2841
1722	0.000000E+00	2.000000E+00	67.2773
1723	0.000000E-00	2.000000E+00	67.2629
1731	0.000000E+00	2.000000E+00	67.3787
1732	0.000000E+00	2.000000E+00	67.3939
1733	0.000000E+00	2.000000E+00	67.4014

1734	0.000000E+00	0.000000E+00	67.3939
1735	0.000000E+00	0.000000E+00	67.3787
1747	2.42030	0.000000E+00	63.4735
1748	2.83227	0.000000E+00	58.3149
1749	3.49394	0.000000E+00	57.4015
1754	1.66988	0.000000E+00	63.8829
1755	2.42323	0.000000E+00	58.8228
1756	3.66191	0.000000E+00	57.3016
1764	0.902641	3.39011	57.4223
1765	1.75756	3.05579	57.4797
1766	2.49965	2.49965	57.5119
1767	3.05579	1.75756	57.4797
1768	3.39011	0.902641	57.4223
1769	0.712238	2.75623	58.4408
1770	1.42849	2.51334	58.6438
1771	2.05840	2.05840	58.7328
1772	2.51334	1.42849	58.6438
1773	2.75623	0.712238	58.4408
1774	0.584343	2.31519	63.6067
1775	1.17403	2.07725	63.8066
1776	1.68799	1.68799	63.8884
1777	2.07725	1.17403	63.8066
1778	2.31519	0.584343	63.6067
1817	0.462878	1.58222	64.0053
1818	0.856340	1.42210	64.1947
1819	1.17939	1.17939	64.2722
1820	1.42210	0.856340	64.1947
1821	1.58222	0.462878	64.0053
1822	0.641819	2.34435	58.9446
1823	1.24164	2.12707	59.1481
1824	1.75303	1.75303	59.2370
1825	2.12707	1.24164	59.1481
1826	2.34435	0.641819	58.9446
1827	0.955389	3.54416	57.3381
1828	1.84306	3.18059	57.4147
1829	2.60258	2.60258	57.4547
1830	3.18059	1.84306	57.4147
1831	3.54416	0.955389	57.3381
1927	4.23715	3.85863	73.1145
1928	11.2464	4.35240	68.7093
2009	-0.379110	15.3211	115.535
2010	0.194195	3.07600	100.950
2015	4.35240	11.2464	68.7093
2016	3.95863	4.23715	73.1145
2046	-2.12123	14.1999	115.538
2047	-0.824341	7.65275	101.090
2052	4.27170	3.69551	68.7720
2053	3.57687	3.32384	73.0966
2074	8.07600	1.194195	100.950
2075	15.3211	-0.379110	115.535
2082	3.32384	3.57687	73.0966
2083	9.69551	4.27170	68.7720
2088	7.65275	-0.824341	101.090
2089	14.1999	-2.12123	115.538

DIRECT AND SHEAR STRESSES IN ELEMENT

ELT No.	Node No.	Compt x-dirn $\times 10^6$	Compt y-dirn $\times 10^6$	Compt z-dirn $\times 10^6$	Compt xy-dirn $\times 10^6$	Compt yz-dirn $\times 10^6$	Compt zx-dirn $\times 10^6$
239	1	72.33	-17.83	20.67	71.88	17.32	3.62
244	5	-17.83	72.33	20.67	71.88	3.62	17.32
251	277	103.61	-16.43	38.73	-1.36	-28.24	-6.21
	70	106.96	-16.64	38.25	-1.20	-27.84	-6.53
	152	82.72	-12.12	58.37	-36.02	-21.18	-4.75
	359	83.20	-12.98	58.47	-35.33	-22.04	-2.26
	278	105.03	-15.26	69.22	-6.37	23.13	-0.77
	71	106.82	-15.15	69.38	-6.53	23.01	-0.98
	153	84.48	-12.09	58.13	-39.64	19.27	-0.23
	360	85.50	-12.67	58.66	-39.20	19.02	1.84
256	319	-12.98	83.20	48.47	-45.33	-2.26	-22.04
	112	-12.12	82.72	48.37	-46.03	-6.53	-21.18
	91	-15.64	106.95	58.25	1.62	-6.21	-27.84
	298	-15.43	103.61	58.73	1.36	-6.21	-28.15
	320	-12.67	86.50	58.66	-49.19	1.84	19.02
	113	-12.09	84.48	58.13	-49.64	-0.23	19.27
	92	-15.15	106.82	68.32	-6.53	-0.98	23.01
	299	-15.27	105.03	69.22	-6.37	-0.77	23.13
259	350	67.85	3.09	56.38	-65.21	0.49	0.54
	143	69.06	3.01	56.84	-65.73	1.35	-0.76
	133	32.70	32.02	56.65	-71.32	7.48	7.31
	340	33.53	33.06	55.66	-70.76	6.80	7.43
	351	60.68	11.36	56.78	-65.22	-0.41	-1.92

	144	62.49	11.71	57.44	-66.00	0.08	-2.70
	134	36.01	35.80	47.18	-70.19	-6.45	-4.58
	341	37.99	33.92	45.99	-70.37	-6.61	-4.52
260	340	34.63	33.53	55.66	-72.76	7.60	6.80
	133	32.02	31.00	56.65	-71.32	7.43	7.40
	123	10.01	59.06	66.84	-71.73	-0.76	1.35
	330	11.09	57.86	66.38	-70.21	0.54	0.41
	341	33.92	38.00	45.99	-69.37	-4.52	-6.61
	134	35.79	36.01	47.18	-70.19	-4.58	-6.45
	124	-5.72	62.49	47.44	-68.00	-2.70	0.08
	331	-5.36	60.68	46.78	-68.22	-1.92	-0.41
262	320	-14.69	85.53	58.70	-44.19	-0.83	-11.97
	113	-13.58	84.97	58.85	-45.64	-2.12	-11.64
	92	-15.60	107.36	69.13	-6.53	-1.39	-15.82
	299	-15.25	105.05	69.24	-6.37	-0.80	-15.75
	321	-12.90	86.34	58.53	-46.96	0.49	7.91
	114	-12.49	85.21	58.50	-44.30	-0.42	8.12
	93	-15.25	105.76	68.90	-9.46	1.24	11.58
	300	-14.61	104.11	69.19	-9.34	1.47	11.64
263	279	103.88	-15.84	68.84	-19.34	-5.81	1.47
	72	105.95	-15.06	69.72	-19.46	-5.82	1.24
	154	86.34	-12.62	58.70	-37.30	-2.98	0.64
	361	85.20	-12.68	58.19	-36.96	3.07	1.03
	280	103.26	-14.43	68.80	-10.02	2.80	1.37
	73	105.16	-15.27	69.08	-10.03	2.75	1.91
	155	84.69	-12.41	57.53	-36.63	0.71	0.16
	362	83.72	-12.55	58.08	-36.32	0.69	0.33

265	351	60.67	4.34	56.75	-65.22	0.96	3.08
	144	62.54	4.77	57.51	-66.00	1.12	3.90
	134	34.88	35.67	47.00	-70.19	2.54	4.36
	341	33.07	33.99	46.09	-69.37	2.48	4.41
	352	61.16	4.01	46.78	-65.20	-2.51	-1.19
	145	63.14	5.50	57.57	-66.02	-2.48	-1.20
	135	35.52	39.85	56.95	-70.61	-3.97	-1.98
	342	34.60	37.09	57.03	-69.73	-3.98	-1.99
266	341	36.99	38.07	47.09	-69.37	4.41	2.48
	134	35.67	39.88	47.00	-70.19	4.35	2.54
	124	4.77	62.54	57.51	-69.00	3.90	1.12
	331	5.34	60.66	56.51	-69.22	3.08	0.96
	342	34.09	37.60	57.03	-69.73	-1.99	-3.98
	135	35.85	39.52	56.95	-70.61	-1.98	-3.97
	125	4.50	63.14	57.57	-69.02	-1.20	-2.48
	332	5.01	61.16	56.78	-68.20	-1.19	-2.51
268	321	-12.68	85.20	58.19	-36.96	1.04	-3.07
	114	-12.62	86.34	58.70	-37.30	0.66	-2.99
	93	-15.06	105.95	69.17	-11.46	1.26	-5.85
	300	-14.83	103.88	68.84	-11.34	1.48	-5.82
	322	-12.55	83.72	58.08	-46.32	0.33	0.70
	115	-12.41	84.69	57.53	-46.63	0.17	0.71
	94	-15.27	105.16	69.08	-10.13	1.47	2.89
	301	-15.43	103.26	68.80	-10.02	1.46	2.86
269	280	102.79	-14.89	68.10	-11.02	0.93	1.46
	73	104.95	-15.27	68.78	-11.13	0.92	1.47
	155	82.58	-12.29	58.37	-36.63	0.93	2.05

	362	84.43	-12.26	57.65	-36.32	0.94	2.01
	281	103.45	-14.49	58.31	-12.84	-2.22	0.18
	74	105.66	-14.49	57.99	-11.95	-2.23	0.20
	156	83.14	-13.63	58.54	-43.85	-2.95	0.77
	363	82.64	-33.57	57.81	-43.53	-2.94	0.75
271	135	35.84	36.17	57.43	-70.61	1.73	5.10
	146	36.01	35.98	57.43	-70.96	-3.06	-1.64
272	135	36.17	35.84	54.43	-70.61	3.67	1.73
	136	35.98	36.01	55.03	-70.96	-1.50	-3.82
274	322	-12.26	83.43	57.65	-42.32	2.00	1.27
	115	-12.30	83.58	58.37	-42.63	2.03	1.26
	94	-15.07	104.95	68.78	-10.13	1.39	0.92
	301	-15.90	102.79	68.10	-10.02	1.39	0.92
	323	-12.57	82.94	57.81	-42.53	0.67	-2.93
	116	-12.63	83.14	58.54	-42.85	0.69	-2.94
	95	-13.49	105.66	58.28	-14.05	0.24	-2.23
	302	-13.94	103.45	58.31	-14.04	0.19	-2.22
275	281	102.92	-14.02	57.52	-12.84	2.98	0.19
	74	105.18	-15.01	58.28	-11.95	2.99	0.24
	156	83.81	-12.31	58.06	-43.25	2.43	2.58
	363	82.60	-12.23	57.30	-43.13	2.43	2.44
	282	104.94	-14.57	57.99	-13.65	-2.33	-0.90
	75	107.30	-14.51	58.78	13.76	-2.33	-0.89
	157	84.75	-12.89	58.54	43.49	-2.68	1.53
	364	83.43	-12.77	67.55	-42.86	-2.67	1.40
277	137	33.20	31.43	57.91	-71.88	-2.73	-0.06
	344	31.43	33.20	57.14	-71.03	-2.71	-0.12

280	323	-12.30	82.60	57.30	-42.53	2.45	2.44
	116	-12.10	83.81	58.06	42.85	2.54	2.43
	95	-15.11	105.18	58.28	-13.95	0.24	3.00
	302	-15.02	102.92	57.52	13.84	0.18	2.98
	324	-12.77	83.43	57.75	-42.16	1.40	-2.68
	117	-12.89	84.75	58.54	-42.49	1.48	-2.68
	96	-15.51	107.30	58.78	-13.76	-0.86	-2.30
	303	-15.57	104.94	57.99	-13.65	-0.90	-2.31
281	282	104.61	-14.90	57.50	-12.65	-2.13	-0.90
	75	106.66	-15.13	57.83	-12.76	-2.10	-0.86
	157	83.25	-12.39	57.79	-43.49	-2.74	1.34
	364	84.25	-12.58	57.48	-43.16	-2.74	1.33
	283	106.44	-14.65	57.89	-12.55	6.42	0.12
	76	108.57	-14.16	58.25	-12.67	6.44	0.16
	158	88.00	-12.74	58.20	-43.07	6.29	2.40
	365	87.92	-12.90	57.86	-42.73	6.28	2.38
283	137	31.00	36.33	57.62	-71.88	-3.34	-0.67
	138	31.99	36.76	57.89	-72.79	4.96	5.42
286	324	-12.58	84.25	57.48	-42.16	1.25	-2.75
	117	-12.39	84.25	57.49	-42.49	1.36	-2.74
	96	-15.13	106.66	57.83	-13.76	-0.85	-2.09
	303	-14.90	104.61	57.50	-13.65	-0.90	-2.10
	325	-12.90	86.92	57.86	-42.73	2.31	6.28
	118	-12.74	87.00	58.20	-43.07	2.39	6.29
	97	-15.16	108.57	58.25	-9.67	0.14	6.45
	304	-14.65	106.44	57.90	-9.55	0.11	6.39
287	283	106.92	-14.16	58.61	-12.55	-20.04	0.11

	76	108.18	-14.24	57.66	-12.67	-20.02	0.14
	158	84.71	-12.45	57.77	-44.07	-19.80	-4.80
	365	83.51	-12.50	58.74	-43.73	-19.60	-4.90
	284	102.99	-14.70	67.76	-9.20	28.10	6.30
	77	104.19	-14.80	66.79	-9.31	27.90	6.30
	159	83.79	-12.73	66.88	-45.25	28.90	1.50
	366	83.65	-12.80	67.87	-45.92	29.10	1.51
292	325	-12.50	86.51	58.74	-42.73	-4.90	19.70
	118	-12.45	87.71	57.77	-42.07	-4.80	19.80
	97	-15.24	108.18	57.66	-9.67	0.13	-20.13
	304	-15.16	106.92	58.61	-9.55	0.09	-20.01
	326	-12.80	81.65	67.87	-43.92	1.51	29.00
	119	-12.73	82.79	66.88	-43.25	1.50	28.87
	98	-14.80	104.19	66.79	-9.31	6.36	28.08
	305	-14.70	102.99	67.76	-9.20	6.36	28.09
764	1237	-2.57	110.27	38.25	17.58	22.39	35.49
765	1229	113.99	-13.45	67.95	-10.89	-51.99	7.21
768	1337	-12.96	33.75	27.31	-21.51	8.73	-3.37
771	1229	114.32	-11.88	67.95	-10.89	48.88	7.21
773	1256	33.98	34.72	57.13	-72.79	-18.21	-9.02
776	1334	-12.79	90.80	69.81	-46.91	6.99	43.02
	1325	-16.84	114.29	69.99	-1.63	6.21	48.78
	1238	-16.88	114.32	67.95	-1.89	7.01	48.96
	1247	-12.86	90.26	68.09	-47.61	9.50	42.42
	1335	-12.87	90.21	69.14	-40.24	-3.74	-50.32
	1326	-13.08	99.80	69.62	-7.02	-5.79	-54.23
	1239	-13.01	95.57	67.16	-7.18	-5.24	-54.02

	1248	-12.22	90.14	67.00	-47.69	-1.64	-50.81
777	1317	97.22	-13.35	63.22	-7.01	62.59	-5.79
	1351	97.64	-12.30	69.75	-45.24	55.57	19.04
	1264	98.01	-12.09	69.77	-43.69	55.60	20.23
	1230	92.47	-13.10	69.98	-7.18	62.95	-5.25
	1318	90.23	-12.98	68.39	-8.12	-64.75	-21.08
	1352	73.95	-12.13	67.81	-33.80	-61.98	5.06
	1265	73.38	-11.51	64.57	-34.11	-61.04	5.88
778	1231	89.52	-13.85	64.88	-8.23	-61.23	-5.01
	1256	84.84	-13.09	66.52	-7.75	-22.95	31.90
	1340	0.27	60.90	46.00	-57.58	-42.34	-36.25
	1253	0.28	60.51	43.34	-58.26	-41.98	-36.25
779	1257	28.30	24.56	52.90	-61.92	-19.91	-46.45
781	1340	25.60	26.21	55.94	-69.33	-8.75	-55.63
	1336	-12.10	71.22	67.86	-37.55	-34.88	-53.25
	1249	-12.59	70.65	64.64	-38.07	-33.96	-53.01
	1253	0.26	62.95	43.34	-63.99	-7.70	-55.90
	1248	-12.52	80.22	69.32	-44.82	10.25	58.28
782	1335	-12.30	79.64	72.75	-43.24	19.05	55.57
	1326	-13.35	92.22	73.22	-17.02	-5.79	62.58
	1239	-13.11	92.47	69.98	-17.18	-4.99	63.96
	1248	-12.09	88.01	69.77	-43.69	20.23	55.61
	1336	-12.14	86.95	67.81	-43.80	7.03	-63.97
	1327	-13.98	79.23	68.39	-8.12	-21.09	-64.84
	1240	-13.85	79.52	64.88	-8.23	-20.93	-64.15
	1249	-12.51	66.38	64.57	-34.11	5.88	-63.95
786	1344	24.07	25.58	44.56	-69.20	39.04	13.29

	1253	0.38	55.20	53.61	-58.26	0.89	44.70
787	1249	-12.47	75.54	69.90	-38.07	-11.09	46.76
	1253	0.54	55.87	55.63	-59.99	33.95	25.68
788	1327	-13.48	79.69	63.53	-8.13	-21.08	43.51
	1240	-13.18	79.55	62.36	-8.24	-20.97	44.86
	1249	12.39	78.26	69.85	-36.11	28.21	36.36
841	587	16.41	-14.68	38.26	-1.04	-70.39	9.28
842	1441	-15.30	5.92	38.07	-4.84	-70.06	-13.81
845	1445	5.92	-15.30	38.07	-4.84	-13.81	-70.06
	1433	-0.12	8.98	83.86	-4.69	-13.33	-67.91
846	605	-14.68	16.41	38.26	-1.04	9.28	-70.20
	597	-14.32	10.05	37.42	-1.00	7.50	-70.39
899	673	-13.71	6.44	109.48	-1.00	-10.51	69.40
	689	-13.48	5.85	108.47	-0.96	31.55	69.39
	1505	-10.06	9.13	112.74	-4.95	12.31	64.40
903	1501	5.67	-11.10	112.74	-5.11	68.51	12.31
	1502	9.13	-0.60	101.22	-4.95	59.40	50.19
997	671	6.44	-13.81	112.70	-0.93	69.40	-9.29
	1542	2.91	-12.60	-112.75	0.74	7.78	-5.42
	1543	-2.59	27.68	101.32	0.78	2.88	-5.88
	681	6.44	-13.46	112.72	-0.96	28.04	-9.57
	1489	5.77	-12.09	112.01	-5.18	48.08	20.99
	1501	5.23	-11.75	112.28	-5.38	25.17	18.84
1001	1489	5.75	-12.83	111.21	-4.39	52.60	4.27
	1501	5.23	-12.58	109.97	-4.73	29.85	-1.51
	1490	3.55	-13.18	108.37	-14.27	41.77	32.36
	1502	4.19	-12.24	106.61	-14.73	20.94	21.47

1005	1490	3.03	-13.37	106.54	-15.11	49.71	18.66
	1491	6.02	5.94	102.13	-5.35	31.77	42.42
	1503	5.62	6.40	101.49	-5.96	14.92	26.26
1009	1504	-12.58	12.64	102.63	-5.67	7.15	29.32
1013	1492	-13.18	13.55	98.37	-4.27	32.36	41.77
	1505	-16.58	7.23	103.97	-3.73	-1.51	29.85
1017	1493	-15.09	8.77	105.01	-2.18	20.99	48.08
	673	31.89	39.29	39.37	-0.63	-9.29	69.40
	1552	-8.85	0.29	-112.56	0.78	-5.42	7.75
	1560	-8.86	1.59	-112.75	0.74	-6.21	2.88
	689	-12.46	12.69	112.69	-0.70	-10.60	69.40
3	605	3.23	13.69	103.35	-0.67	8.02	-52.16
	597	4.19	12.50	101.39	-0.74	8.34	-28.77
1285	2053	-6.70	-11.58	-2.12	2.17	20.38	-27.65
	1039	-12.80	-0.69	0.43	-0.31	-23.41	25.09
1287	2009	-17.13	-14.16	-6.22	-3.97	8.63	-28.40
	2046	-13.40	-17.84	-6.22	4.66	7.34	-29.14
1319	1082	-11.58	-6.70	-2.11	2.17	-27.65	20.38
1321	2075	-14.16	-17.13	-6.22	-3.97	-22.55	6.98
	2089	-17.84	-13.40	-6.22	4.66	-22.81	7.31